# การพัฒนาแบบจำลองเชิงสโตแคสติกและการจำลองการเกาะแบบกลุ่มก้อนของแอโรซอลบนเส้นใยอิเลกเทรต

นางสาว วีรยา แซ่ลิ่ม

วิทยานิพนธ์นี้เป็นส่วนหนึ่งของการศึกษาตามหลักสูตรปริญญาวิศวกรรมศาสตร์ดุษฎีบัณฑิต
สาขาวิชาวิศวกรรมเคมี ภาควิชาวิศวกรรมเคมี
คณะวิศวกรรมศาสตร์ จุฬาลงกรณ์มหาวิทยาลัย
ปีการศึกษา 2548

ISBN 974-53-1861-2

ลิขสิทธิ์ของจุฬาลงกรณ์มหาวิทยาลัย

# STOCHASTIC MODEL DEVELOPMENT AND SIMULATION OF AGGLOMERATIVE DEPOSITION OF AEROSOL ON AN ELECTRET FIBER

Miss Weeraya Sae-lim

A Dissertation Submitted in Partial Fulfillment of the Requirements
for the Degree of Doctor of Engineering Program in Chemical Engineering
Department of Chemical Engineering
Faculty of Engineering
Chulalongkorn University
Academic year 2005

ISBN 974-53-1861-2

| | |
|---|---|
| Thesis Title | STOCHASTIC MODEL DEVELOPMENT AND SIMULATION OF AGGLOMERATIVE DEPOSITION OF AEROSOL ON AN ELECTRET FIBER |
| By | Miss Weeraya Sae-lim |
| Filed of study | Chemical Engineering |
| Thesis Advisor | Professor Wiwut Tanthapanichakoon, Ph.D. |
| Thesis Co-advisor | Professor Chikao Kanaoka, Ph.D |

---

Accepted by the Faculty of Engineering, Chulalongkorn University in Partial Fulfillment of the Requirements for the Doctor's Degree

DL Lavansiri ……………………………Dean of the Faculty of Engineering
(Professor Direk Lavansiri, Ph.D.)

THESIS COMMITTEE

…………………………………………….. Chairman
(Associate Professor Tawatchai Charinpanitkul, D.Eng.)

Wiwut Tanthapanichakoon ……… Thesis Advisor
(Professor Wiwut Tanthapanichakoon, Ph.D.)

Chikao Kanaoka ……………….. Thesis Co-advisor
(Professor Chikao Kanaoka, Ph.D.)

…………………………………………….. Member
(Assistant Professor Vichitra Chongvisal, Ph.D.)

Sirikalaya Suvachittanont ………. Member
(Associate Professor Sirikalaya Suvachittanont, Ph.D.)

Mana Amornkitbamrung ... Member
(Assistant Professor Mana Amornkitbamrung, D.Eng.)

วีรยา แซ่ลิ่ม: การพัฒนาแบบจำลองเชิงสโตแคสติกและการจำลองการเกาะแบบกลุ่มก้อนของแอโรซอลบนเส้นใยอิเลกเทรต (STOCHASTIC MODEL DEVELOPMENT AND SIMULATION OF AGGLOMERATIVE DEPOSITION OF AEROSOL ON AN ELECTRET FIBER) อ. ที่ปรึกษา: ศ.ดร. วิวัฒน์ ตัณฑะพานิชกุล, อ.ที่ปรึกษาร่วม: ศ.ดร. ชิคาโอะ คานาโอกะ 117 หน้า. ISBN 974-53-1861-2.

ประสิทธิภาพการกรองของแผงกรองอิเลกเทรต แตกต่างจากประสิทธิภาพของแผงกรองที่ใช้โดยทั่วไป เนื่องจากประสิทธิภาพการกรองในช่วงต้นของเส้นใยอิเลกเทรตอาจจะลดลงเมื่อมีภาระฝุ่นเพิ่มขึ้น การศึกษาในที่นี้จะทำนายค่าสัมประสิทธิ์การเพิ่มประสิทธิภาพ(efficiency enhancement factor) ในการจับอนุภาคบนเส้นใยภายใต้ภาระฝุ่นสำหรับอนุภาคที่ไม่มีประจุและมีประจุจากผลการทดลองที่มีผู้ตีพิมพ์ไว้แล้ว พบว่าค่าประสิทธิภาพการจับอนุภาคบนเส้นใยอิเลกเทรต สามารถคำนวณได้จากผลบวกของประสิทธิภาพเชิงไฟฟ้าและประสิทธิภาพเชิงกล ผลที่ได้แสดงว่า ค่าประสิทธิภาพการกรองของแผงกรองอิเลกเทรตที่ได้มาจากการคำนวณ สอดคล้องกันค่อนข้างดีกับผลการทดลองที่เคยรายงานไว้ทั้งในกรณีอนุภาคที่มีประจุและไม่มีประจุ นอกจากนี้ยังได้ขยายผลของแบบจำลองเชิงสโตแคสติก เพื่อจำลองลักษณะการเกาะตัวแบบกลุ่มก้อนของอนุภาคบนเส้นใยอิเลกเทรต และได้ศึกษาถึงผลของค่าพารามิเตอร์ของการสกัดกั้น ค่าพารามิเตอร์ของแรงทางไฟฟ้า ทั้งกรณีของแรงเหนี่ยวนำ (กรณีอนุภาคไม่มีประจุ) และแรงคูลอมบ์ (กรณีอนุภาคมีประจุ) จากการศึกษาทั้งกรณีอนุภาคที่มีประจุและไม่มีประจุ พบว่าเมื่อค่าพารามิเตอร์ของการสกัดกั้นมีค่าน้อย การเกาะของอนุภาคจะหนาแน่น ส่วนผลของแรงทางไฟฟ้าต่อรูปทรง พบว่ากรณีที่แรงทางไฟฟ้ามีค่ามาก ลักษณะของเดนไดรต์จะสูงขึ้น ตรงขึ้น และเรียวขึ้น กว่ากรณีที่แรงทางไฟฟ้ามีค่าน้อย

นอกเหนือจากที่กล่าวมาแล้วข้างต้น ได้ศึกษาและเปรียบเทียบค่าประสิทธิภาพของแผงกรองอิเลกเทรต 4 ชิ้น ที่มีค่าเฉลี่ยความหนาแน่นในการบรรจุเท่ากัน แต่การกระจายตัวของเส้นใยตามทิศความหนาของแผงกรองมีค่าไม่เท่ากัน ผลที่ได้พบว่าสามารถยืดอายุการใช้งานของแผงกรองได้ด้วยการทำให้เส้นใยมีความหนาแน่นในการบรรจุต่ำทางด้านขาเข้าของแผงกรอง และค่อยๆเพิ่มความหนาแน่นในการบรรจุมากขึ้นไปยังด้านขาออก

ภาควิชา..... วิศวกรมมเคมี.......................... ลายมือชื่อนิสิต วีรยา แซ่ลิ่ม
สาขาวิชา.....วิศวกรรมเคมี......................... ลายมือชื่ออาจารย์ที่ปรึกษา วิวัฒน์ ตัณฑะพานิชกุล
ปีการศึกษา...2548............................ ลายมือชื่ออาจารย์ที่ปรึกษาร่วม Chikao Kanaoka

# # 4471822721 : MAJOR CHEMICAL ENGINEERING
KEY WORD: ELECTRET FIBER/ DUST LOADING EFFECT/ STOCHASTIC SIMULATION/COLLECTION EFFICIENCY ENHANCEMENT FACTOR

WEERAYA SAE-LIM: STOCHASTIC MODEL DEVELOPMENT AND SIMULATION OF AGGLOMERATIVE DEPOSITION OF AEROSOL ON AN ELECTRET FIBER. THESIS ADVISOR: PROF. WIWUT TANTHAPANICHAKOON, Ph.D., THESIS CO-ADVISOR: PROF. CHIKAO KANAOKA, Ph.D., 117 pp. ISBN 974-53-1861 -2.

Unlike ordinary filters, the initial high collection efficiency of the electret filter (E) might briefly fall as dust load increases. Here, the electrical enhancement factor of the electret fiber ($\lambda_E$) under dust-loaded condition for uncharged and charged particles is obtained from published experimental results. It is found that the collection efficiency of the electret fiber ($\eta$) can be approximated as the sum of the electrical and mechanical collection efficiency. The predicted values of E are shown to agree well with reported experimental observations for both uncharged and charged particles. In addition, a three-dimensional stochastic model is extended to simulate collection and agglomeration of particles on the cylindrical electret fiber. Effect of interception, induced force (for uncharged particles) and coulombic force (for charged particles) parameters are studied. For both charged and uncharged particles, when the interception parameter is small, captured particles are densely packed. The effect of high electrical forces on the morphology makes the dendrites taller, straighter and more slender than those of small electrical forces.

Next, the dust-loaded collection efficiencies of four identical electret filters with the same average packing density but different spatial distributions of packing density along the filter thickness are calculated and compared. The results show that we can significantly lengthen the filter service life by packing the filter loosely on the inlet side and progressively more densely towards the outlet side.

Department......Chemical Engineering........Student's signature Weeraya Saelim
Field of study...Chemical Engineering.......Advisor's signature W. Tanthapanichakoon
Academic year...2005..........................Co-advisor's signature Chikao Kanaoka

# ACKNOWLEDGEMENTS

Firstly, the author sincerely wishes to thank Professor Wiwut Tanthapanichakoon, thesis advisor, and Professor. Chikao Kanaoka, thesis co-advisor, for their encouraging guidance and suggestions throughout this study. Their comments and suggestions not merely provide valuable knowledge but broaden her perspective in practical applications as well.

The author received the full-expense scholarship under The Royal Golden Jubilee (RGJ) Ph.D. Program from Thailand Research Fund (TRF) , and also got 1-year Student Exchange Scholarship from Association of International Education Japan (AIEJ) to study and do research at Kanazawa University (2003-2004). This work was also partially supported by Thailand-Japan Technology Transfer Project (TJTTP-JBIC) and TRF-RTA Project of Prof. Wiwut Tanthapanichakoon

Next, the author is thankful to Associate Professor Tawatchai Charinpanitkul, Assistant Professor Vichitra Chongvisal, Associate Professor Sirikalaya Suvachittanont, and Assistant Professor Mana Amornkitbamrung for their useful comments and participation as thesis committee.

Moreover, the author wants to give credit to all friends in Powder Technology and Material Processing Laboratory members especially Mr. Apiluck Eiad-eua who have supported and given her very helpful advice.

Eventually, the author would like to express the appreciation to her parents, younger sister, and younger brother for their encouragement, understanding, inspiration and very useful help.

# CONTENTS

Page

**ABSTRACT IN THAI**………………………………………………………………. iv

**ABSTRACT IN ENGLISH**…………………………………………………………. v

**ACKNOWLEDGEMENTS**………………………………………………………… vi

**CONTENTS**……………………………………………………………………. vii

**LIST OF TABLES**…………………………………………………………….. xi

**LIST OF FIGURES**…………………………………………………………… xii

**NOMENCLATURE**………………………………………………………….. xix

**CHAPTER**

**I. INTRODUCTION**………………………………………………………1

1.1 Aerosol particles………………………………………………… 1

1.2 Clean room………………………………………………………... 4

1.3 Introduction to electret filter……………………………………… 7

1.4 Objectives of research…………………………………………10

1.5 Scope of research……………………………………………... 10

**II. LITERATURE REVIEW** ……………………………………………. 11

2.1 Modeling study of single fiber…………………………………….. 11

2.2.1 Deterministic approach……………………………………… 12

2.2.2 Stochastic approach for non-electret fiber…………………… 15

2.2.3 Stochastic approach for electret fiber……………………….. 16

2.2 Air filtration using electret filter ………………………………….. 18

Page

**III. THEORY…………………………………………………………….. 22**

3.1 Filtration phenomena in the filter……………………………….22

3.2 Trajectory and deposition mechanism of aerosol on a … …………25
single fiber

3.2.1 Kuwabara flow field………………………………………25

3.2.2 Interception……………………………………………..28

3.2.3 Diffusion………………………………………………..29

3.2.4 Inertial impaction……………………………………….30

3.2.5 Gravitational settling……………………………………...31

3.2.6 Electrostatic deposition …………………………………..31

3.3 Relationship between E of a filter and η of a single fiber……….....32

3.4 The stochastic dendritic growth model for a single fiber………….34

3.4.1 Deposition via convective Brownian diffusion ……………..36

3.4.2 Deposition via inertial impaction …………………………...37

**IV. CALCULATION PROCEDURE FOR EFFICIENCY ENHANCEMENT FACTOR OF AN ELECTRET FIBER……...40**

4.1 Calculation procedure to determine correlation for the…………...40
efficiency enhancement factor of a single electret fiber
from experimental results

4.2 Stochastic simulation procedure to predict the collection………..44
efficiency of a single electret fiber via Monte-Carlo Technique

Page

4.3 Evaluation/Estimation of filter service life……………………………50

**V. EXPERIMENTAL EVIDENCE…………………………………….....52**

5.1 Experimental set-up of electret filter filtration……………………..52

5.2 Penetration of aerosol particles under dust loading………………...54

5.3 Pressure drop of electret filter under dust loading…………………56

**VI. RESULTS AND DISCUSSION……………………………………...59**

6.1 Correlation of the collection efficiency enhancement factor………59

6.1.1 Comparison between experimental and simulated results…...59

6.1.2 Electrical enhancement factor, $\lambda_E = \beta \ln m + \gamma$……………...62

6.1.3 Normalized single-fiber collection efficiency……………….67

6.2 Collection efficiency of an electret fiber via Monte-Carlo………...68 technique

6.2.1 Validation of model……………………………………….71

6.2.1.1 Cases in which Brownian diffusion mechanism is ……..71 assumed to be dominant

6.2.1.2 Cases in which inertial impaction mechanism is ……….73 assumed to be dominant

6.2.1.3 Selection of suitable stochastic model…………………..76

6.2.2 Effect of electrical degradation factor……………………….80

6.2.3 Effect of interception parameter…………………………...81

6.2.4 Effect of coulombic force parameter…………………………83

6.2.5 Effect of induce force parameter……………………………..85

Page

6.2.6Effect of Peclet number……………………………………88

6.2.7 Correlation for the simulated collection ……………………92
efficiency enhancement factor

6.3 Structural improvement to lengthen service life …………………..98
of the electret filter

**VII. CONCLUSION AND RECOMMENDATION……………………102**

7.1 Conclusion………………………………………………… 102

7.2 Recommendation…………………………………………... 104

**REFERENCES………………………………………………………….. 105**

**APPENDICES…………………………………………………………….109**

APPENDIX A Derivation of collection efficiency of …………….110
electret filer under dust loading

APPENDIX B Publications resulting from this …………………..116
research work

**VITA……………………………………………………………………117**

# LIST OF TABLES

Page

**Table 4.1** Simulation conditions used (a) Based on Walsh's …………...........43 experiments on stearic acid particles (1997) (b) Based on Lee's experiments (2002)

**Table 4.2** Packing density of the electret filter………………………………...51

**Table 5.1** Characteristics of electrically active material……………………......53

**Table 6.1** Electrical enhancement factor ($\lambda_E = \beta \ln m + \gamma$) of an………………63 electret fiber from clean state to clogging point

**Table 6.2** Stochastic simulation conditions for aerosol agglomerative ……….70 depostion on an electret fiber

**Table 6.3** Interception parameter of various particle sizes respect with ……...81 fiber diameter 20 μm

# LIST OF FIGURES

Page

**Figure 1.1** Range of aerosol concentration ($g/m^3$)……………………………3

**Figure 1.2** Comparison of particle size……………………………………….6

**Figure 3.1** Time dependency of particle agglomerates on a tungsten wire …….23 $d_f$ = 10 μm, $d_p$ = 1 μm, v = 50 cm/s, $\rho_p$ = 11.34 $g/cm^3$, Stk =3.5, R=0.1 (Kanaoka, 1998)

**Figure 3.2** Particle agglomerates formed by electrostatic effect; $d_f$ = 30 μm, ....24 $d_p$ = 0.39 μm, v = 15 m/s,$\rho_p$ = 2.33 $g/cm^3$ , Stk =0.015, Pe=$5\times10^4$, R=0.013. (a) Uncharged particles $K_{In}$ = 0.004, V = $4.8\times10^{-4}$ ; (b) Uncharged particles $K_{In}$ =0.004, V= $1.5\times10^{-3}$; (c) Charged particles $K_c$= 0.016, V= $4.9\times10^{-4}$

**Figure 3.3a** Vorticity around cylinders (the broken lines represent zero………. 26 vorticity)

**Figure 3.3b** Mean flow velocity around cylinders…………………………....26

**Figure 3.4** Cross section of Kuwabara's cell…………………………………..27

**Figure 3.5** Shape of particle accumulates by the change of collection ………. 28 mechanism

**Figure 3.6** Streamlines near a cylindrical fiber lying transverse to flow, …….33 and the definition of single fiber efficiency

**Figure 4.1** Collection efficiency, electrical collection efficiency …………….41 and mechanical collection efficiency of 1.03 micron stearic acid charged particles at face velocity 0.1 m/s

Page

**Figure 4.2** Simplified flow chart of the iteration procedure……………………44

**Figure 4.3** Schematic diagram of Kuwabara's cell……………………………46

**Figure 4.4** Region of high gradient electrostatic field…………………………47

**Figure 4.5** Flow chart of the stochastic simulation procedure………………....49

**Figure 4.6** The filter packing density distribution along thickness …………...51 of 4 filters.

**Figure 5.1** Sketch of the aerosol filtration test rig…………………………….53 (Walsh and Stenhouse,1995)

**Figure 5.2** Penetration through filter samples loaded with stearic acid ……...55 particles of Boltzmann equilibrium charge distribution, over a size range 0.46 – 1.40 μm at face velocity 0.1 m/s

**Figure 5.3** Penetration through filter samples loaded with uncharged ………55 and charged stearic acid particles of 0.61 and 1.26 μm at face velocity 0.1 m/s

**Figure 5.4** Pressure drop across filter samples loaded with ………………....57 stearic acid particles of Boltzmann equilibrium charge distribution at a face velocity of 0.1 m/s

**Figure 5.5** Pressure drop across filter samples loaded with …………………58 uncharged and charged particles of 1.26, 0.61 particle size at 0.1 m/s face velocity.

Page

**Figure 6.1** Comparison between experimental results and ……………………61 simulation results of stearic acid over size range 0.46 – 1.26 micron at face velocity 0.1 m/s :(a) charged particles (b) uncharged particles

**Figure 6.2** Electrical collection efficiency enhancement factor ($\lambda_E$) …………66 of charged particles: (a) over size range 0.61- 1.26 micron at face velocity 0.1 m/s (b) uncharged and charged 1.03 micron stearic acid particles at face velocity 0.1 m/s

**Figure 6.3** Normalized collection efficiency of charged ………………………68 stearic acid particles, over a size range 0.46 – 1.26 micron at face velocity 0.1 m/s

**Figure 6.4** Typical configuration of dendrites for the case of $K_c = 0.20$, …….71 $R_i = 0.0515$, Pe = 75372, Gamma = 90, $\phi = 0.01$, layers = 40

**Figure 6.5** Typical configuration of dendrites for the case of $K_{In} = 0.20$, ……72 Ri = 0.0515, Pe = 75372, $\phi = 0.01$, layer = 40

**Figure 6.6** Normalized collection efficiency for the case of $K_C = 0.2$ , ……...72 Ri = 0.0515, Pe = 75372,$\phi$= 0.01

**Figure 6.7** Normalized collection efficiency for the case of $K_{In} = 0.2$ ,……....73 Ri = 0.0515,Pe = 75372, $\phi = 0.01$

**Figure 6.8** Typical configuration of dendrites for the case of $K_c = 0.20$,……..74 $R_i = 0.0515$, Stk = 0.017,Gamma = 90, $\phi = 0.01$, layer = 40

Page

**Figure 6.9** Typical configuration of dendrites for the case of $K_{In}$ = 0.20, ……75
$R_i$ = 0.0515, Stk = 0.017,$\phi$ = 0.01 , layer = 40

**Figure 6.10** Normalized collection efficiency for the case of $K_C$ = 0.2 ,……….75
$R_i$ = 0.0515, Stk = 0.017, Gamma = 90 , $\phi$ = 0.01

**Figure 6.11** Normalized collection efficiency for the case of $K_{In}$ = 0.2 ,………76
$R_i$ = 0.0515, Stk = 0.017, $\phi$ = 0.01

**Figure 6.12** Experimental results of dendrite morphology on an ……………….77
electret fiber with low dust load for uncharged particles at conditions: $d_f$ =30 μm, $d_p$= 0.039 μm, $R_i$ = 0.013, u=15 cm/s, $\rho_p$=2.33 g/cm$^3$, $K_{In}$=0.004, Pe= 50000 and Stk = 0.015

**Figure 6.13** Experimental results of dendrite morphology on an ………………78
electret fiber with high dust load for uncharged particles at conditions: $d_f$ =30 μm, $d_p$= 0.039 μm, $R_i$ = 0.013, u=15 cm/s, $\rho_p$=2.33 g/cm$^3$, $K_{In}$=0.004, Pe= 50000 and Stk = 0.015

**Figure 6.14** Experimental results of dendrite morphology on an ………………78
electret fiber with low dust load for charged particles at conditions : $d_f$ =30 μm, $d_p$= 0.039 μm, Ri = 0.013, u=15 cm/s, $\rho_p$=2.33 g/cm$^3$, $K_C$=0.016, Pe= 50000 and Stk = 0.015

**Figure 6.15** Experimental results of dendrite morphology on an ……………...79
electret fiber with high dust load for charged particles at conditions: $d_f$ =30 μm, $d_p$= 0.039 μm, Ri = 0.013, u=15 cm/s, $\rho_p$=2.33 g/cm$^3$, $K_C$=0.016, Pe= 50000 and Stk = 0.015

Page

**Figure 6.16** Normalized collection efficiency for the case of $K_C = 0.2$ , ………80
Ri = 0.0515,Pe = 75372 and $\phi = 0.005, 0.01$ or0.03

**Figure 6.17** Typical configuration of dendrites with $K_c = 0.20$, $\phi= 0.01$ ………82
a) Ri = 0.0515 ; b) Ri = 0.063

**Figure 6.18** Typical configuration of dendrites for the case of $K_c = 0.10$, ……..83
Ri = 0.0515, Pe = 75372.

**Figure 6.19** Typical configuration of dendrites for the case of $K_c = 0.05$, ……..84
Ri = 0.0515 Pe = 75372.

**Figure 6.20** The normalized collection efficiency for the cases of $K_C = 0.05$, …84
0.1 and 0.2 , respectively ( Ri = 0.0515, Pe =75732,$\phi = 0.01$)

**Figure 6.21** Typical configuration of dendrites for the case of $K_{In} = 0.20$, ……86
Ri = 0.0515, Pe = 75372,$\phi = 0.01$

**Figure 6.22** Typical configuration of dendrites for the case of $K_{In} = 0.10$, ……87
Ri = 0.0515, Pe = 75372, $\phi$ =0.01

**Figure 6.23** Typical configuration of dendrites for the case of $K_{In} = 0.05$, ……87
Ri = 0.0515, Pe = 75372, $\phi = 0.01$

**Figure 6.24** Normalized collection efficiency for the cases of $K_{In} = 0.05$, …….88
0.1 and 0.2, respectively ( Ri = 0.0515, Pe = 75372,$\phi = 0.01$)

**Figure 6.25** Typical configurations of dendrites a) $K_c = 0.20$; b) $K_{In} = 0.20$ …..89
with $R_i = 0.0515$, Pe = 1000, $\phi = 0.01$

**Figure 6.26** Typical configuration of dendrites a) $K_c = 0.20$; b) $K_{In} = 0.20$……90
with $R_i = 0.0515$, Pe = 5000, $\phi = 0.01$

Page

**Figure 6.27** Typical configurations of dendrites a) $K_c = 0.20$; b) $K_{In} = 0.20$……91
with $R_i = 0.0515$, Pe = 50000, $\phi = 0.01$

**Figure 6.28** Single fiber collection efficiency for the case of $K_C = 0.2$ and …….94
$\phi = 0.01$ for charged particles over a size range
0.46 – 1.26 micrometer

**Figure 6.29** Normalized collection efficiency for the case of $K_C = 0.2$ ,……….94
Ri = 0.023 and $\phi = 0.01$

**Figure 6.30** Normalized collection efficiency for the case of $K_C = 0.2$ , ………95
Ri = 0.0305 and $\phi = 0.01$

**Figure 6.31** Normalized collection efficiency for the case of $K_C = 0.2$ ,……….95
Ri = 0.0515 and $\phi = 0.01$

**Figure 6.32** Normalized collection efficiency for the case of $K_C = 0.2$ , ………96
Ri = 0.063 and $\phi = 0.01$

**Figure 6.33** Normalized collection efficiency for the case of $K_{In} = 0.2$ ,………96
Ri = 0.023 and $\phi = 0.01$

**Figure 6.34** Normalized collection efficiency for the case of $K_{In} = 0.2$ , ……...97
Ri = 0.0305 and $\phi = 0.01$

**Figure 6.35** Normalized collection efficiency for the case of $K_{In} = 0.2$ , ……...97
Ri = 0.0515 and $\phi = 0.01$

**Figure 6.36** Normalized collection efficiency for the case of $K_{In} = 0.2$ ,………98
Ri = 0.063 and $\phi = 0.01$

Page

**Figure 6.37** Penetration through 4 different by packed electret filters …………99
under dust loading condition

**Figure 6.38** Distribution of dust inside electret filters; (a) Filter A; ……………101
(b) Filter B; (c) Filter C; (d) Filter D

# NOMENCLATURE

$A(t)$ = fluctuating term (cm/s)

$B$ = mobility of particle ($=C_m/3\pi\mu d_p$) (s/kg)

$C_e$ = effluent particle concentration (kg/m$^3$)

$C_i$ = influent particle concentration (kg/m$^3$)

$C_m$ = Cunnigham’s correction factor (-)

$E_m$ = collection efficiency of filter (dimensionless)

$d_f$ = fiber diameter (m)

$d_p$ = particle diameter (m)

$D_{BM}$ = diffusion coefficient ($= \frac{C_m kT}{3\pi\mu D_p}$) (m$^2$/s)

$e$ = elementary electric charge ($=1.6*10^{-19}$) (C)

$E$ = particle collection efficiency of filter (-)

$F_C$ = dimensionless coulombic force (-)

$F_G$ = dimensionless gradient force (-)

$F_R$ = dimension high-gradient force (-)

$F$ = external force vector (N)

$Gr$ = gravitation settling parameter ($=\frac{U_\infty}{V_g}$) (-)

$h$ = thickness of filter (m)

$H$ = half height of generation plane (-)

$K$ = hydrodynamic factor (-)

$K_C$ = dimensionless electrical parameter for coulombic force (-)

$K_{In}$ = dimensionless electrical parameter for induced force (-)

L = Sample size (-)

m = dust load in a unit filter volume (kg/m$^3$)

n = standard normal random vector = ($n_x$,$n_y$,$n_z$)

$n_E$ = number of electron on particle (-)

N = total number of sampling points (-)

p = position vector (m)

P = dimensionless position vector (-)

Pe = Peclet number (=$\frac{D_f U_\infty}{D_{BM}}$ ) (-)

Pn = penetration (dimensionless)

$r_E$ = radius of hemisphere of influence of high-gradient force (-)

Ri = interception parameter ($d_p$/$d_f$) (-)

$R_c$ = dimensionless radius of Kuwabara's cell (-)

$R_f$ = radius of fiber (m)

$R_p$ = radius of particle (m)

Stk = Stoke number (=$\frac{C_m U_\infty \rho_p d_p^2}{9\mu d_f}$ ) (-)

t = time (s)

$\Delta t$ = time step (s)

u = fluid velocity (-)

$U_X$ = fluid velocity in x-direction (-)

$U_Y$ = fluid velocity in y-direction (-)

$U_Z$ = fluid velocity in z-direction (-)

$U_\infty$ = approach velocity of air (m/s)

v = particle velocity (-)

$V_g$ = settling velocity (m/s)

x = x-coordinate (m)

X = dimensionless x-coordinate (-)

y = y-coordinate (m)

Y = dimensionless y-coordinate (-)

z = z-coordinate (m)

Z = dimensionless z-coordinate (-)

$\eta$ = single-fiber collection efficiency

$\eta_{0E}$ = electrical single-fiber collection efficiency of the clean fiber

$\eta_{0M}$ = mechanical single-fiber collection efficiency of the clean fiber

$\lambda_E$ = electrical enhancement factor ($m^3$/kg)

$\lambda_M$ = mechanical enhancement factor ($m^3$/kg)

$\alpha$ = packing density of filter (-)

# CHAPTER I

# INTRODUCTION

## 1.1 Aerosol particles

The microscopic particles that float in the air are of many kinds: resuspended oil particles, smoke from power generation, photochemical by formed particles, salt particles formed from ocean spray, and atmospheric clouds of water droplets or ice particles. They vary greatly in their ability to affect not only visibility and climate but also our health and quality of life. These airborne particles are all examples of aerosols. An aerosol is defined in its simplest form as a collection of solid or liquid particles and the gas in which they are suspended. They include a wide range of phenomena such as dust, fume, smoke, mist, fog, haze, clouds, and smog.

An understanding of the properties of aerosols is of great practical importance. Aerosol properties influence the production, transport, and ultimate fate of atmospheric particulate pollutants. Aerosols can be subdivided according to the physical form of the particles and their method of generation. There is no strict scientific classification of aerosols. The following definitions correspond roughly to common usage and are precise enough for most scientific description.

**Aerosol:** A suspension of solid or liquid particles in gas phase. Aerosols are usually stable for at least a few seconds and in some cases may last a year or more. The term *aerosol* includes both the particles and the suspending gas, which is usually air. Particle size ranges from about 0.002 to more than 100 μm.

**Cloud:** A visible aerosol with defined boundaries.

**Dust:** A solid-particle aerosol formed by mechanical disintegration of a parent material, such as by crushing or grinding. Particles range in size from sub micrometer to more than 100 μm and are usually irregular in shape.

**Fume:** A solid-particle aerosol produced by the condensation of vapors or gaseous combustion products. These submicrometer particles are often clusters or chains of primary particles. The latter are usually less than 0.05 μm. Note that this definition differs from the popular use of the term to refer to any noxious contaminant in the atmosphere.

**Haze:** An atmospheric aerosol that affects visibility.

**Smog:** 1. A general term for visible atmospheric pollution in certain areas. The term was originally derived from the words smoke and fog. 2. Photochemical smog is a more precise term referring to an aerosol formed in the atmosphere by the action of sunlight on hydrocarbons and oxides of nitrogen. Particles are generally smaller than 1 or 2 μm.

Particle size is the most important parameter for characterizing the behavior of aerosols. A major dividing line is 1 μm, which marks the upper limit of the submicrometer range ( less than 1.0 μm) and the lower limit of the micrometer size range (1-10 μm). In general, dust, ground material, and pollen are in the micrometer range or larger, and fumes and smokes are submicrometer. The smallest aerosol particles approach the size of large gas molecules and have many of their properties. Ultrafine particles range from large gas molecules to about 100 nm (0.001 to 0.1 μm). Particles less than 50 nm are called nanometer particles or nanoparticles. Solid aerosol particles usually have complex shapes. In the development of the theory of aerosol properties, it is usually necessary to assume that the particles are spherical. Correction factor and the use of equivalent diameters enable these theories to be applied to nonspherical particles. An equivalent diameter is the diameter of the sphere that has the same value of a particular physical property as that of an irregular particle.

The most commonly measured aerosol property, and the most important one for health and environmental effects, is the *mass concentration*, the mass of particulate matter in a unit volume of aerosol. Common units are g/m$^3$, mg/m$^3$. Another common measure of concentration is *number concentration*, the number of particles per unit volume of aerosol, commonly expressed as number/cm$^3$ or number/m$^3$. **Figure 1.1** shows the extremely wide range of aerosol concentration.

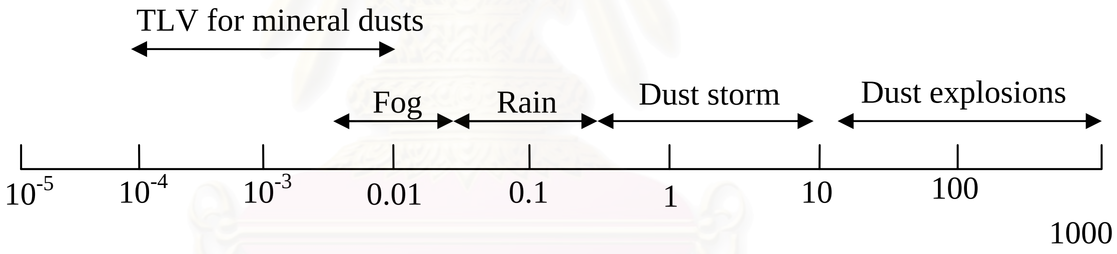

**Figure 1.1** Range of aerosol concentration (g/m$^3$).

Once aerosols are in the atmosphere, they can be removed by several processes. Aerosol filtration by a fibrous air filter is a widely adopted and highly efficient method for removing submicron particles from gas stream with the additional advantage of low energy consumption. Filtration is a simple, versatile, and economical means for collecting aerosol particles. At low dust concentrations, fibrous filter are the most economical means for achieving high-efficiency collection of sub micrometer particles. Aerosol filtration is used in various applications, such as respirator protection, air cleaning, and clean rooms.

## 1.2 Clean room

In the high technological industries such as electronics, optical and biological industries, the newly developed commodities are manufactured with precise fabrication as a basic process. Both production yield and product quality are affected by invisible airborne particles or fine dust. For example in the manufacturing of semiconductors, the design rule of ULSI is now minimized to the line width of sub micrometer. In this case, the size of particle to be eliminated in the clean room is smaller than 0.05 micrometer, namely, 1/5 — 1/10 of the design rule, which means that only a super clean environment can be accepted for its production process. Also, in food processing, medical or pharmaceuticals, how to control the micro-organism is a key point to maintain the quality, which can be achieved with the clean room.

The clean room is defined as a specially constructed room in which the air supply, air distribution, dust and airborne particles, room pressure, temperature and humidity are environmentally regulated to meet an appropriate cleanliness level. The particle referred here means a particle as small as 1/1000 of human hair in diameter, which is equivalent to 1/100 of the smallest visible limit. These small particles affect the production yield and product quality to a great extent. Also many factors other than air supply are to be carefully managed to achieve and mention clean environment condition. The clean room is what solves these issues.

The clean room is divided into two kinds by application; one is Industrial Clean Room and the other Biological Clean Room. The latter, together with clean room function, controls contamination density of micro-organism and plays an important role in clinical research and examination, development of medicines, research and improvement of cultivation cycle and plant breeding, etc. The clean air technology development has taken further steps along with the progress of the APO LO Program by NASA. During this progress, a high efficient filter has been put into practical use, and its development has now advanced from 0.3 micrometer HEPA Filter (High Efficient Particulates Air Filter) to ULPA Filter (Ultra Low Penetration Air Filter) which can eliminate 0.1-0.2 micrometer particles in diameter at efficiency as high as 99.999% by number.

The dust and particles controlled in the clean room are very small and invisible as shown in **Figure 1.2.** A visible particle is generally larger than 10 micrometer, which is removed out at the stage of Pre-Filter. In case of clean room, so called submicron particle, smaller than 1 micrometer, is the subject to control. According to the United States Federal Standards the cleanliness is defined on the basis of 0.5 micrometer particle in diameter. In **Figure 1.2**, around 0.5 micrometer particles are smog, oil mist, cigarette smoke, etc. These are visible only when they are condensed, but not directly. Like this, in the clean room, the subjects are such small particles that they can not be visible without using microscopy.

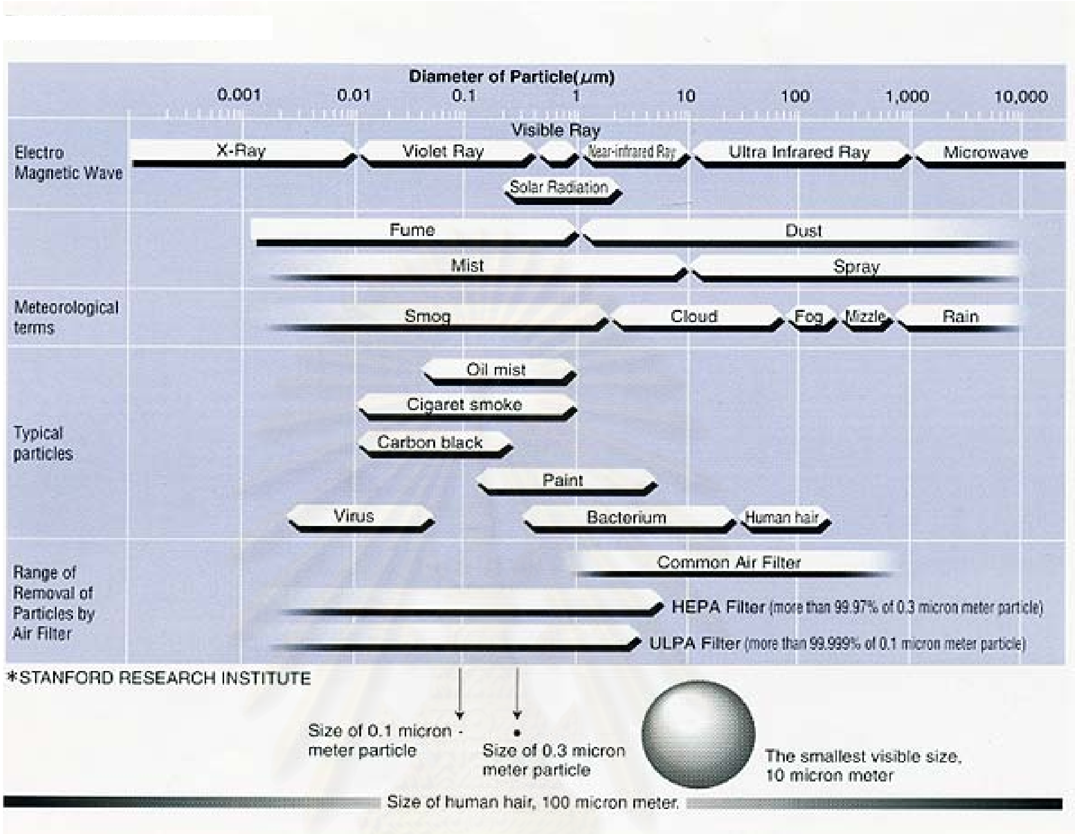

**Figure 1.2** Comparison of particle size

HEPA Filter used in a clean room can remove particles 0.3 micrometer in diameter with more than 99.97% collection efficiency. ULPA Filter now being used in Super Clean Room for semiconductor industries has more than 99.999% for 0.1 micrometer particle, and is able to make the supply air free from particles. An electret filter carries permanent positive and negative charges inside each fiber. The aerosol collection efficiency of the electret fiber can be significantly higher than the non-electret one, even if the aerosol particles are uncharged. Unsurprisingly, electret fibers have been used to enhance the collection efficiency of HEPA and ULPA filters.

## 1.3 Introduction to electret filter

Electrically charged filter material has a history of several decades. The advantage of materials of this type is that the charge on the fibers considerably augments the filtration efficiency without making any contribution to the air flow resistance. Several materials carrying permanent electric charge now exist, finding wide use in situations where a high efficiency is required along with a minimum flow resistance, such as in respirator filters.

The electret filter can be classified according to how the filter material becomes electrically charged. There are three principal charging processes: triboelectric charging, corona charging and charging by induction. Although it is difficult to explain at the microscopic level, charged fibers can greatly enhance filter collection. This characteristic is used for filters that require both high collection efficiency and low pressure drop, such as respirator filters (Hinds, 1999). The oldest type of charged-fiber filter is the resin-wool or Hansen filter, made of wool fiber impregnated with insulating resin particles about 1 μm in diameter. The charging of a plastic comb on vigorous contact with human hair is a familiar example of this charging process. The mechanical action of carding the felt causes the resin particles to become highly charged, and they retain their charge for years under favorable conditions. The presence of this highly charged particles in the filter greatly enhances its collection efficiency without increasing its resistance. Unfortunately, charged fiber filters lose their charge and their effectiveness when exposed to ionizing radiation, high temperature, high humidity or organic liquid aerosols. Also accumulated dust can mask the charge and reduce its effectiveness.

Another type of charged fiber is the electret fiber. Electric charge can be placed on a polymer by means of a corona discharge. A pointed electrode at a high potential emits ions of its own sign, and these will drift, under the influence of the field produced by the electrode, to any surface at a lower potential. If the surface is insulating, a charge will develop. If the insulator is a thin sheet of polymer, resting on a conductor, a compensating charge of the opposite sign will develop as the polymer is stripped away from its conductor backing to give charge in a sheet dipole configuration. Their similarity to a magnet, which has permanent magnetization, is reflected in the similarity between the words electret and magnet. Electret fiber filters have advantages and limitations similar to those of resin-wool filters.

The collection performance of an electret fiber has been investigated theoretically and experimentally. As a result, the collection efficiency of a single electret fiber was well correlated by a function of coulombic force and induced force parameters, when electrostatic effects are prevailing. Electret filters can be used in particular for respirators, clean rooms and probably for the highly-efficient cleaning of waste laboratory air (e.g. in the case of toxic or radioactive pollution). The advantages of the electret filters are, in all cases, high initial collection efficiencies combined with a low flow resistance.

An electret filter carries permanent positive and negative charges inside each fiber. The aerosol collection efficiency of the electret fiber can be significantly higher than a non-electret one, even if the aerosol particles are uncharged. Thus electret fibers have been used to enhance the collection efficiency of HEPA and ULPA filters. In some instances the collection efficiency of an electret fiber may drop substantially as deposition of particles progresses. Typically air filters are not equipped with any dust-cleaning systems and are discarded when captured particles clog the air passage. Kanaoka (1998) showed how to double the service life by designing a filter with larger dust-holding capacity at the same final pressure drop. This is achievable because filter performance depends not only on filtration conditions and particle properties but also on filter properties, such as fiber diameter, packing density and packing structure.

The collection efficiency of the clean electret fiber in the initial stage is remarkably high because of its strong electrostatic effects. As dust loading proceeds, the collection efficiency of the electret filter might briefly fall as a function of dust load because the electrostatic effect exhibited by the fiber surface is screened or masked by the deposited particles. It is known that most on-coming particles are collected on already captured particles to form complicated agglomerates on an electret fiber. As a consequence, the mechanical effect on the overall efficiency gradually picks up and ultimately becomes the dominant collection mechanism.

As more and more particles deposit on a fiber inside a filter and/or on previously captured particles, they form complicated accumulates. As the constituent fibers are covered with collected particles, the filter characteristics change with the dust load. Therefore, it is necessary for the rational design and operation of the electret filter to know the collection efficiency of an electret fiber under dust-loaded condition.

The process of filtration is complicated although the general principles are well known. There is a gap between theory and experiment. Nevertheless, filtration is an active area for theoretical and experimental research, and there is an extensive scientific literature on the subject.

## 1.4 Objectives of research

1. To predict the collection efficiency enhancement factors under dust loading condition for both charged and uncharged particles.

2. To lengthen the electret filter service life by changing the distributions of packing density along the filter thickness

3. To develop and apply a stochastic model to predict the dendritic growth of aerosol particles and the corresponding aerosol collection efficiency on a dust-loaded electret fiber for the case of uncharged and charged particles.

## 1.5 Scopes of research

1. The model derived from studying the dendritic growing on a single electret fiber was applied to electrostatic deposition mechanism.

2. Fortran programming language was chosen to code the model program. The resulting computer code will be tested on a personal computer.

3. The stochastic model was simulated under various filtration conditions such as Peclet number or inertial parameter, electrical parameters and particle size to obtain additional stochastic simulation results for the collection efficiency raising factors.

4. The results will be compared to both the experimental results and the previously simulated results of other researchers.

# CHAPTER II

# LITERATURE REVIEW

The review of literature consists of two parts. The first part is a review of modeling study. Two different approaches can be discerned: first is the deterministic approach, and second is the stochastic approach. The second part is a review of experimental study of aerosol filtration using the electret filter.

Investigations, both experimental and theoretical, on aerosol filtration have been carried out extensively, and are too numerous to cite individually. Generally, the performance characteristics of clean air filters are well known and have widely been reported. However, only a few studies are concerned about the performance characteristics changing with dust loading. It is necessary for the rational design and operation of the electret filter to know the collection efficiency and pressure drop of an electret fiber under dust-loaded condition. The present study will focus mostly on the collection efficiency aspect.

## 2.1 Modeling study

In formulating a theoretical model of the phenomenon, two different approaches can be discerned: one is deterministic, and the other stochastic. The deterministic approach formulates a mathematical model in which there is no uncertainty in the values of the variables and parameters. The stochastic approach employs variables and parameters to describe the input-output relationship, which are not known precisely but governed by certain probability laws. The latter approach is, in general, more difficult to employ than the former but in many cases the stochastic approach provides more insight into the characteristics and behavior of a real process. The deterministic approach has been pursued mostly by Payatakes (1976a, 1976b, 1076c, 1977, 1980a, 1980b) for interception, and/or convective diffusional, and/or inertial impaction, whereas the corresponding stochastic approach for the same case have been carried out by Tien et al. (1977); Wang et al. (1977); Kanaoka et al. (1980, 1981, 1983).

### 2.2.1 Deterministic approach

Radushkevich (1964) was the first to model the growth of particle clusters on collectors. He assumed that a given dendrite can be completely characterized by just the number of member particles. This implied that no distinction existed between member particles at different positions in a dendrite, so no prediction regarding the dendrite configuration is possible, even though its configuration was a factor of primary importance in the determination of the effect of the dendrites on both the filtration efficiency and resistance to flow. Furthermore, the facts that a new dendrite is generally of a slimmer structure protruding from the collector surface into the bulk flow and that the probability of new particle additions depends on the site of deposition along the dendrite suggest that the configuration of the dendrite should significantly affect its rate of growth.

Payatakes and Tien (1976) proposed a preliminary math model for the formation of chain-like agglomerates on a fiber during the filtration of aerosols in fibrous media. Their work was intended for the description of filtration performance, both filtration efficiency and pressure drop, over the entire dust loading period. The model was limited by two assumptions; first, the dendrite layer adjacent to the collector could contain only one particle at most; second, the particles colliding with the upper half of a dendrite particle became members of the immediately higher layer. Then, they showed that the idealized dendrite configurations predicted theoretically were in agreement with those observed experimentally form a photograph of particle dendrites on a single fiber (Billing 1966).

Payatakes (1977) extended their previous work, which consider only contribution of particle deposition from the tangential flow component by pure interception. He developed a revised and generalized version of the model. The following major revisions were made: allowance is made for collisions with a particle in a given dendrite layer that lead to retention in the same layer, radial as well as angular contribution to depositions are considered, and the dendrite layer adjacent to the collector is allowed to contain more than one particle. These revisions led to a substantially more realistic theoretical model. The behavior of this model was demonstrated in the simple case of deposition by pure interception. The proposed treatment of deposition by pure interception is more rigorous than and superseded that adopted in previous work.

Payatakes and Gradon (1980) extended the model to include the case of deposition by inertial impaction and interception mechanism. Also the shadow effect was incorporated in the analysis. Furthermore, the model can be extended to deal with the case of deposition by convective Brownian diffusion. They showed the calculated profiles of the expected dendrite configuration as a function of age and angular position and the transient behavior of a fibrous filter of different thickness. These observations were in agreement with experimental data.

Payatakes and Gradon (1980a) extended the model to include the case of submicron particles, where the main transport mechanism of the model is convective Brownian diffusion. They presented solutions for the cases of non-slip flow around the fiber; and nonslip, slip and free molecular flow around particles. They found that dendrites form over the entire fiber surface. Moreover, the profiles of the expected dendrite configuration depend strongly on the angular position. In addition, a larger interception parameter value leads to more pronounced dendrite deposition.

Tanthapanichakoon et al. (1993) developed a simple population balance model for predicting dendritic growth of aerosol particles and the accompanying increase in the collection efficiency on a single fiber via convective diffusional deposition by using only a personal computer without requiring much computational time. The simulation results of the new simplified model agreed fairly well with those obtained previously by Monte-Carlo simulation of the stochastic model.

Areephant (1996) studied the growth of dendrites on a fiber in an air filter by using the deterministic dendritic growth model which Tanthapanichakoon et al.(1993) developed on the basis of population balance. This model was modified for particle deposition via convective diffusion and via inertial impaction. The optimal parameter values of the model could be estimated by comparison with the stochastic simulation results.

### 2.2.2 Stochastic approach for non-electret fiber

Tien et al. (1977) were the first to use the stochastic approach to represent the random locations of incoming particles in their simulation. They proposed a model for the formation and growth of dendrites on a two dimensional collector placed in an aerosol stream. Their simulations were carried out on a cross section of the collector by taking into account the randomness of individual particles together with the corresponding trajectories determined from the equation of motion. The formation and growth of particle dendrites were simulated and found to resemble those obtained from experiments.

Kanaoka et al. (1980, 1980a) simulated the growing process of particles dendrites on a dust-loaded fiber via Monte-Carlo simulation of a stochastic model for inertial interception collection mechanism. They found that the shapes of dendrites thus obtained agreed fairly well with experimental investigations and the ratio of single fiber collection efficiency with dust load to that of a clean fiber was expressed as a linear function of the mass of deposited particles in a unit filter volume. In addition, the values of a collection efficiency raising factor $\lambda$ were in qualitative agreement with previous experimental study.

Kanaoka et al. (1983) proposed a three-dimensional stochastic model for the case of deposition of aerosol particles by convective Brownian diffusion. This model was developed starting from Langevin's equation and used to simulate the collection and agglomeration processes of particles on a cylindrical fiber. The equation of motion of particles including the Brownian effect was considered. The effect of Peclet number, interception parameter and the accumulated mass of particles on a fiber on the distribution of captured particles on the fiber and the evolution of the collection efficiency of the dust-loaded fiber were also discussed through the simulation. Furthermore, they found that the ratio of the collection efficiency of single dust-loaded fiber to that of the clean fiber was expressed as a linear function of the mass of particles in a unit filter volume. In addition, the coefficient in the linear function and collection efficiency raising factor depended on the Peclet number and interception parameter.

Wongsri et al. (1991) proposed a three-dimensional method for the stochastic simulation of dendritic growth of polydisperse particles for the case of convective Brownian diffusion. They found that this study were almost the same as those obtained for monodispersed aerosols and the range of standard deviation of polydispersity of the aerosol particles did not affect the average performances of the dust-loaded fiber.

### 2.2.3 Stochastic approach for electret fiber

Emi et al. (1984) studied collection efficiency of an electret filter, both theoretically and experimentally by means of monodisperse particles in different charging states, namely, uncharged, singly or doubly charged, and charged in Boltzmann equilibrium. Moreover, the theoretical collection efficiencies of a clean single electret fiber were calculated by considering the effects of both induced and coulombic forces, and approximate expressions of the efficiencies were obtained for the induced force effect, coulombic force effect and the combined effect of both. Experimentally, the collection efficiency of the filter is markedly influenced by the change in the charging state of particles, and both coulombic and induced forces affect the collection of particles simultaneously. Finally, a semi-empirical expression for the collection efficiency of a clean single electret fiber was obtained.

Emi et al. (1987) experimentally studied the collection performance of an electret filter by means of very fine particles in different charging states, that is, uncharged, singly or multiply charged and charged in equilibrium at filtration velocity ranging from 5 to 200 cm/sec. They found that a general expression of a clean single electret fiber efficiency for fine particles was obtained by considering Brownian diffusion together with coulombic and induced forces. The expression successfully explained the complex behavior of penetration curve of particles charging in equilibrium.

Hiragi (1995) studied experimentally and employed a practical three-dimensional simulation method for predicting the agglomerative deposition process of submicron aerosol particles on an electret fiber. The simulated results were shown to agree quite well with the experimental observations for both uncharged and charged particles dealing with gradient force and coulombic force respectively. This study led to prediction of how the morphology of particle accumulates on a constituent fiber changed and affected the collection efficiency and pressure drop of the filter under the dust-loaded condition. Furthermore, he applied fractal geometry to describe the characteristic of dendrite.

Kanaoka (1998) reviewed the performance of a dust-loaded air filter in which particles deposit and form complicated accumulates, thus increasing its collection efficiency and pressure drop. The following topics were reviewed: 1) The collection process of particles and morphology of particle accumulates on a single fiber plus experimental observation and computer simulation by various collection mechanism,

2) collection efficiency and pressure drop of a dust-loaded filter, 3) prediction of filter performance with dust load and 4) improvement of filter service life.

Kanaoka et al. (2001) proposed a practical three-dimensional simulation method for predicting the agglomerative deposition process of submicron aerosol particles on an eletret fiber. The simulated results are shown to agree quite well with the experimental observations for both uncharged and charged particles. For the former only the gradient force and for the latter only the coulombic force needs to be considered as long as an oncoming particle has not come in close proximity to any previously deposited particles. In contrast, once the oncoming particle enters a region of close proximity to a deposited particle at the tip of a dendrite or chain-like agglomerate, it suffices to consider only the high-gradient or particle-string formative force in the employed stochastic model.

Tanthapanichakoon et al. (2003) modified a three dimensional stochastic model to simulate the deposition process on an electret fiber by considering the effect of Brownian diffusion in the model. The model was shown to predict the agglomerative deposition process reasonably well, and in the case of weak electrical effects, they also approximated the collection efficiency enhancement factor as linear function of dust load.

## 2.2. Air filtration using electret filter

As mentioned earlier, Emi et al.(1984) studied the collection efficiency of a single electret fiber using monodisperse sodium chloride particles ranging from 0.01-0.4 μm in diameter for filtration velocity from 5 to 200cm/s, under different charging state of particles, i.e., uncharged, singly or doubly charged, and charged in Boltzmann equilibrium. It was found that the experimental clean fiber efficiency was markedly influenced by the small change in the charging state of particles.

Baumgartner et al. (1986) studied the determination of single fiber charge and collection efficiency. They presented fractional separation functions for different types of electret filters and for the particle size range from 10 nm to 10 μm at the filtration velocity of 10 cm/s. The initial efficiencies were compared to that of a conventional (glass fiber) filter and also to those of electret filters in discharged state. The results of long-term filtration experiments showed that a complex time-dependent behavior existed for different filter materials. Furthermore, two experimental methods were presented and discussed for determining the charge characteristics of single electret fibers.

Brown et al. (1988) studied the natural process of deterioration performance of electrically charged filter material by exposing respirator filter materials, on site, to industrial aerosols, comprising aerosols produced during foundry fettling operations, foundry burning, lead component manufacture, lead smelting, silica sand quarrying, refractory brick production, coking, and asbestos textile manufacture. Equal masses of different aerosols were found to cause widely different changes in performance. They found that loading filters with homogeneous aerosols caused the penetration to increase exponentially, with a constant of proportionality that quantifies the ability of the aerosol to degrade the filter. Their experimental results were shown to be consistent with a charge-screening process.

Otani et al. (1993) proposed equations of clean electret fiber collection efficiency for small electrostatic effect between particles and electret fibers accounting for the interception effect, and comparing with the experimental data.

They also studied the stability of electret charge when the electret filters was exposed to liquid and humid air. They found that the electret charge is fairly stable in humid air, but the collection efficiency for liquid droplets gradually decreases because captured droplets covered the fiber and thus weakened the electrical field around the fibers.

As mentioned earlier, Hiragi (1995) studied how the agglomerates of uncharged and charged particles, respectively, change with filtration time and location on an electret fiber. When uncharged particles were collected, they attached all around the fiber and formed chainlike agglomerates, which subsequently became irregular and complicated as the electrostatic effect gradually weakened. In the case of charged particles, the shape is similar to the former but agglomerates tended to concentrate in a limited area of opposite polarity to the particles.

Walsh and Stenhouse (1997) studied the characteristics of an electrically active fibrous filter material loaded with particles. They showed that small particles accelerated filter clogging and rapidly reduced the initial filtration efficiency. They suggested that electrically active materials had greater dust holding capacity than the conventional ones did. These studies indicate that the charge of a test particle is a key parameter affecting the initial and long-term performance characteristics of electret filters.

Lee et al. (2002) predicted the collection performance of high-performance electret filters (HPEF).They carried out experiments on HPEF using the particles whose diameter ranged from 0.01 to 0.3 micrometer, whereas the face velocity was varied from 0.5 to 50 cm/s. They found that the HPEF had electrical charge density twenty times as high as previous research of them (Otani et al.,1993), and that the

HPEF was fairly stable against organic solvent, retaining one-third of initial charge after soaking it with ethanol.

Ji et al. (2004) tested electret filter media used in manufacturing cabin air filters by applying two different charging states to the test particles. These charging states were achieved by spray electrification through the atomization process and by bipolar ionization with an aerosol neutralizer, respectively. They found that the amount of charge, the mean particle size, and the particle material significantly affected the collection performance of the electret filter for submicron particles. The collection efficiency of electret filter degraded as more particles were loaded, and showed minimum efficiency at a pseudo steady state. The filter media loaded with liquid DOS particles showed collection efficiencies much lower than those loaded with solid NaCl particles.

# CHAPTER III

# THEORY

This chapter presents a brief review of the basic theory of aerosol filtration.

## 3.1 Filtration phenomena in the filter

The process of filtration is complicated, and although the general principles are well known, there is still a gap between theory and experiment. Fibrous filters consist of a mat of fine fibers arranged so that most are perpendicular to the direction of airflow. As particles deposit on a fiber inside the filter and/or on previously captured particles, they form complicated accumulates, which lead to a marked increase in collection efficiency and pressure drop. Since air filter is operated under dust load, prediction of filter performance is indispensable to the improvement of filter service life. Depending on the aerosol particle size and operating conditions, various filtration mechanisms such as interception, inertial impaction, and Brownian motion, simultaneously influence deposition process on a fiber. The process is enhanced by electrostatic effects with the application of an external electric field or the use of an electret filter.

To understand the behavior of fibrous air filters, and the way in which they collect aerosol particles, it is important to consider the structure of the fibrous mats. Fibrous filters have very open structure, and traditionally they have been modeled by considering the behavior of aerosol particles with respect to a single cylindrical fiber within the depth of the media. Kanaoka (1998) observed the deposition pattern of aerosol particles on a tungsten wire as shown in **Figure 3.1.** When the fiber is still clean, particles are collected directly on it, but once a few particles are collected, the flow pattern around them changes, and the existence of captured particles enhance the collection of additional particles. This can clearly be seen from **Figure 3.1**, which shows the time evolution of accumulates of lead particles ( $d_p$ = 1 μm) on a tungsten wire ($d_f$ = 10 μm) at a velocity of v = 50 cm/s (Stk = 3.5). At 1.5 min, few particles are collected on the fiber surface but the number of particles increases enormously from 1.5 to 10 min. Furthermore, the average spatial distribution of captured particles does not change much with time; i.e., the maximum deposition appears around the front stagnation and then decreases gradually to the side edge of the fiber.

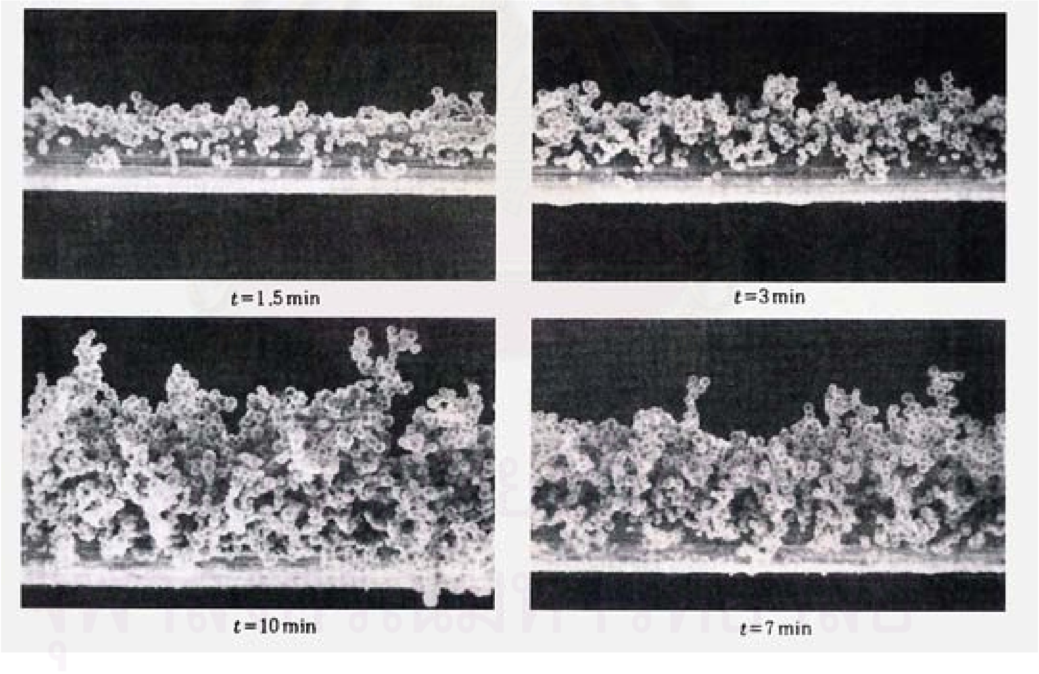

**Figure 3.1** Time dependency of particle agglomerates on a tungsten wire $d_f$ = 10 μm, $d_p$ = 1 μm, v = 50 cm/s, $\rho_p$ = 11.34 g/cm$^3$, Stk =3.5, R=0.1 (Kanaoka, 1998)

When particles and/or the fiber are electrically charged, the deposition pattern is different from mechanical collection because of electrostatic effects. **Figure 3.2** shows the particles on an electret fiber. When uncharged particles are collected, they attach all around the fiber and form chainlike agglomerates and then they become irregular and complicated because of the weak electrostatic effect. For charged particles, the shape is similar to the former but agglomerates concentrate in a limited area of opposite polarity to the particles.

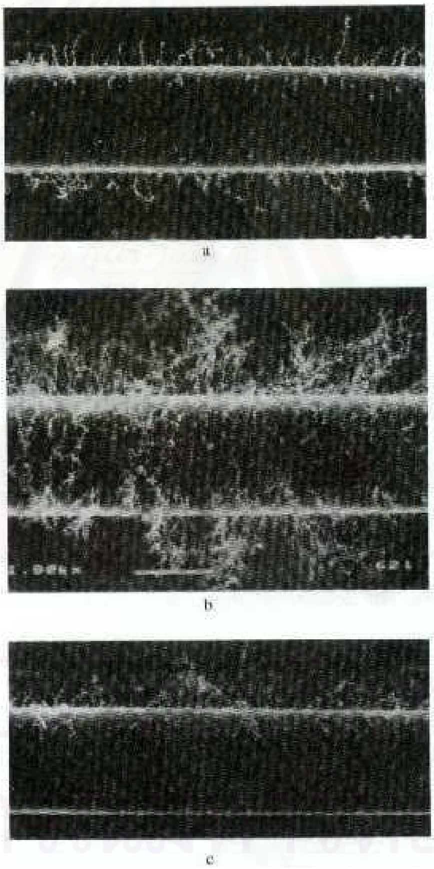

**Figure 3.2** Particle agglomerates formed by electrostatic effect; $d_f$ = 30 μm, $d_p$ = 0.39 μm, v = 15 m/s, $\rho_p$ = 2.33 g/cm$^3$ , Stk =0.015, Pe=$5\times10^4$, R=0.013. (a) Uncharged particles $K_{In}$ = 0.004, V = $4.8\times10^{-4}$ ; (b) Uncharged particles $K_{In}$ =0.004, V= $1.5\times10^{-3}$; (c) Charged particles $K_c$= 0.016, V= $4.9\times10^{-4}$

## 3.2. Trajectory and deposition mechanism of aerosol on a single fiber

### 3.2.1. Kuwabara flow field

Kuwabara (1959) solved the Navier-Stokes equations for viscous flow. **Figure 3.3** shows the flow cells in a fibrous filter consisting of parallel fibers, spaced randomly and transverse to the flow. The mean flow is directed from left to right with a velocity equal to U. The vorticity would be negative on the upper side of a cylinder and positive on the lower side of a cylinder. An ideal cell for the mathematical model is shown in **Figure 3.4.** Kuwabara considered that each cylinder of radius $R_f$ is enclosed by an imaginary cylindrical cell of radius $R_c$. If there are *n* parallel fibers per unit volume of filter, the volume fraction or packing density $\alpha$ is

$$\alpha = n\,\pi\,R_f^2 \tag{3.1}$$

and $R_c$ is adjusted so that

$$n\,\pi\,R_c^2 = 1 \tag{3.2}$$

Thus

$$R_c = \frac{R_f}{\sqrt{\alpha}} \tag{3.3}$$

The boundary conditions used by Kuwabara were that air velocity is zero on the surface of the fiber. The stream function, $\psi$, and the velocity component, $U_x$, $U_y$ and $U_z$, obtained by Kuwabara and expressed in dimensionless form are

$$\psi = \frac{Y}{2K}\left[(1-\frac{\alpha}{2})\frac{1}{X^2+Y^2} - (1-\alpha) + \ln(X^2+Y^2) - \frac{\alpha}{2}(X^2+Y^2)\right] \tag{3.4}$$

$$U_x = \frac{\partial\psi}{\partial Y},\ U_y = \frac{\partial\psi}{\partial X},\ U_z = 0 \tag{3.5}$$

where $K = -\frac{1}{2}\ln\alpha + \alpha - \frac{\alpha^2}{4} - \frac{3}{4}$ and $X = \frac{x}{R_f},\ Y = \frac{y}{R_f},\ Z = \frac{z}{R_f}$

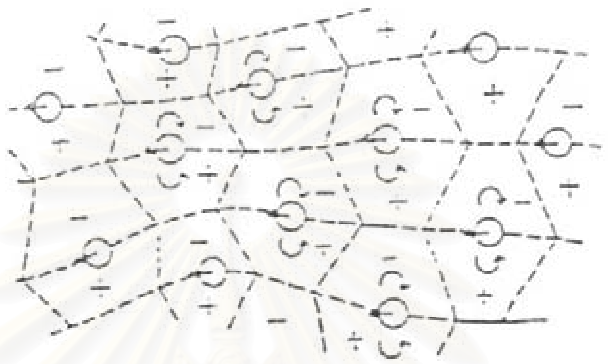

**Figure 3.3a** Vorticity around cylinders (the broken lines represent zero vorticity)

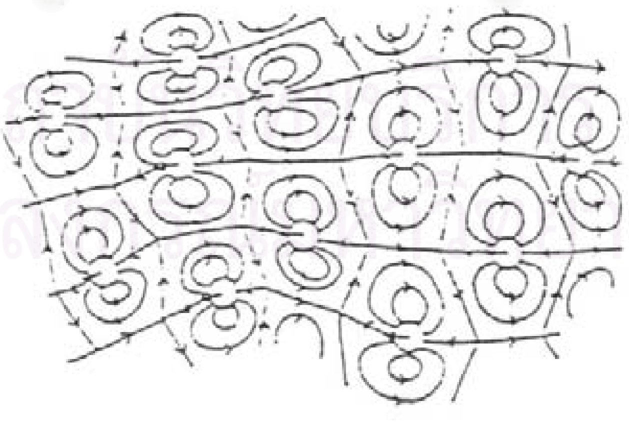

**Figure 3.3b** Mean flow velocity around cylinders

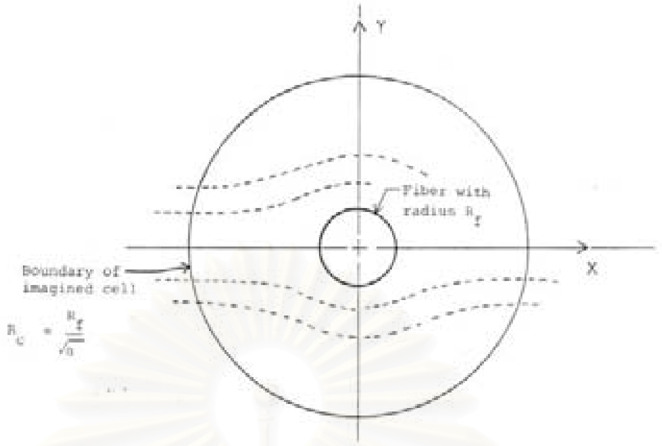

**Figure 3.4** Cross section of Kuwabara’s cell

The filtration by a fibrous air filter depends on several mechanisms. The important mechanisms causing particle deposition are interception, diffusion, inertial impaction, gravitational settling and electrostatic attraction. The single fiber efficiency $\eta$ can be estimated as the sum of the individual efficiencies caused by diffusion, $\eta_D$, interception, $\eta_R$, inertial impaction, $\eta_I$, gravitational settling, $\eta_G$ and electrostatic attraction, $\eta_E$, mechanisms. Based on numerous experimental observations, the general features of the deposition patterns may be summarized as shown in **Figure 3.5**

These five deposition mechanisms form the basis set of mechanisms for all types of aerosol particle deposition, including deposition in a lung, in a sampling tube, or in an air cleaner. The method of analysis and prediction may be different for each situation, but the deposition mechanisms are the same. The first four mechanisms are called mechanical collection mechanisms. Each of the five deposition mechanisms is described below, along with equations that predict the single fiber efficiency due to that mechanism. The theoretical analysis is complex, and only simplified equations are presented. Still, these equations are accurate enough to show the trend of collection efficiency with filter parameters. Wherever possible, the equations are based on experimentally verified theory and except where noted, are valid for standard conditions and $0.005 < \alpha < 0.2$, $0.001 < U_0 < 2$ m/s (0.1-200 cm/s) and $0.01 < d_f < 50$ μm.

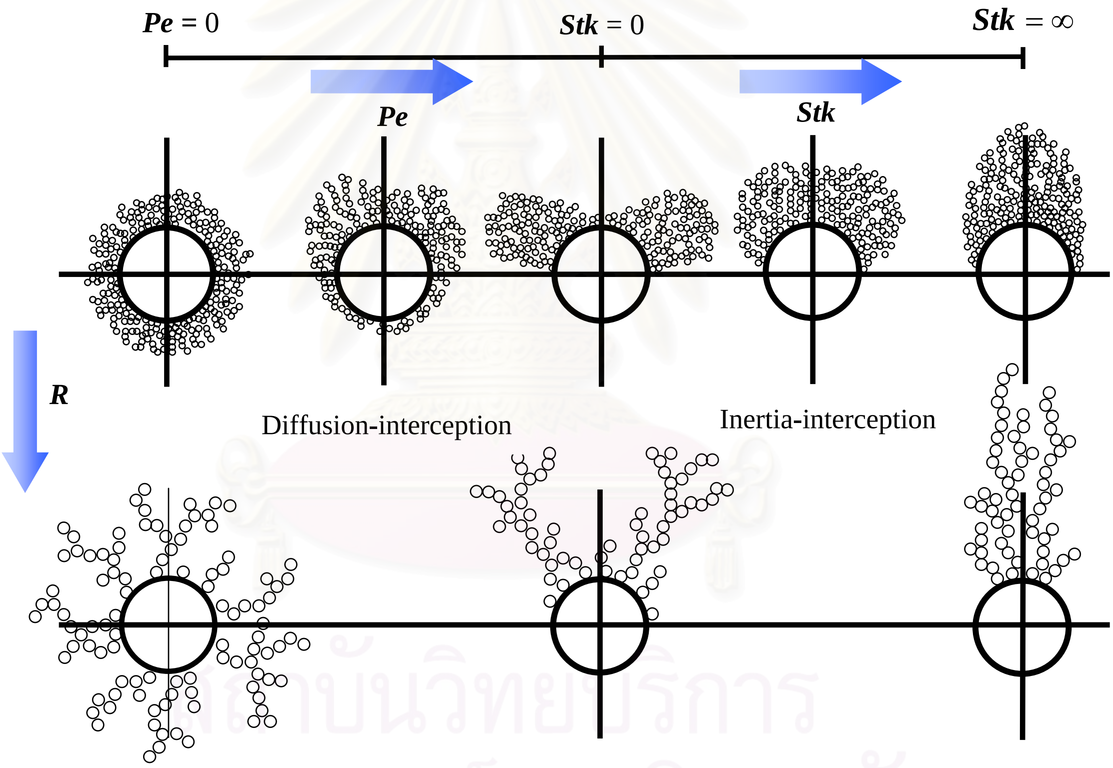

**Figure 3.5** Shape of particle accumulates by the change of collection mechanism.

### 3.2.2 Interception

Even if a particle does not deviate from its streamline, if the distance between the particle to a capturing surface is less than one particle radius, the particle may be collected on the surface by the interception mechanism. The particle would adhere to it due to Van der Waal's force. This mechanism is directly related to the relative size of the particle. The dimensionless parameter describing the interception effect is the interception parameter R defined as the ratio of the particle diameter to the fiber diameter.

$$R = \frac{d_p}{d_f} \tag{3.6}$$

where $d_p$ is the particle diameter and $d_f$ is the fiber diameter.

If the Kuwabara flow field is used, the single fiber efficiency caused by interception can be expressed by

$$\eta_R = \frac{1+R}{2K}[2\ln(1+R) - 1 + \alpha + (\frac{1}{1+R})^2(1-\frac{\alpha}{2}) - \frac{\alpha}{2}(1+R)^2] \tag{3.7}$$

### 3.2.3 Diffusion

When a particle is very small, in the submicrometer order, the main deposition mechanism is Brownian diffusion. Generally, the particle does not follow its streamline but continuously diffuse away from it. Thus the particle may be captured even on the rear surface. The diffusion effect of particles increase when the particle size and air velocity decrease. From the convective diffusion equation describing this process, a dimensionless parameter called the Peclet number, Pe, can be defined as

$$Pe = \frac{d_f U_\infty}{D_{BM}} \tag{3.8}$$

where $U_\infty$ is the average air velocity.

$D_{BM}$ is the diffusion coefficient of the particle.

The physical meaning of Peclet number is that Peclet number describes the relationship between diffusion and convection in a manner similar to the role played by the Reynolds number in fluid flow. When the Peclet number is small, molecular diffusion predominates. When it is large, convective transport predominates and diffusion can be neglected (Reist, 1993). Moreover, the single fiber efficiency, based on Kuwabara flow field, can be expressed by (Stechkina and Fuchs, 1966)

$$\eta_D = 2.9K^{-\frac{1}{3}}Pe^{-\frac{2}{3}} + 0.624Pe^{-1} \tag{3.9}$$

$$\eta_{DR} = 1.24K^{-\frac{1}{2}}Pe^{-\frac{1}{2}}R^{\frac{2}{3}} \tag{3.10}$$

### 3.2.4 Inertial impaction

Particles with a finite mass may not follow the streamlines exactly due to their inertia. If the streamlines are highly curved and the particle mass is high, the particle will deviate from the streamlines to collide with the capturing surface. Unlike the diffusion mechanism, the inertial impaction mechanism increases with an increase in particle size and/or air velocity. The effect of inertia on particle deposition can be described by the dimensionless number Stokes number, Stk, defined as

$$Stk = \frac{C_m d_p^2 \rho_p U_\infty}{9\mu d_f} \tag{3.11}$$

The single fiber efficiency is calculated by Stechkina et al. (1969), using the Kuwabara flow field. Their expression gave

$$\eta_I = \frac{1}{(2K)^2} I.Stk \tag{3.12}$$

where $I = [(29.6 - 28\alpha^{0.62})R^2 - 27.5R^{2.8}]$

### 3.2.5 Gravitational settling

When a particle is in a gravitational force field, they will settle with a finite velocity. If the settling velocity is large, the particle may deviate from the streamlines and deposit on the capturing surface. The gravitational settling mechanism is important only for large particles and at low flow velocity. The dimensionless parameter governing the gravitational settling mechanism is

$$\mathrm{Gr} = \frac{U_\infty}{V_g} \tag{3.13}$$

where $V_g$ is the terminal settling velocity of the particle.

The single fiber efficiency due to gravity,$\eta_G$, can be approximated (Davies 1973) as

$$\eta_G = \frac{\mathrm{Gr}}{1 + \mathrm{Gr}} \tag{3.14}$$

### 3.2.6 Electrostatic deposition

Electrostatic deposition can be extremely important, but is difficult to quantify because it requires knowledge of the charge on the particles and on the fibers. Electrostatic collection is often neglected, unless the particles or fibers have been charged in some quantifiable way. Increasing the charge on either the particles or the fibers and reducing the velocity, increases the collection efficiency. The theory of particle collection by charged fibers, charged particles or both is reviewed by Brown (1993). Charged particles are attracted to oppositely charged fibers by coulombic attraction. A neutral particle can also be attracted to a charged fiber: The electric field created by the charged fiber induces a dipole, or charge separation, in the particles. In the non-uniform field around the fiber, the near side of the particle experiences an attractive force that is greater than the repulsive force on the far side; hence, a net force exists in the direction of the fiber, and the particle migrates in that direction. Finally, a charged particle can be attracted to a neutral fiber at close range by image forces. The charged particle induces an equal but opposite charge in the fiber surface and thus creates its own field for attraction. Image forces are weaker than coulombic forces.

A single fiber collection efficiency is expressed by a function of dimensionless induced force and coulombic force parameter ($K_{In}$, $K_C$), neglecting mechanical collection mechanisms. The single collection efficiency is obtained as (Lee et al., 2002):

for charged particles,

$$\eta_{In} = 1.48 K_{In}^{0.93} \qquad ; 10^{-4} < K_{In} < 10^{-2} \tag{3.15}$$

$$\eta_{In} = 0.51 h_k^{-0.35} K_{In}^{0.73} \qquad ; 10^{-2} < K_{In} < 1 \tag{3.16}$$

$$\eta_{In} = 0.54 h_k^{-0.60} K_{In}^{0.40} \qquad ; 1 < K_{In} < 100 \tag{3.17}$$

for uncharged particles,

$$\eta_C = 0.78 K_C \qquad ; 10^{-3} < K_{In} < 10^{-1} \tag{3.19}$$

$$\eta_C = 0.59 h_k^{-0.17} K_C^{0.83} \qquad ; 10^{-1} < K_{In} < 10 \tag{3.20}$$

where $h_k = -0.5 \ln\alpha + \alpha - 0.25\alpha^2 - 0.75$

## 3.3 Relationship between E of a filter and η of a single fiber

A fibrous filter consists of a mass of fibers which are placed perpendicular to the direction of flow and oriented randomly. The single fiber may be used to explain the performance of a fibrous filter. When an air filter is composed of uniformly packed fibers with the same diameter, its efficiency is estimated by equation (3.21) , but cannot be used under dust-loaded condition. Let the total length of every fiber in unit thickness of unit cross flow area be L. The packing density ($\alpha$) or volume fraction of the fibers is the ratio of the total volume of all the fibers to the volume of the filter.

$$E = 1 - \exp\left( \frac{-4}{\pi} \cdot \frac{\alpha}{1-\alpha} \cdot \frac{L}{d_f} \cdot \eta \right) \tag{3.21}$$

The definition of the dust collection efficiency of a single fibers, $\eta$, is the ratio of the distance between two the limiting streamline of the flow approaching the fiber to the fiber radius (cf. **Figure 3.6**).

$$\eta = \frac{Y}{R_f} \tag{3.22}$$

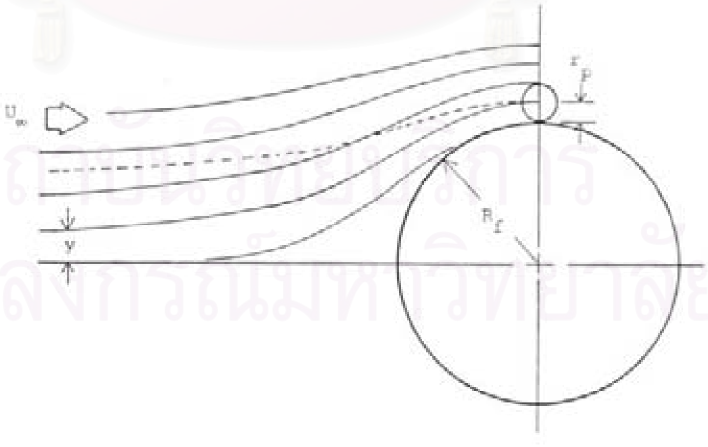

**Figure 3.6** Streamlines near a cylindrical fiber lying transverse to flow, and the definition of single fiber efficiency

Under dust-loaded condition, the local aerosol concentration C and dust load m in the filter can be obtained by integrating equations (3.23)-(3.24) together with equation (4.2) and the applicable initial and boundary conditions.

$$\frac{\partial C}{\partial x} = -\frac{4}{\pi} \cdot \frac{\alpha}{1-\alpha} \frac{\eta}{d_f} C \tag{3.23}$$

$$\frac{\partial C}{\partial x} = -\frac{1}{v} \cdot \frac{\partial m}{\partial t} \tag{3.24}$$

Initial condition $t = 0 : m=0$ for $0 < x < L$

Boundary condition $x = 0 : C = C_i$ for $t > 0$

The filter collection efficiency is calculated from $C_e$ at $x = L$ as follows.

$$E_m = 1 - \frac{C_e}{C_i} \tag{3.25}$$

$$E_m = 1 - \frac{C_e}{C_i} = 1 - \frac{\exp(-\lambda B C_i v t)}{\exp(-\lambda B C_i v t) + \exp(BL) - 1} \tag{3.26}$$

Dust load

$$m = -\frac{1}{\lambda} \cdot \frac{\exp(-\lambda B C_i v t) - 1}{\exp(-\lambda B C_i v t) + \exp(Bx) - 1} \tag{3.27}$$

where $B = \frac{4}{\pi} \cdot \frac{\alpha}{1-\alpha} \frac{\eta_{\alpha 0}}{d_f}$

### 3.4 The stochastic dendritic growth model for a single fiber

Stochastic or random processes abound in nature such as the path of a particle in Brownian diffusional motion, the growth of population of bacteria, and the mixing of pigment in plastics. If investigators would like to study these phenomena, they can easily make use of the theory of stochastic process.

This study applies the previous stochastic model (Maneeintr, 2001) which was used to simulate the induced-force and coulombic-force deposition of the aerosol particles via Monte Carlo method.

To calculate the collection performance of a single fiber, the motion of the air flow around the fiber can be described by Kuwabara stream function, which was expressed by equation (3.4). **Figure 4.3** is a schematic diagram of a representative fiber surrounded by Kuwabara's cell. Due to its stochastic nature, a set of uniform random numbers is used to represent the random location of each oncoming particle at the generation plane of Kuwabara's cell. Furthermore, the standard normal random vector, $n_{i-1}$, in Equation (3.29) and (3.30) plays the role of a directional vector of Brownian motion of each particle in the direction of x, y and z. Assuming no interparticle interaction, the motion of each particle is governed by the Langevin's equation plus the effect of electrical forces on the particle, as follows:

$$\frac{dv}{dt} = -\beta(v - u) + A(t) + \frac{FB}{\Delta t} \qquad (3.28)$$

where v is the velocity of the particle

u is the velocity of fluid stream

A(t) is a fluctuation force

F is the external force

B is the mobility of the particle

### 3.4.1 Deposition via convective Brownian diffusion

In the case of convective diffusional deposition, the position vector p of a particle at time $t_i = t_{i-1} + \Delta t$ can be approximated by equation (3.29) and (3.30), respectively, which were derived by Kanaoka et al. (1983)

$$p_i = p_{i-1} + u_{i-1}\Delta t + \sigma n_{i-1} + FB\,\Delta t \qquad (3.29)$$

where $\sigma = \sqrt{2 D_{bm} \Delta t}$

$\sigma$ is the standard deviation

$n = (n_x, n_y, n_z)$ is a standard normal random vector with zero mean and unit variance

Transform these variables to dimensionless form then equation (3.29) become

$$P_i = P_{i-1} + U_{i-1}\Delta\tau + 2\sqrt{\frac{\Delta\tau}{P_e}}\, n_{i-1} + F'B'\Delta\tau \qquad (3.30)$$

Here, the fluid velocity U of viscous flow across a random array of parallel fibers having packing density $\alpha$ is given by equation (3.5), and Pe is Peclet number. On the right of the equation, the second term represents the convective movement of the particle, the third term represents the diffusion movement of particle and the last term represents the electrical force.

F’B’ in electrical dimensionless term is meant for either an uncharged or charge particle and is defined as

for uncharged particle: $F'B' = K_{In}F_g$ (3.31a)

for charged particle: $F'B' = K_C F_c$ (3.31b)

In addition, the equations to find these electrical parameters are shown below.

Dimensionless electrical parameters

$$K_C = \frac{C_m n_p e \overline{\sigma}}{6 \varepsilon_0 (1 + \varepsilon_f) \mu d_p u} \tag{3.32a}$$

$$K_{In} = \frac{C_m \pi^2 \overline{\sigma}^2 d_p^2 (\varepsilon_p - 1)}{6 \varepsilon_0 (\varepsilon_p + 2)(1 + \varepsilon_f)^2 \mu d_f u} \tag{3.32b}$$

In the case of the non-electret fiber, the electrical term is omitted and equation (3.30) becomes

$$P_i = P_{i-1} + U_{i-1} \Delta\tau + 2\sqrt{\frac{\Delta\tau}{P_e}}\, n_{i-1} \tag{3.33}$$

3.4.2 Deposition via inertial impaction

In the case of the inertial impactional deposition, the position of a particle at time $t_i = t_{i-1} + \Delta t$ can be approximated by the following equations

$$St \frac{d^2X}{dt^2} + \frac{dX}{dt} - U_x = BF_x \tag{3.34}$$

$$St \frac{d^2Y}{dt^2} + \frac{dY}{dt} - U_y = BF_y \tag{3.35}$$

For the case of non-electret fiber, these equations are reduced to equations (3.36) and (3.37)

$$St \frac{d^2X}{dt^2} + \frac{dX}{dt} - U_x = 0 \tag{3.36}$$

$$St \frac{d^2Y}{dt^2} + \frac{dY}{dt} - U_y = 0 \tag{3.37}$$

In short, Equations (3.30), (3.34) and (3.35) can be used to simulate the movement of a particle in Kuwabara’s cell for the electret fiber. To complete the stochastic simulation of the dendritic growth on the electret fiber, the following assumptions have been made.

1) Existence of dendrites on the fiber has little effect on the flow field around the fiber.

2) Spatial and time distribution of the oncoming particles are random microscopically.

3) The next particle will not enter the Kuwabara’s cell until the present one in it either deposits or passes through the cell.

4) A particle is always retained once it is captured on a dendrite or fiber surface.

5) There is no re-entrainment or detachment of captured particles or dendrites from the fiber.

6) The particle size is monodisperse.

7) Both positive and negative charges on the fiber surface are permanent.

8) The charge on each particle is equal to –1.

# CHAPTER IV

# SIMULATION PROCEDURE

Simulation is a powerful technique for solving a wide variety of problems and imitates the behavior of a system or phenomena under study. The basic idea behind simulation is simple, namely, to model the given system by means of mathematical equations, and then determine its time-dependent behavior. The simplicity of the approach, when combined with the computational power of a high speed personal computer, makes simulation a powerful and efficient apparatus. Fundamentally, simulation is used when either an exact analytical expression for the behavior of the system under investigation is not available, or the analytical solution takes too much time or cost.

In modeling natural phenomena, two different approaches are available: deterministic and stochastic. Deterministic models are those in which each variable and parameter can be assigned a definite number, or a series of definite numbers, for any given set of conditions. In contrast, for stochastic or random models, uncertainty is introduced. The variables or parameters used to describe the structure of the elements (and the constraints) may not be precisely known. The former approach is less demanding computationally than the latter and could frequently be solved analytically.

To represent random variables, a source of randomness is required. A random number generator and its appropriate use play significant roles of any simulation experiments involving a stochastic system. Methods of generating random numbers are obtained by Tanthapanichakoon (1978). This chapter presents the simulation procedure of the deterministic and stochastic model to simulate correlation for the efficiency enhancement factor of a single electret fiber, and flow chart of simulation procedure.

## 4.1 Calculation procedure to determine correlation for the efficiency enhancement factor of a single electret fiber

It is postulated that the collection efficiency of an electret fiber under dust loading can be approximated as the sum of two mechanisms: the electrical and the mechanical collection efficiency. Kanaoka et al. (1983) approximated the mechanical collection efficiency of the dust-loaded fiber as a linear function of the accumulated mass of particles in a unit filter volume. They also looked at the effect of Peclet number and interception parameter on the collection efficiency enhancement factor. Tanthapanichakoon et al. (2003) simulated a three dimensional stochastic model and found that the collection efficiency of the electret fiber with dust load can be approximated as a linear function in the case of weak electrical effects.

In the present study, the correlation for the collection efficiency of the electret fiber ($\eta$) is found by summing a logarithmic function for the electrical collection efficiency ($\eta_E$) and the previously obtained linear function of mechanical collection efficiency ($\eta_M$).

$$\eta = \eta_E + \eta_M = \eta_{0E}[1+(\beta \ln m + \gamma)m] + \eta_{0M}[1+\lambda_M m] \tag{4.1}$$

or

$$\eta = \eta_{0E}[1+\lambda_E m] + \eta_{0M}[1+\lambda_M m] \tag{4.2}$$

where $\lambda_E = \beta \ln m + \gamma$

**Figure 4.1** illustrates the concept. The mechanical collection efficiency of the clean fiber ($\eta_{0M}$) was estimated as the sum of efficiencies attributed to the inertia, diffusion and interception mechanism (William C. H., 1998). The mechanical collection efficiency enhancement factor, $\lambda_{M,}$ can be estimated from an existing correlation (Kanaoka et al., 1983; Kanaoka, 1998). Here the electrical collection efficiency enhancement factor, $\lambda_E$, will be estimated from published experimental data (Walsh and Stenhouse, 1997).

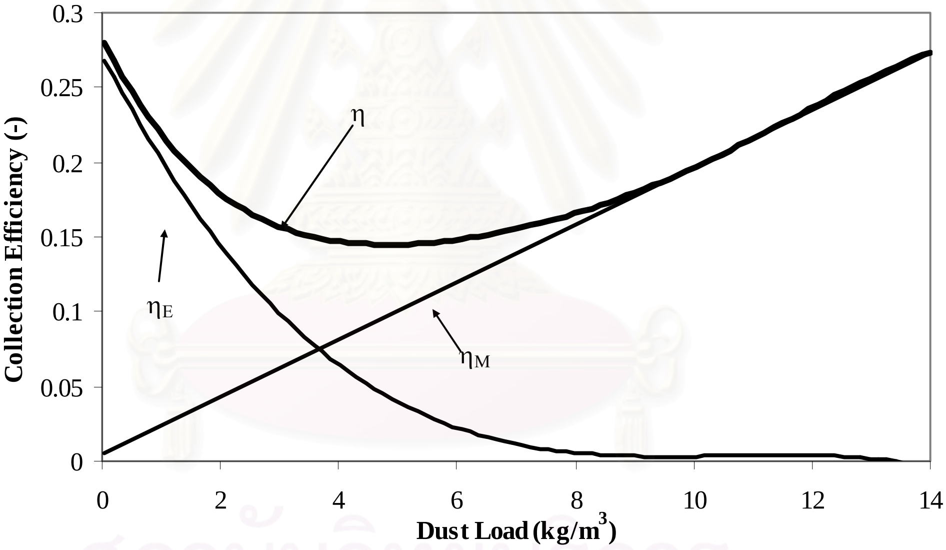

**Figure 4.1** Collection efficiency, electrical collection efficiency and mechanical collection efficiency of 1.03 micron stearic acid charged particles at face velocity 0.1 m/s

Under dust-loaded condition, the local aerosol concentration C and dust load m in the filter can be obtained by numerically integrating equations (3.23) and (3.24) together with equation (4.2) and the applicable initial and boundary conditions. To estimate the collection efficiency of the electret filter under dust-loaded condition, the following assumptions are made:

(1) The local collection performance (between x and $x+\Delta x$) can be regarded as constant for a sufficiently short time interval (t and $t+\Delta t$).

(2) When the local dust load on a single fiber is the same, the local electrical enhancement factor is the same regardless of the fiber location in the filter and filtration time.

As shown in **Table 4.1**, the simulation conditions are a) Based on Walsh's experimental conditions and b) Based on Lee's experiments (2002). The simulation is carried out until the filter becomes clogged. The % penetration P is defined as $P = 100(1-E_m)$. The values of $\beta$ and $\gamma$ are estimated by a straight-forward iterative method to obtain the layer by layer collection efficiency. The iteration is repeated until a good fit with the experimental results is found. A simplified flow chart of the simulation procedure is shown in **Figure 4.2**.

**Table 4.1** Simulation conditions used (a) Based on Walsh's experiments on stearic acid particles (1997) (b) Based on Lee's experiments (2002)

| | (a) | (b) |
|---|---|---|
| Influent dust concentration ,$C_i$ [kg/m$^3$] | 0.2 | $1\times10^{-8}$ |
| Electret fiber diameter, $d_f$ [μm ] | 20 | 2.64 |
| Electret fiber charge [coulomb/m$^2$] | $5\times10^{-10}$ | $1.2\times10^{-4}$ |
| Packing density of filter,$\alpha$ [-] | 0.04 | 0.04 |
| Filter thickness, L [m] | 0.003 | 0.003 |
| Particle diameter, $d_p$ [μm] | 0.46, 0.61, 1.03, 1.26 | 0.3 |
| Face velocity of filtration [m/s] | 0.1 | 0.1 |
| Differential filter thickness, $\Delta x$ [m] | 0.00002 | 0.00002 |
| Time step, $\Delta t$ [s] | 0.03 | 0.03 |

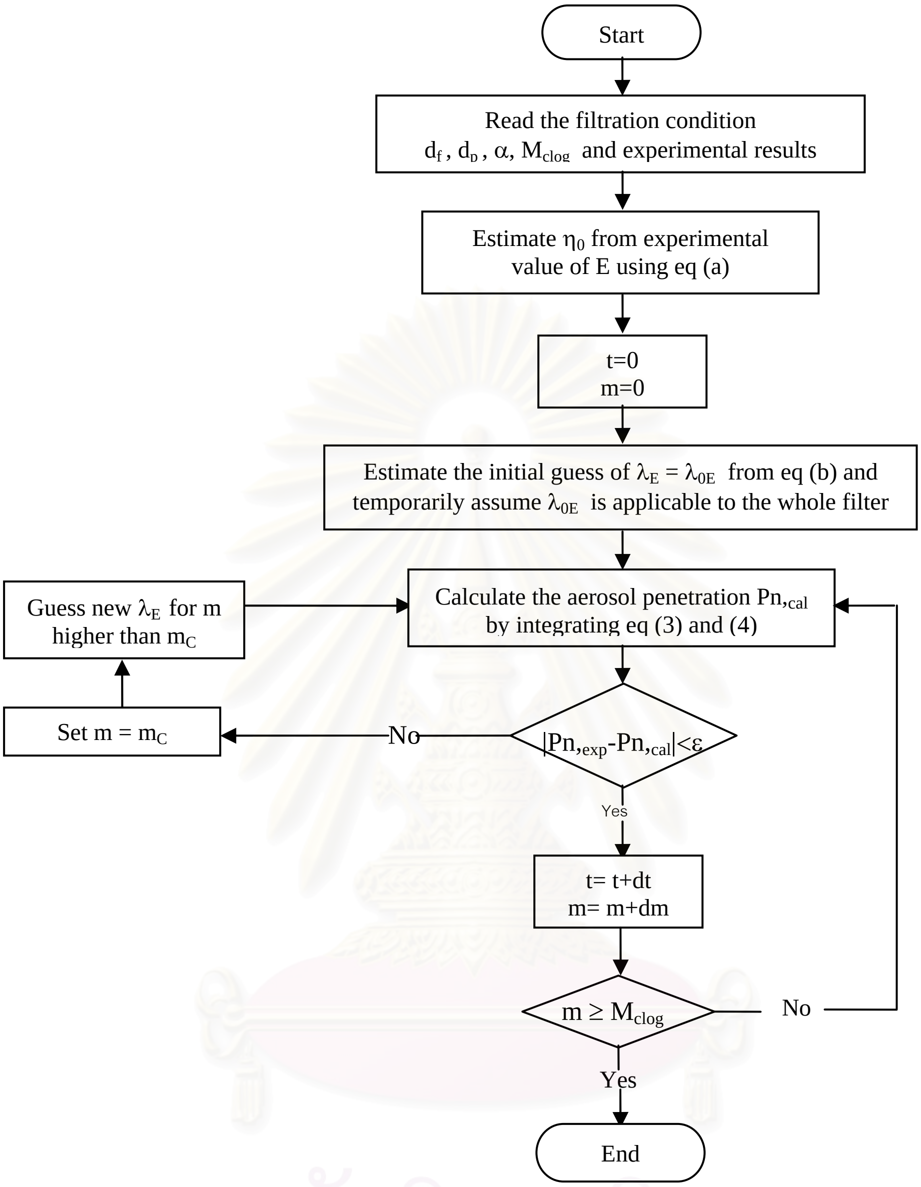
Start
Read the filtration condition
$d_f$ , $d_p$ , $\alpha$, $M_{clog}$ and experimental results
Estimate $\eta_0$ from experimental value of E using eq (a)
t=0
m=0
Estimate the initial guess of $\lambda_E = \lambda_{0E}$ from eq (b) and temporarily assume $\lambda_{0E}$ is applicable to the whole filter
Calculate the aerosol penetration $Pn_{,cal}$ by integrating eq (3) and (4)
Guess new $\lambda_E$ for m higher than $m_C$
Set m = $m_C$
No
$|Pn_{,exp}-Pn_{,cal}|<\varepsilon$
Yes
t= t+dt
m= m+dm
$m \geq M_{clog}$
No
Yes
End

**Figure 4.2** Simplified flow chart of the iteration procedure

### 4.2 Stochastic simulation procedure to predict the collection efficiency of a single electret fiber via Monte-Carlo Technique

The random position at the aerosol generation plane of Kuwabara's cell is represented by a uniform random number. Furthermore, the dimensionless radius of the Kuwabara’s cell ($R_c$) is related to the packing density $\alpha$ by

$$R_c = \frac{1}{\sqrt{\alpha}} \tag{4.3}$$

The total length of the fiber is subdivided into 5 sections with length $Z_1$, $Z_2$, $Z_3$, $Z_4$, $Z_5$, respectively (**Figure 4.3**). However, the effective length of the fiber was $Z_3$, which was expected to resemble those obtained from using a very long fiber. Here the length of the generation plane $Zgen=Z_1 + Z_2 + Z_3 + Z_4 + Z_5$ with $Z_1=Z_5$, and $Z_2=Z_4$.

For the case of electret fiber, there are so many kinds of forces acting on both particles and fiber. Coulombic forces $F_C$ (between the particle and fiber), $F_{CP}$ (between the particle and another nearby particle) and image force $F_I$ come into play only when a particle has electric charge. For both charged and uncharged dielectric particles, the long-range non-uniform electric field around the electret fiber and the agglomerates lead respectively to the long-range gradient force $F_G$ and particle-string formative or high-gradient force $F_R$. Under typical filtration conditions, Hiragi (1995) has calculated that $F_R$ becomes dominant when an oncoming particle comes in close proximity to a deposited particle and that, until this proximity region is reached, only either $F_C$ in the case of charged particles or $F_G$ in the case of uncharged particles need to be considered. His conclusions agree with Zebel (1963) and are adopted here.

The flow of fluid around the fiber is Kuwabara flow. For uncharged particles, the trajectory of an oncoming uncharged particle is essentially determined by the gradient force $F_G$ except in a region of close proximity to a deposited particle. Since $F_G$ depends only on the radial coordinate r and not on the polarization direction $\gamma$ . For charged particles, the coulombic force $F_C$ essentially determines the trajectory, except in the region of close proximity to some deposited particle. Since $F_C$ depends on the polarization direction $\gamma$ as well as the coordinates r and $\theta$, the resulting trajectory changes drastically with $\gamma$.

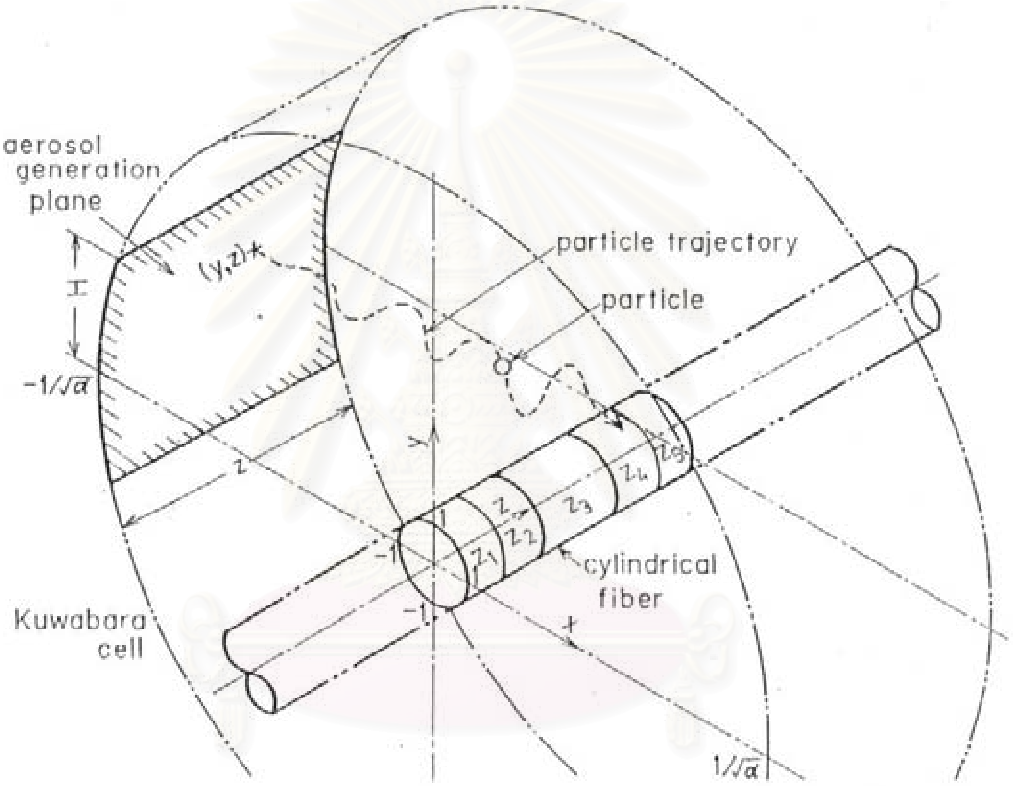
aerosol generation plane
H
$-1/\sqrt{\alpha}$
(y,z)
particle trajectory
particle
z
y
$z_5$
$z_4$
$z_3$
$z_2$
$z_1$
$z_1$
$z_2$
-1
-1
cylindrical fiber
Kuwabara cell
x
$1/\sqrt{\alpha}$

**Figure 4.3** Schematic diagram of Kuwabara's cell

The simulation is carried out according to the following procedure.

1. The starting point $P_0$ of an incoming particle was chosen randomly on the generation plane, which overlaps the cell surface and has height 2H and width Z. Two mutually independent uniform random number, $Y_0$ and $Z_0$, ($-H \leq y_0 \leq H$, $0 \leq z_0 \leq Z$),

were generated by using subroutine RANDOM (Tanthapanichakoon, 1978) to give $K_0 = (-\sqrt{R_c^2 - y_0^2}, y_0, z_0)$.

2. For convective Brownian diffusional deposition, the movement of the particle at each successive time interval, $\Delta t$, is simulated by using the equation (3.30), and the next position vector $P_i$ was calculated. The random component in equation (3.30) uses three mutually uncorrelated standard normal random numbers, $n_x$, $n_y$, and $n_z$, which are generated by using subroutine RND (Tanthapanichakoon, 1978). In contrast, in the case of inertial impaction deposition, the next position vector $P_i$ of the particle at each time step, was calculated by using the equation (3.34) and (3.35).

3. The new position vector $P_i$ at the end of the each time step is checked to see whether the particle has come in close proximity to the end of deposited particle or dendrite tip. If it does so, its movement is controlled by the high-gradient force $F_R$ which is prominent only at the tip of the particle string (dendrite). Thus only the electrostatic field around the dendrite tip needs to be considered. Once an oncoming particle enters this projected hemisphere of influence of the high-gradient field at the dendrite tip, it is assumed to deposit at the center of the hemisphere. And the location of captured particle is stored as you see in **Figure 4.4**.

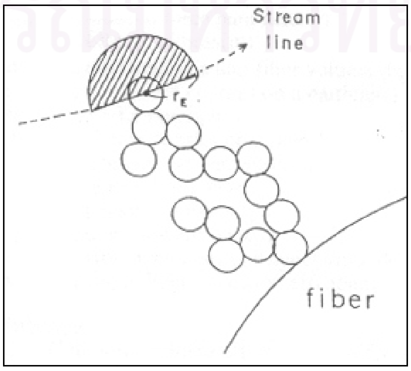

**Figure 4.4** Region of high gradient electrostatic field

4. However, if an oncoming particle is not in radius of hemisphere of influence, then the model of diffusion mechanism is used to check that particle has collided on the fiber surface or with any of the previously captured particles. If collision has occurred the coordinates of the location of capture is stored, and step 5 is executed next. If no collision has occurred, step 2, 3 and 4 are repeated until the particle either is captured or moves out of the boundary of Kuwabara's cell.

5. Steps 1, 2, 3 and 4 are repeated until one of the dendrites on the fiber surface grows up to a predetermined height of given-particle layer.

6. Steps 1, 2, 3, 4 and 5 are repeated for a number of samples to yield enough information for stochastic analysis.

A flow chart of the computational procedure is given in **Figure 4.5**. Monte Carlo simulations are carried out under various filtration conditions. Time step $\Delta t$ and fiber length Z are the two most important parameters which control the accuracy and computational time of the simulation. A short time step and a longer fiber length would enhance accuracy but consume very large computer memory and much computational time. Their suitable values in previous study (Kanaoka et al., 2001 and Hiragi, 1995) are adopted in this study. A compromise of 50 samples is selected in this study.

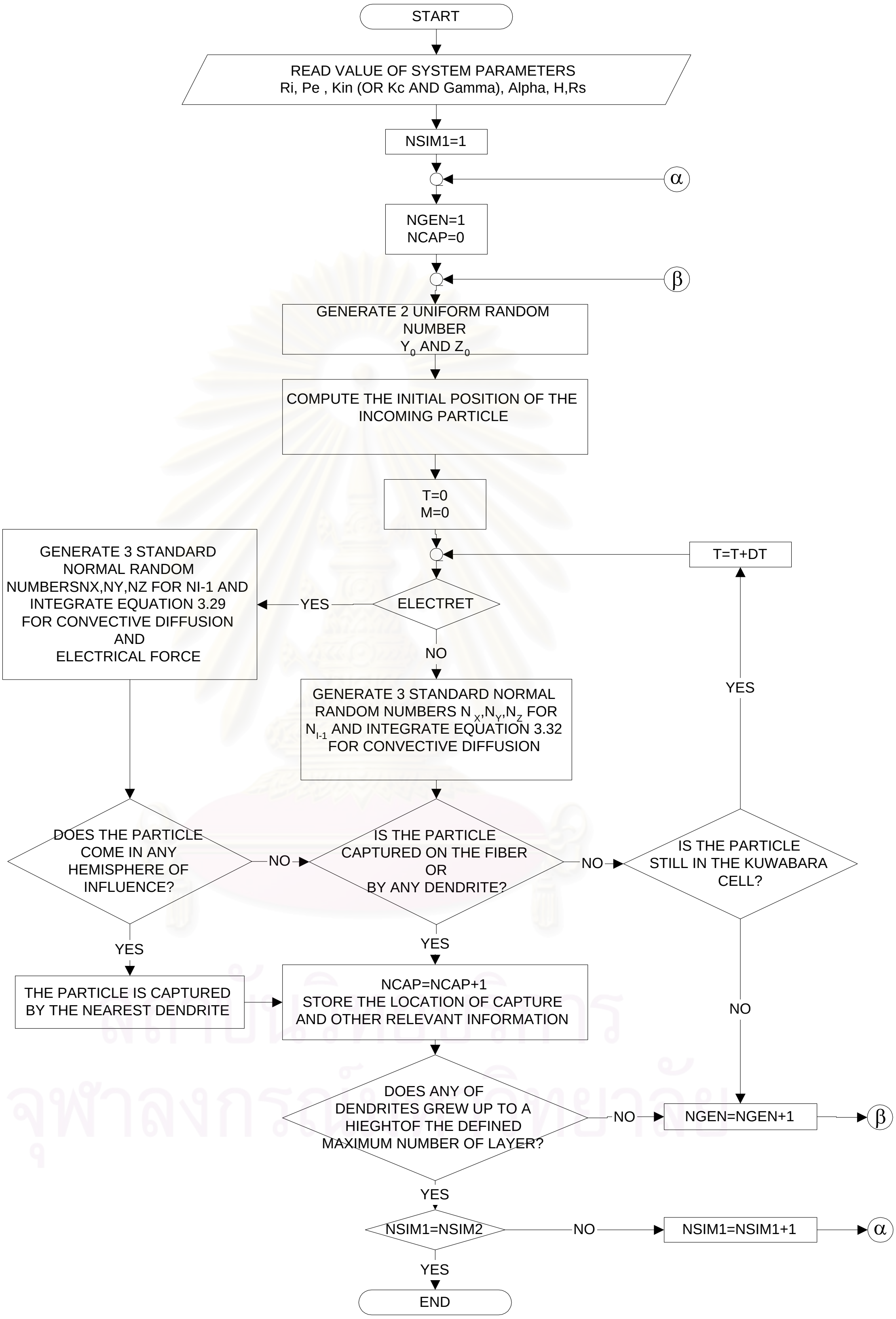
START
READ VALUE OF SYSTEM PARAMETERS
Ri, Pe , Kin (OR Kc AND Gamma), Alpha, H,Rs
NSIM1=1
α
NGEN=1
NCAP=0
β
GENERATE 2 UNIFORM RANDOM NUMBER
Y0 AND Z0
COMPUTE THE INITIAL POSITION OF THE INCOMING PARTICLE
T=0
M=0
T=T+DT
ELECTRET
YES
GENERATE 3 STANDARD NORMAL RANDOM NUMBERSNX,NY,NZ FOR NI-1 AND INTEGRATE EQUATION 3.29 FOR CONVECTIVE DIFFUSION AND ELECTRICAL FORCE
NO
GENERATE 3 STANDARD NORMAL RANDOM NUMBERS NX,NY,NZ FOR NI-1 AND INTEGRATE EQUATION 3.32 FOR CONVECTIVE DIFFUSION
YES
DOES THE PARTICLE COME IN ANY HEMISPHERE OF INFLUENCE?
NO
IS THE PARTICLE CAPTURED ON THE FIBER OR BY ANY DENDRITE?
NO
IS THE PARTICLE STILL IN THE KUWABARA CELL?
YES
YES
THE PARTICLE IS CAPTURED BY THE NEAREST DENDRITE
NCAP=NCAP+1
STORE THE LOCATION OF CAPTURE AND OTHER RELEVANT INFORMATION
NO
DOES ANY OF DENDRITES GREW UP TO A HIEGHTOF THE DEFINED MAXIMUM NUMBER OF LAYER?
NO
NGEN=NGEN+1
β
YES
NSIM1=NSIM2
NO
NSIM1=NSIM1+1
α
YES
END

**Figure 4.5** Flow chart of the stochastic simulation procedure

### 4.3 Evaluation/Estimation of filter service life

As fine particles deposit on the fibers, the single-fiber and overall filter collection efficiencies increase while the filters gradually become clogged. Since the expensive electret filter can not practically be cleaned and re-used, it is crucial to devise some means to lengthen its service life without compromising its collection efficiency. Filter collection efficiency depends not only on filtration condition and particle properties, but also on the filter properties, such as fiber diameter, packing density, packing structure. In the case of ordinary air filters it has been shown that suitable improvement in the fiber packing structure can lead to a significant increase in their service life (Kanaoka, 1998).

The objective here is to show the some approach can lead to several fold increase in service life in the case of the electret fiber. The simulation conditions for improvement in the filter service life are listed in **Table 4.1(b)**. **Table 4.2** shows the equation of the filter packing density of four identical filters with the same average packing density, $\alpha = 0.04$, but different spatial distributions of packing density along the filter thickness. **Figure 4.6** shows the filter packing density distribution along thickness of 4 filters. Fibers are packed uniformly in filter A. For filters B, C and D, the packing density changes along the filter thickness, with a minimum packing density at the inlet side and a maximum packing density at the outlet side of filter. The simulation of the filter service life estimation can be applied from the simulation in **section 4.1** and the procedure of simulation is shown in **Figure 4.2**.

**Table 4.2** Packing density of the electret filter

| Filter | Packing density (α) |
|---|---|
| A | 0.04 |
| B | 0.02(x/L)+0.03 |
| C | 0.04(x/L)+0.02 |
| D | 0.06(x/L)+0.01 |

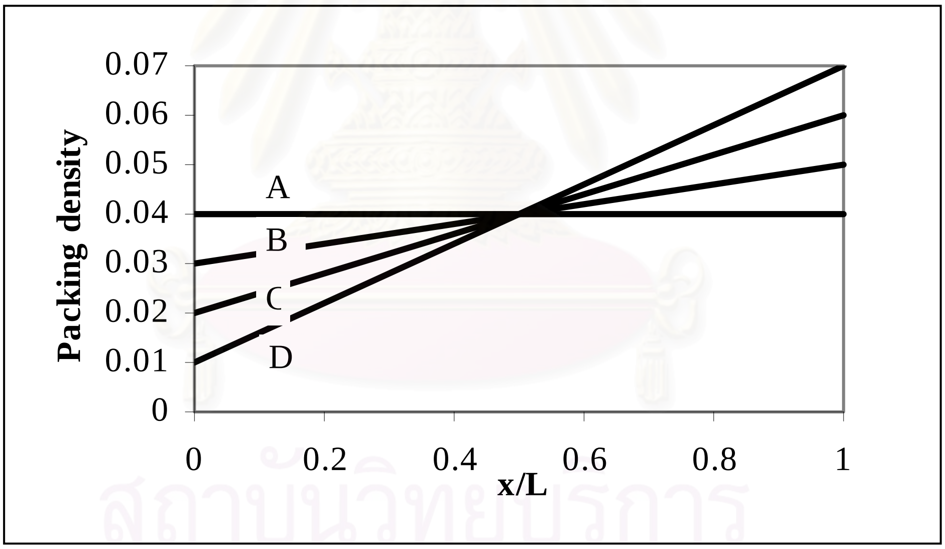

**Figure 4.6** The filter packing density distribution along thickness of 4 filters.

# CHAPTER V

# EXPERIMENTAL EVIDENCE

## 5.1 Experimental set-up of electret filter filtration

Experimental results were obtained by Walsh and Stenhouse (1997) for uncharged and charged particles under dust-loaded condition. In their work, they used stearic acid over a size range of 0.46 - 1.40 micrometers, as measured with an API Aerosizer (Aerosizer Mach 2, Amherest Process Instruments Inc., United States). Monodisperse particles were produced in the MAGE (Monodisperse Aerosol Generator, Lavoro E Ambiente, Bologna, Italy) by first atomizing a very dilute saline solution to produce very fine seed particles, and then passing this aerosol through heated stearic acid, where the gas became saturated with stearic acid vapour. As this mixture was allowed to cool under controlled conditions, the stearic acid condensed on the seed to form monodisperse spheres. Aerosol from MAGE was exposed to a radiation source (Krypton-85), which brings the particles' charge distribution to Boltzmann equilibrium. The smallest particles used (0.46 micron) had a mean charge at Boltzmann equilibrium of 1.6 unit charge. The aerosol was diluted by the addition of clean filtered air. The particle concentration of this diluted aerosol was measured using a light scattering photometer (LSP), before it challenged a filter sample. The particle concentration was measured again downstream of the filter using a second LSP. A diagram of the filtration test rig is shown in **Figure 5.1**. The filter properties are shown in **Table 5.1**.

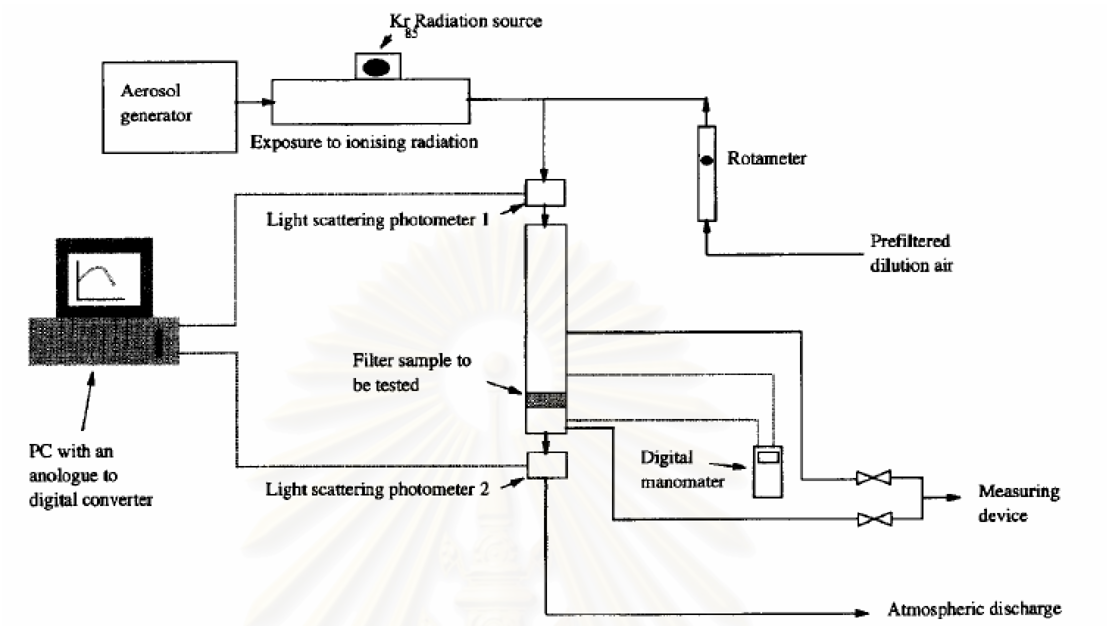
Kr 85 Radiation source
Aerosol generator
Exposure to ionising radiation
Rotameter
Light scattering photometer 1
Prefiltered dilution air
Filter sample to be tested
Digital manomater
Measuring device
PC with an anologue to digital converter
Light scattering photometer 2
Atmospheric discharge

**Figure 5.1** Sketch of the aerosol filtration test rig (Walsh and Stenhouse,1995)

**Table 5.1** Characteristics of electrically active material

| Parameter | Value |
|---|---|
| Fiber diameter | 20 μm |
| Packing density | 0.04 |
| Filter depth | 0.003 m |
| Filter fiber charge | 5×10$^{-10}$ c/m |
| Weight per unit area | 92 g/m$^2$ |

## 5.2 Penetration of aerosol particles under dust loading

**Figure 5.2** shows that the penetration of charged aerosol particles begins from a low initial value because the filter is initially clean and the electrostatic effect is still strong. The penetration initially increases with the dust load because of the gradually degradation of the electrostatic effect. Slowly but surely, the mechanical effect gradually picks up and becomes dominant as the deposited particles form chainlike agglomerates. At the maximum penetration point, the monotonically increasing mechanical collection efficiency equals the reduction in electrostatic collection efficiency. Subsequently the penetration monotonically decreases as the filter gradually clogs up. The significance of Walsh’s experimental results is that they covered the whole history of the changes on an electret fiber under different situations. However, the experimental data are somewhat scattered perhaps because of imperfectly controlled condition. Nevertheless, they clearly reveal the trend of the collection efficiency of an electret filter in the initial stage.

These data show that smaller particles cause a more rapid degradation in the electrical efficiency. The maximum penetration is also attained more quickly when filter samples are loaded with smaller particles, and falls to zero more quickly. Filter clog more quickly when loaded with smaller aerosol particles (Baumgarter and Loffer,1986; Walsh and Stenhouse, 1995). As dendrites grow more quickly when filter samples are loaded with smaller particles, they become clogged at lower mass deposits, and the mechanical contribution to the filtration efficiency becomes significant more than the initial stage; so penetration reaches a maximum more quickly. Moreover, a cake forms at the surface more quickly and thus the penetration falls to zero more quickly with smaller particles.

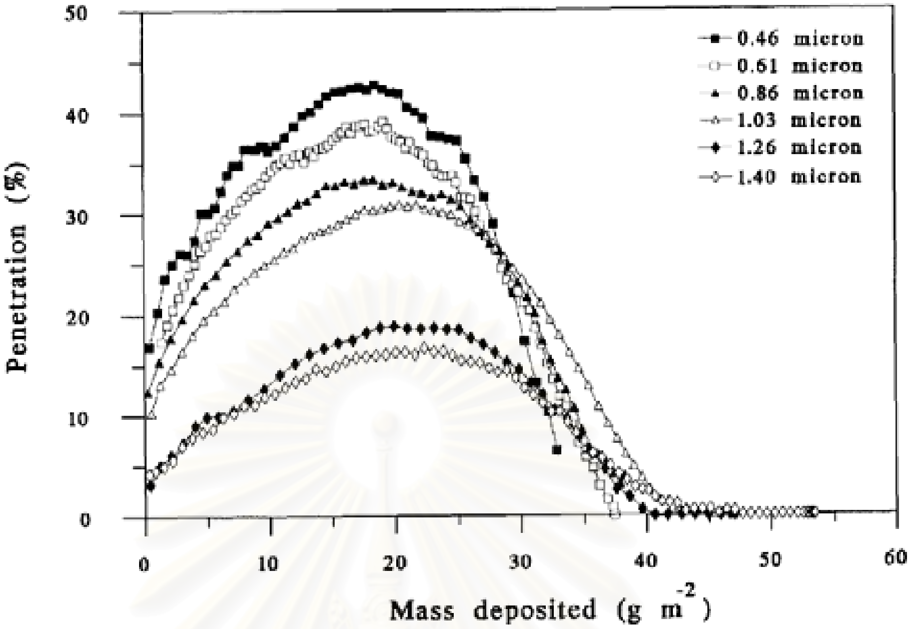

**Figure 5.2** Penetration through filter samples loaded with stearic acid particles of Boltzmann equilibrium charge distribution, over a size range 0.46 – 1.40 μm at face velocity 0.1 m/s

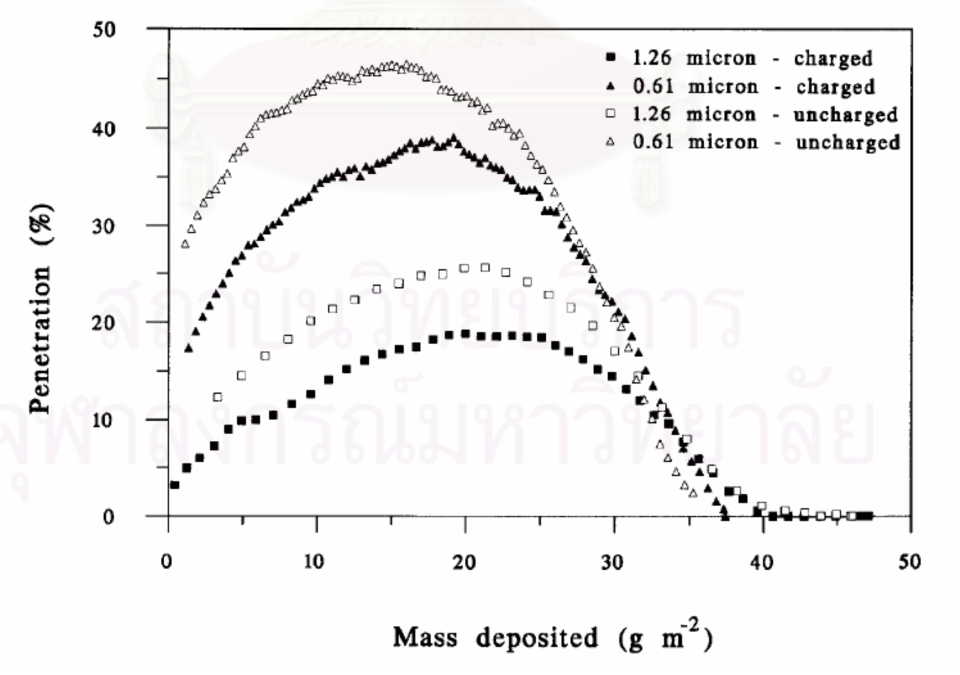

**Figure 5.3** Penetration through filter samples loaded with uncharged and charged stearic acid particles of 0.61 and 1.26 μm at face velocity 0.1 m/s

**In Figure 5.3** we see that the initial penetration of uncharged aerosol particles is higher than that of charged particles. The corresponding maximum penetration of the former happens earlier and its value is also higher. Then the penetration drops quickly below that of the charged particles. Concerning the cake structure, it will be affected simultaneously by electrostatic and mechanical forces. The cake consists of pearl chain structure protruding from the surface for both charged and uncharged particles but the spatial distribution of dendrites and the dendrite length are not the same. For uncharged particles, the dendrites are distributed randomly but uniformly on the whole fiber surface and grow almost perpendicular to the fiber surface. However, for charged particles, the dendrites also form pearl chain structure along the electric force lines but are scattered only in the region with opposite charge to the particles' polarity. When particles are collected beyond the effective reach of the electrostatic effect, they start to form random structured deposit (Kanaoka et al., 2001).

## 5.3 Pressure drop of electret filter under dust loading

In the early stages of filter loading the increase in pressure drop per unit aerosol particle deposit is initially very low, as aerosol particles are initially deposited on the surface of individual filter fibers deep within the filter bed. As loading continues, dendrites begin to form and the pressure drop accelerates. These dendrites ultimately join together and a filter cake is formed on the front edge of the filter. At the point of complete cake formation the pressure drop has reached its maximum rate of increase, and there-after the pressure drop is a linear function of aerosol particle deposited. The point at which it clogs is a strong function of aerosol particle size, as has been found with the conventional filter, with smaller aerosol particles being most clogging. The slope of the linear part of the pressure drop curve, after clogging is different for the various sizes of aerosol particles, the sharpest slope being for smallest aerosol particles as shown in **Figure 5.4**. For charged and uncharged aerosol particles, it is found that at the clogging point the pressure drop curve of uncharged particles are steeper than that of charged particles, so uncharged aerosol particles cause the filter to become clogged more quickly as shown in **Figure 5.5** (Walsh, 1995).

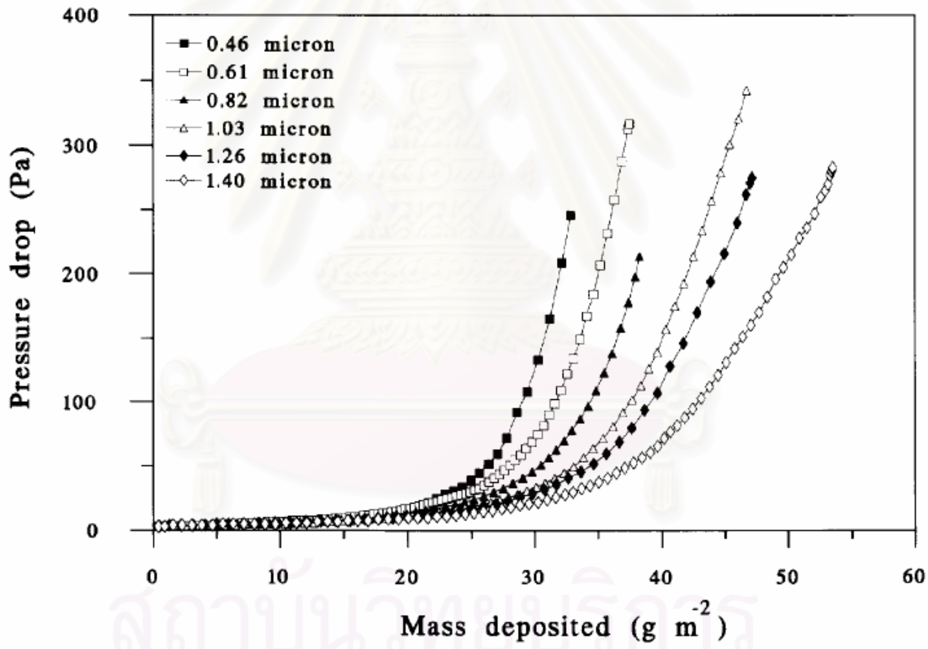

**Figure 5.4** Pressure drop across filter samples loaded with stearic acid particles of Boltzmann equilibrium charge distribution at a face velocity of 0.1 m/s

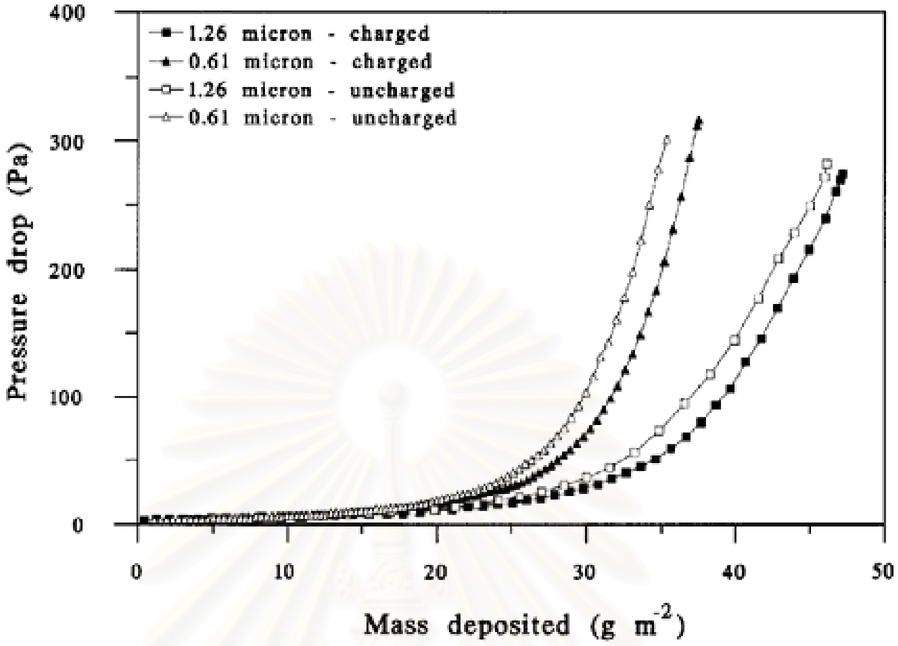

**Figure 5.5** Pressure drop across filter samples loaded with uncharged and charged particles of 1.26, 0.61 particle size at 0.1 m/s face velocity.

# CHAPTER VI

# RESULTS AND DISCUSSION

## 6.1 Correlation for the electrical collection efficiency enhancement factor

Based on the simulation procedure described in section 4.1, the obtained simulation results are shown and discussed in this section. The correlation for the collection efficiency of the electret fiber ($\eta$) is obtained by summing a logarithmic function of dust load for the electrical collection efficiency ($\eta_E$) and the conventional linear function of dust load for the mechanical collection efficiency ($\eta_M$). The adopted simulation conditions are listed in **Table 4.1** (a) which correspond to Walsh's experiments using stearic acid particles.

### 6.1.1 Comparison between experimental and simulated results

First of all, simulation results are compared with the experimental results previously reported by Walsh and Stenhouse (1997). **Figures 6.1(a) and 6.1(b)** compare the experimental and simulated results for the cases of charged and uncharged particles, respectively. Good agreement is observed for both charged and uncharged monodisperse particles of various sizes. In the proposed empirical correlations, only a single dominant type of electrical forces – coulombic force for the case of charged and induced force for uncharged particles – is considered. In reality, however, both induced and coulombic forces are present simultaneously. Walsh and Stenhouse (1997) did not actually neutralize the charges on their generated aerosol particles but assumed that the aerosol from the MAGE is uncharged because vapour condensing on a nucleus neither imparts nor removes electrostatic charge, and that the seed particles are so small that even at breakdown charge distribution its charge should be negligible; for example, 0.025 μm seed particles have only 0.3 unit charges at breakdown (see Brown, 1993). Both assumptions could be the reasons why our empirical correlations show a similar effect of the particle size on the electrical enhancement factor in **Table 6.1** for both charged and uncharged particles. As for the effect of particle charge, penetration of 0.46 micrometer uncharged particles appear slightly higher than the corresponding case of charged particles, but the difference is not significant. In the case of 0.61 micrometer charged and uncharged particles, the former shows less penetration than the latter as expected. There are two possible reasons for the unexpected penetration result in the case of 0.46 micron particles. First, as mentioned above, Walsh and Stenhouse (1997) did not actually neutralize the charges on their aerosol particles but assumed that the aerosol from the MAGE was uncharged. Second, there was significant scattering of experimental data because of imperfectly controlled condition.

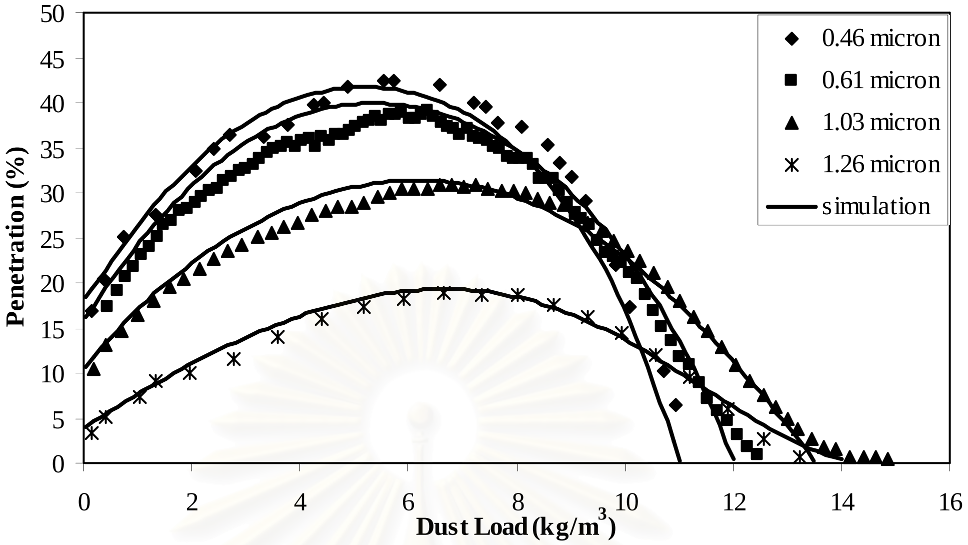

(a)

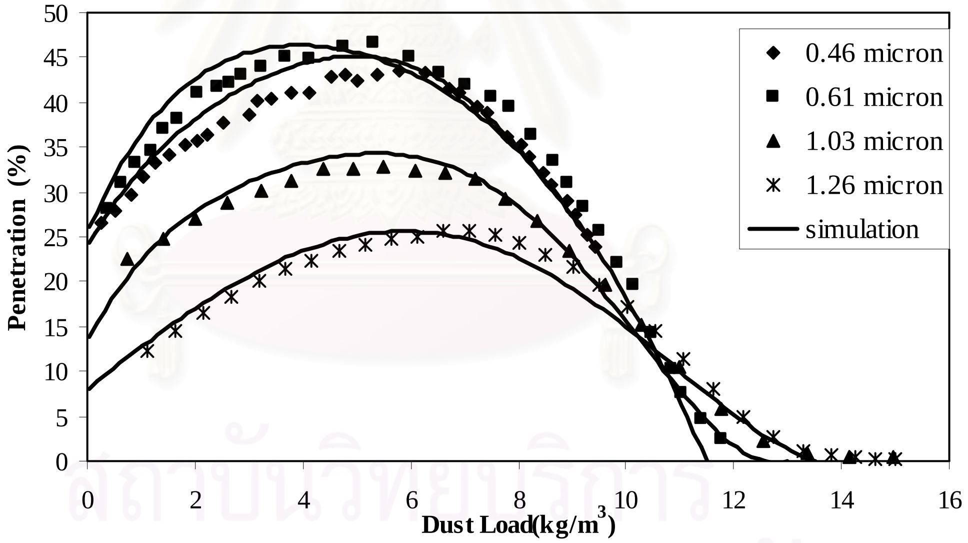

(b)

**Figure 6.1** Comparison between experimental and simulation results for stearic acid particles over size range 0.46 – 1.26 micrometer at face velocity 0.1 m/s : (a) charged particles (b) uncharged particles

### 6.1.2 Electrical enhancement factor, $\lambda_E = \beta \ln m + \gamma$

It is well known that the collection efficiency of an ordinary fiber always increases as dust particles are loaded on the fiber (Kanaoka et al., 1983). However, for an electret filter, the collection efficiency of aerosol particles reportedly decreases exponentially with the operation time in its early stage of collection until it loses electrical forces (Brown et al., 1988). Then the electrical collection efficiency becomes negligible but the overall efficiency increase with time because of the mechanical collection mechanism (Ji et al., 2003). The quantity of effective charge on the electret fiber and amount of particles deposited on the fiber surface as well as the particle size and shape do affect the aerosol collection efficiency (Brown et al., 1988; Walsh and Stenhouse, 1997).

As can be seen from **Table 6.1**, the electrical enhancement factor can be expressed as a logarithmic function of m: $\lambda_E = \beta \ln m + \gamma$. In the table, the values of both $\beta$ and $\gamma$ decrease as the size of aerosol particles increases. This may be attributed to the fact that the smaller the particle size, the closer they lie in contact with the fiber surface, thereby enhancing the charge-screening and neutralizing effect. In addition, the charged particles have smaller $\beta$ and $\gamma$ values than the uncharged particles. As expected, the differences in $\beta$ and $\gamma$ between charged and uncharged particles increase as the particle size increases. For 0.46 micrometer particles, the values of $\beta$ and $\gamma$ for charged and uncharged particles are nearly the same because, as mentioned above in relation to **Figure 6.1**, the aerosol particles were not actually neutralized but Walsh and Stenhouse (1997) assumed that the aerosol from the MAGE was uncharged and there was also significant scattering of the experimental data.

**Table 6.1** Electrical enhancement factor ($\lambda_E = \beta \ln m + \gamma$) of an electret fiber from clean state up to clogging point

| Particle size (micrometer) | Charged particles | Uncharged particles |
|---|---|---|
| 0.46 | 0.13 ln m – 0.40 | 0.133 ln m – 0.40 |
| 0.61 | 0.11 ln m – 0.35 | 0.12 ln m – 0.37 |
| 1.03 | 0.10 ln m – 0.33 | 0.11 ln m -0.355 |
| 1.26 | 0.086ln m – 0.30 | 0.098ln m – 0.335 |

As for the effect of the gas flow velocity, Walsh (1995) experimentally investigated the penetration at 0.1, 0.3 and 0.8 m/s filtration velocity for 1.03 micrometer particles. It is found that the higher the flow velocity, the smaller the electrical enhancement factor becomes. The empirical correlation for 1.03 μm particles reveals that $\beta$ = 0.10, 0.25, 0.26 and $\gamma$ = 0.33, 0.56, 0.47 for v = 0.1, 0.3 and 0.8 m/s, respectively. Generally, several collection mechanisms occur simultaneously in a complicated manner. They are: diffusion/Brownian motion, inertial impaction, interception, gravitational settling and electrostatic forces. The particle size of interest here ranges from 0.46 – 1.26 μm, the filter diameter is 20 μm and the face velocity of filtration of interest is 0.1 m/s. In this case, the Peclet number of the particles (Pe) ranges from 28,724 to 94,570; Stokes number (stk), from 0.0041- 0.0257; and the interception parameter, from 0.023 to 0.063. Therefore, the dominant mechanical collection mechanism is diffusional/Brownian motion, followed by interception. As evident from **Figure 4.1**, the electrostatic effect is dominant only in the initial stage up to a dust load of around 2 $kg/m^3$. Beyond the dust load of 6 $kg/m^3$, the mechanical collection mechanism takes over.

During the initial stage of particle deposition on the electret fiber, particles are either captured directly on the fiber surface as single particles and short dendrites (Kanaoka and Hiragi, 1990). During this period, the negative charge–screening effect of the particles, neutralization effect of the charges on the fiber by deposited particles lying in direct contact with the electret fiber and possible chemical interactions between the aerosol particles and fiber material might take place (Ji. et al., 2003). Nevertheless, during this initial period, the electrical enhancement factor $\lambda_E$ could briefly be approximated as a linear function of the dust load m [Brown et al., 1998]. As dust loading proceeds, the deposited particles form tall porous dendritic agglomerates with complicated shapes. The negative effects of additional particles on the fiber charge become less and less pronounced while the absolute effect of electrostaticity gradually dies out. Though Walsh's experimental results can be explained quite well by $\lambda_E = \beta \ln m + \gamma$ , this empirical correlation is restricted to the following conditions: $0.46\ \mu m < d_p < 1.26\ \mu m$ , $v = 0.1$ m/s, $d_f = 20 \mu m$, and electret fiber charge = $5\times 10^{-10}$ coulomb/$m^2$.

**Figure 6.2(a)** compares the calculated values of the electrical enhancement factor ($\lambda_E$) of charged particles over a size range of 0.46 – 1.26 micrometer at the face velocity of 0.1 m/s. We see that $\lambda_E$ remains negative throughout the filtration time of interest because of the degradation of electrical effect. In the early stage, $\lambda_E$ value of small particles is smaller than that of large particles. Above certain dust load, $\lambda_E$

increases more gradually and finally becomes nearly equal. Though not shown here, a similar trend is also observed in the case uncharged particles. As an example, **Figure 6.2(b)** compares the electrical enhancement factor ($\lambda_E$) of uncharged and charged particles. As pointed out in **Table 6.1**, $\lambda_E$ value of uncharged particles is slightly more negative than that of charged particles at low dust load. Then the difference in $\lambda_E$ gradually decreases as the electrical effect is degraded by dust load. Since the electrical collection of uncharged particles relies on induced forces which are generally smaller than the corresponding columbic forces of charged particles, the electrical enhancement factor and collection efficiency in the case of charged particles is higher than that of uncharged particles. Though not shown in **Figure 6.2(b)**, the estimated electrical enhancement factor of 0.46, 0.61 and 1.26 micrometer particles of charged particles are also found to be higher than the corresponding case of uncharged particles.

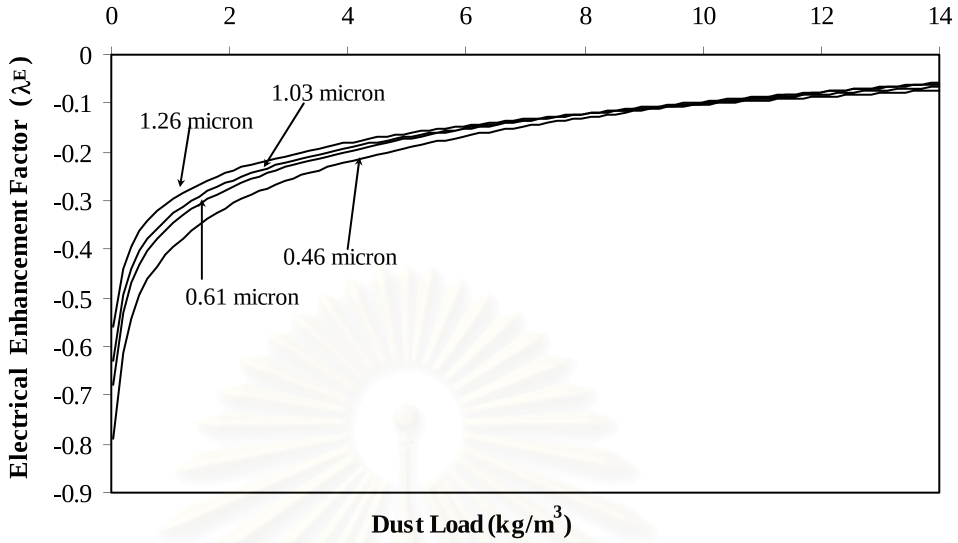

(a)

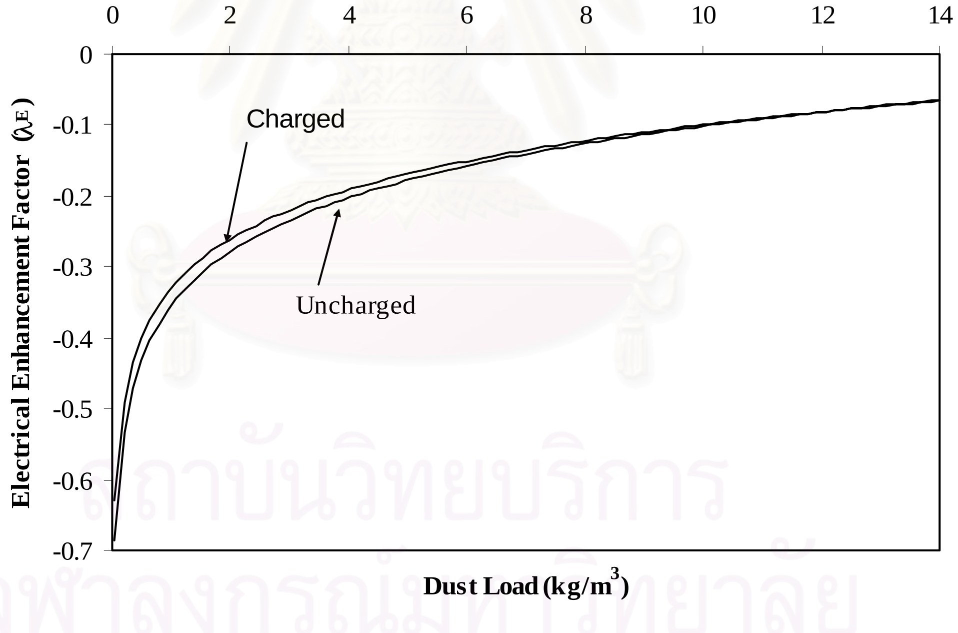

(b)

**Figure 6.2** Electrical collection efficiency enhancement factor ($\lambda_E$) of charged particles: (a) over size range 0.61- 1.26 micrometer at face velocity 0.1 m/s (b) uncharged and charged 1.03 micrometer stearic acid particles at face velocity 0.1 m/s

### 6.1.3 Normalized single-fiber collection efficiency

The normalized collection efficiency ($\eta/\eta_0$) is the ratio of the dust-loaded collection efficiency,$\eta$, to that of the clean-fiber, $\eta_0$. In the case of an ordinary fiber or a weak electret fiber, the normalized collection efficiency has been shown to increase monotonically as a linear function of dust load (Kanaoka et al, 1983; Tanthapanichakoon et al., 2003). This phenomena, however, does not hold in the case of a strong electret fiber.

As an example, **Figure 6.3** shows the normalized single-fiber efficiency of charged particles over a size range of 0.46-1.26 micrometers. Instead of increasing linearly, $\eta/\eta_0$ initially decreases from unity down to a minimum point as the number of deposited particles increases. Beyond the minimum, the monotonically increasing mechanical effect more than compensates the degradation of electrical forces and becomes dominant. The smaller particles show more rapid degradation in electrostatic efficiency. In addition, the clogging point of a filter is attained more easily when it is loaded with smaller particles, which is consistent with published experimental results (Baumgartner&Loffler, 1986; Walsh & Stenhouse, 1997).

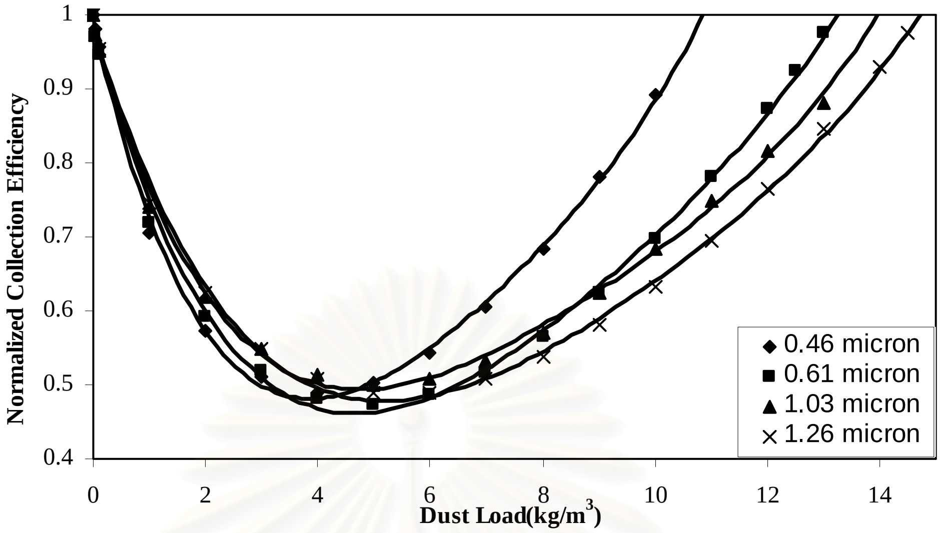

**Figure 6.3** Normalized collection efficiency of charged stearic acid particles, over a size range 0.46 – 1.26 micrometer at face velocity 0.1 m/s

## 6.2 Collection efficiency of an electret fiber via Monte-Carlo technique

Based on the simulation procedure described in **section 4.2**, the obtained simulation results are shown and discussed in this section. The adopted simulation conditions are listed in **Table 6.2**. Monte Carlo simulations are carried out under various filtration conditions. However, the packing density of the filter and the particle density are fixed at 0.04 and 1g/cm$^3$, respectively. As the electrostatic field strength is degraded while dust load increases, the collection efficiency of the electret filter might briefly fall as a function of dust load because of screening of the filter charges, neutralization of charges on the fibers, and possible chemical interaction between the aerosol particles and filter material (Ji et al. 2003). Therefore, the electrical force parameters must be assumed to degrade as a function of dust load.

In this study, the electrical force parameters are assumed to degrade as an exponential function of dust load as the follows.

For charge particle: $K_C = K_{C0}\, e^{(-\phi Ncap)}$ (6.1)

For uncharged particle: $K_{In} = K_{In0}\, e^{(-\phi Ncap)}$ (6.2)

where $K_{C0}$ = Initial coulombic force parameter of the electret fiber

$K_{In0}$ = Initial induce force parameter of the electret fiber

Ncap = Number of captured particles on the fiber

$\phi$ = electrical degradation factor ($\phi>0$)

In the present study, the normalized collection efficiency against dimensionless dust load will be shown discussed under various dust loading conditions.

The dimensionless dust load is defined by the following equation:

$$M\_ = M_{dep} / M_{(\eta/\eta 0 = 1)} \quad (6.3)$$

where M_ = dimensionless dust load

$M_{dep}$ = dust loaded at the filtration time t

$M_{(\eta/\eta 0=1)}$ = non-zero dust load at which $\eta/\eta_0$ reaches unity

**Table 6.2** Stochastic simulation conditions for aerosol agglomerative depostion on an electret fiber

| | | |
|---|---|---|
| Packing density of filter $\alpha$ (-) | | 0.04 |
| Dimensionless initial electrical parameter | | |
| Induced force $K_{In0}$ (-) | | 0.05 , 0.1 and 0.2 |
| Coulombic force $K_{C0}$ (-) | | 0.05 , 0.1 and 0.2 |
| Dimensionless length of fiber section | | |
| I | $Z_1$ (-) | 3 $d_p$ |
| II | $Z_2$ (-) | 5 $d_p$ |
| III | $Z_3$ (-) | 20 $d_p$ |
| IV | $Z_4$ (-) | 5 $d_p$ |
| V | $Z_5$ (-) | 3 $d_p$ |
| Dimensionless radius of fiber $R_f$ (-) | | 1 |
| Dimensionless half height of generation plane H (-) | | 2 |
| Dimensionless step size $\Delta t$ (-) | | 0.05 |
| Dimensionless number of simulation $N_{sim2}$ (-) | | 50 |
| Dimensionless radius of hemisphere of influence $R_e$ (-) | | 1.5 $d_p$ |

### 6.2.1 Validation of model

#### 6.2.1.1 Cases in which Brownian diffusion mechanism is assumed to be dominant

In this section, the morphology of deposited particles and normalized collection efficiency of a single electret fiber are discussed. **Figures 6.4** and **6.5** show typical examples of the morphology of the dendrites for the cases of charged and uncharged particles, respectively. The condition used in this section are $K_c$ = 0.20, $K_{In}$ = 0.20, $R_i$ = 0.0515, Pe = 75372, Gamma = 90 and $\phi$ = 0.01. Generally particle dendrites tend to grow perpendicular to the fiber surface and straight for both charged and uncharged particles, but for charged particles the agglomerates concentrate in a limited area of opposite polarity to the particles. **Figures 6.6** and **6.7** show the normalized collection efficiency against dimensionless dust load for charged and uncharged particles, respectively.

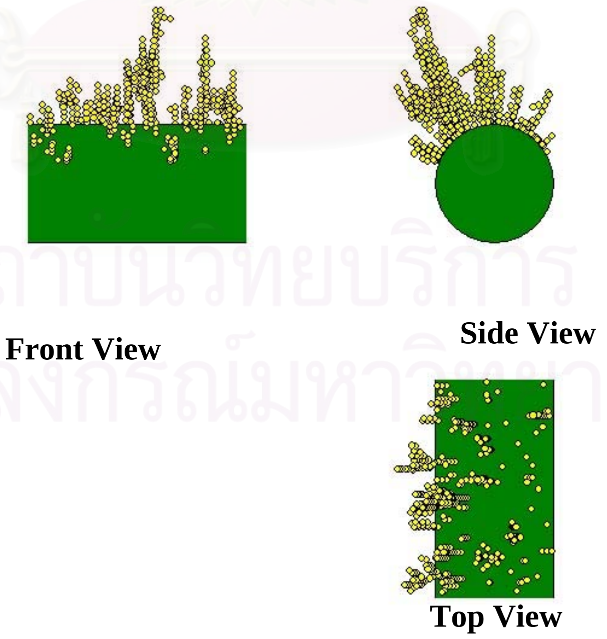

**Front View**

**Side View**

**Top View**

**Figure 6.4** Typical configuration of dendrites for the case of $K_c$ = 0.20, $R_i$ = 0.0515, Pe = 75372, Gamma = 90, $\phi$ = 0.01, layers = 40

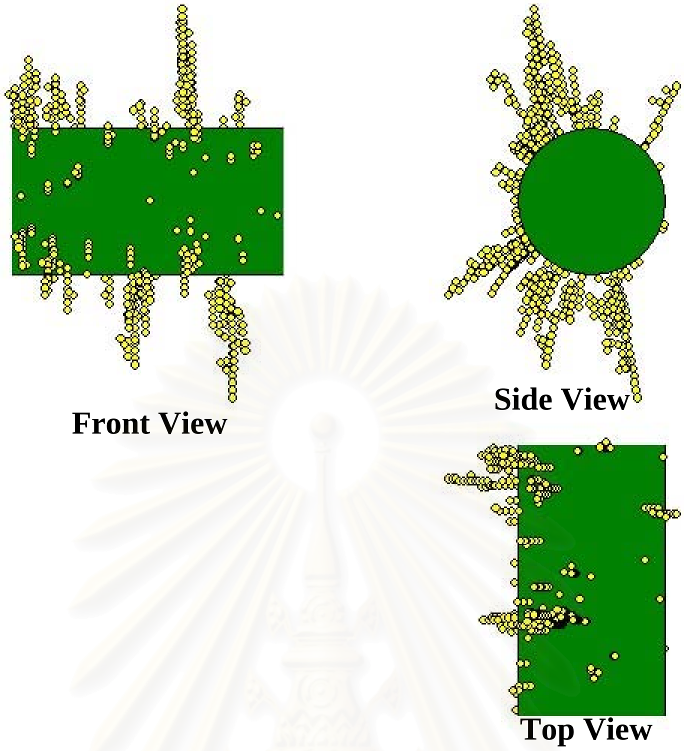
Front View
Side View
Top View

**Figure 6.5** Typical configuration of dendrites for the case of $K_{In} = 0.20$, Ri = 0.0515, Pe = 75372, $\phi = 0.01$, layer = 40

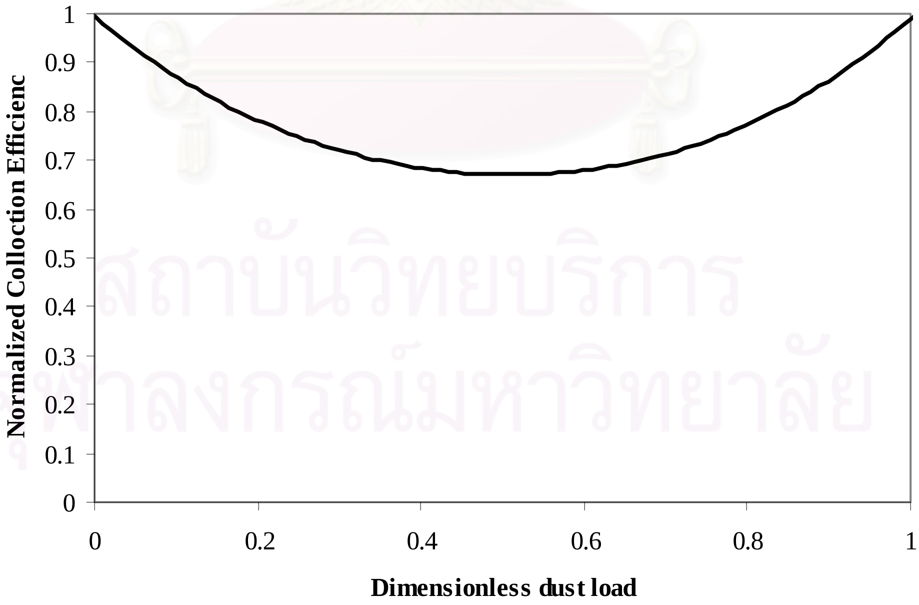

**Figure 6.6** Normalized collection efficiency for the case of $K_C = 0.2$ , Ri = 0.0515, Pe = 75372,$\phi$= 0.01

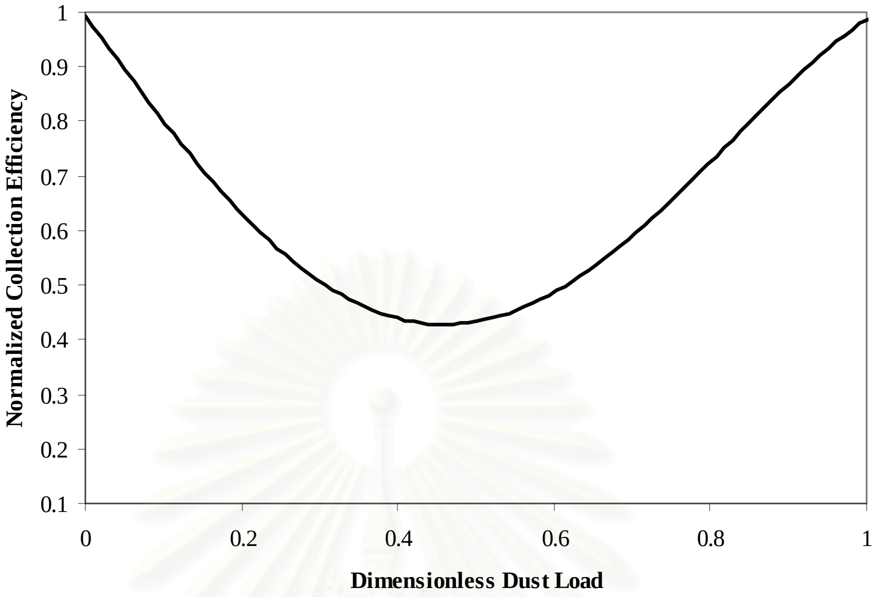

**Figure 6.7** Normalized collection efficiency for the case of $K_{In}$ = 0.2 ,Ri = 0.0515 Pe = 75372, $\phi$ = 0.01

6.2.1.2 Cases in which inertial impaction mechanism is assumed to be dominant

In this section, the simulation results for the case of inertial impaction mechanism dominant are shown and discussed. **Figures 6.8** and **Figure 6.9** show typical examples of the morphology of the dendrites for the cases of charged and uncharged particles, respectively. It can be seen that none of the dendrites in **Figure 6.8** are found in the lower half of the fiber because the Stk value is very small (small effect of inertial impaction). **Figure 6.9** shows deposition of particles collected all around the fiber surface again because of small inertial effect and induction mechanism (for uncharged particles). **Figures 6.10** and **6.11** show the predicted the normalized collection efficiency for charged and uncharged particles, respectively. It shows rapid degradation of the normalized collection efficiency with the increasing dimensionless dust load in both cases. Compared with the experimental results of Walsh and Stenhouse (1997)(see **Figure 6.3**), the normalized collection efficiencies in **Figures 6.10** and **6.11** degrade too fast and not realistic.

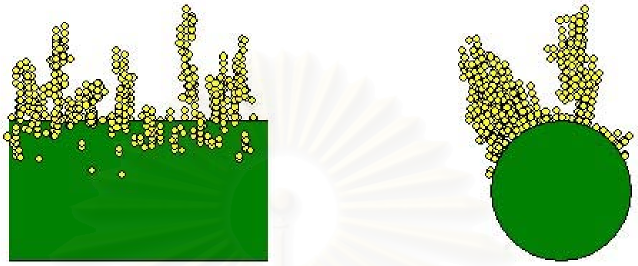

**Front View**

**Side View**

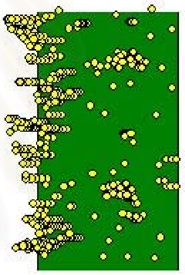

**Top View**

**Figure 6.8** Typical configuration of dendrites for the case of $K_c = 0.20$, $R_i = 0.0515$, Stk = 0.017,Gamma = 90, $\phi = 0.01$, layer = 40

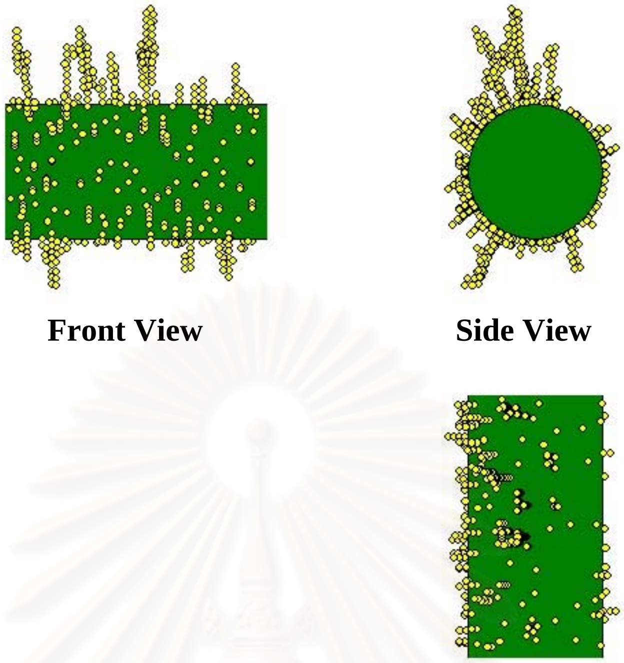

**Front View**

**Side View**

**Top View**

**Figure 6.9** Typical configuration of dendrites for the case of $K_{In} = 0.20$, $R_i = 0.0515$, Stk = 0.017, $\phi = 0.01$ , layer = 40

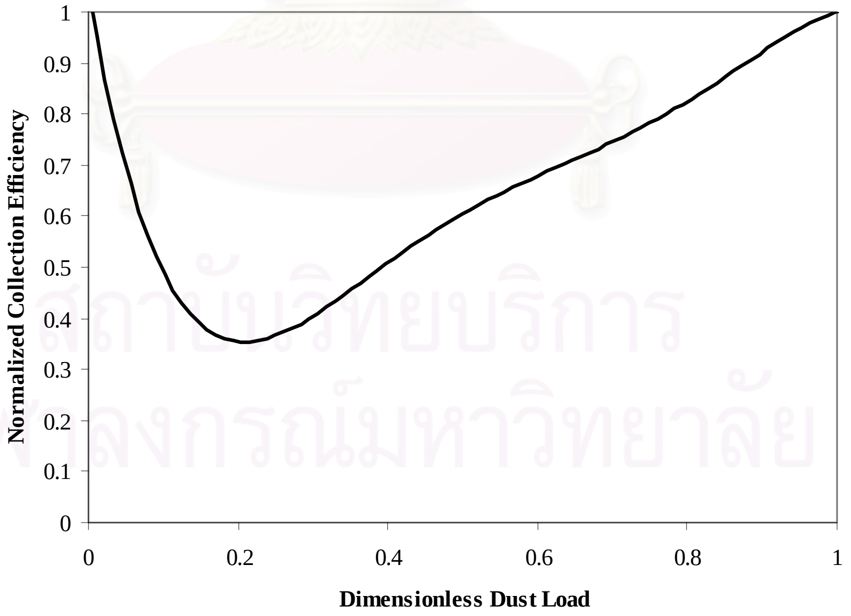

**Figure 6.10** Normalized collection efficiency for the case of $K_C = 0.2$ , $R_i = 0.0515$, Stk = 0.017, Gamma = 90 , $\phi = 0.01$

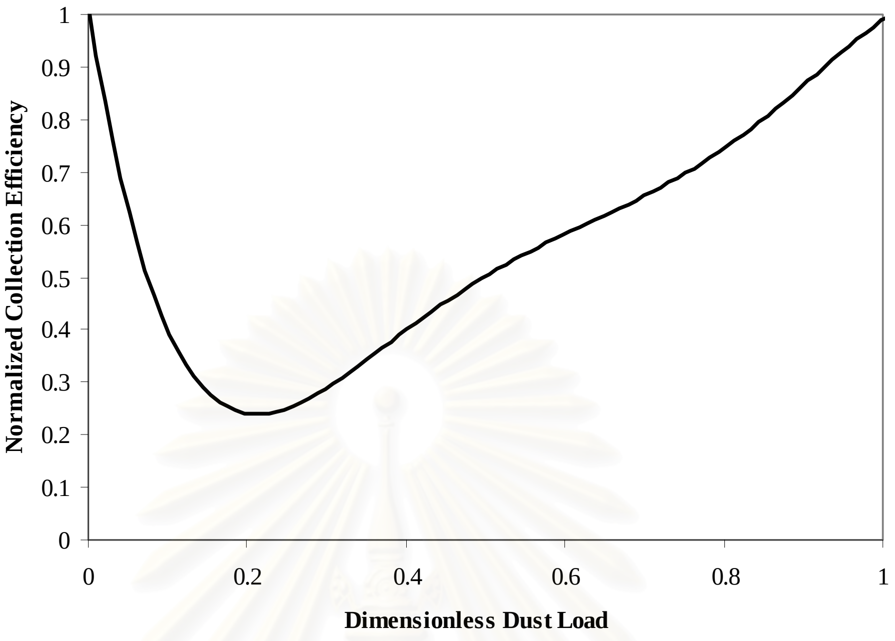

**Figure 6.11** Normalized collection efficiency for the case of $K_{In} = 0.2$ , $R_i = 0.0515$, Stk = 0.017, $\phi = 0.01$

### 6.2.1.3 Selection of suitable stochastic model

The experimental results of Kanaoka (1998) are shown in **Figures 3.2, 6.12 and 6.13**. When induced forces dominate, i.e., uncharged particles are collected on the electret fiber, the particle are uniformly collected all around the fiber surface regardless of charge distribution on the fiber at the initial stage. Most of them form chainlike agglomerate and grow almost perpendicular to the surface until a certain height. Then the shapes of the agglomerates become random and complicated. **Figures 6.12** and **6.13** are the experimental results for uncharged particles at low and high dust loads, respectively. It can be seen that there are more particles collected on the front side than the back side. Comparing **Figure 6.12** and **6.13** with either **Figure 6.9** or **Figure 6.5**, we may conclude that the morphology of dendrites in **Figure 6.5** is more realistic.

**Figures 6.14** and **6.15** show the experimental results for charged particles at low and high dust loads, respectively. When coulombic force prevails, i.e., charged particles are collected, the shapes of the agglomerates are quite similar to the case of induced forces except that the agglomerates concentrate on surface area of opposite polarity to the particles. **Figure 6.4** shows that the straight dendrites growing perpendicular to the fiber surface is more realistic than that shown in **Figure 6.8**. By the way, the particle size of interest here ranges from 0.46 – 1.26 μm, the filter diameter is 20 μm and the face velocity of filtration of interest is 0.1 m/s. In this case, Pe ranges from 28,724 to 94,570; Stokes number, from 0.0041- 0.0257; and interception parameter, from 0.023 to 0.063. Therefore, the dominant mechanical collection mechanism is diffusional/Brownian motion, followed by interception.

In conclusion, Brownian diffusion is much more significant for the present simulation than inertial impaction. Therefore, the suitable stochastic model is the one in which diffusional mechanism is dominant.

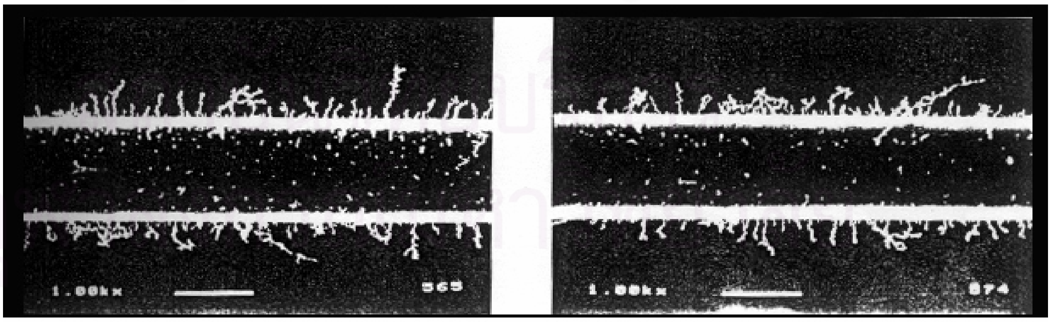

Front View Rear View

**Figure 6.12** Experimental results of dendrite morphology on an electret fiber with low dust load for uncharged particles at conditions: $d_f$ =30 μm, $d_p$= 0.039 μm, $R_i$ = 0.013, u=15 cm/s, $\rho_p$=2.33 g/cm$^3$, $K_{In}$=0.004, Pe= 50000 and Stk = 0.015

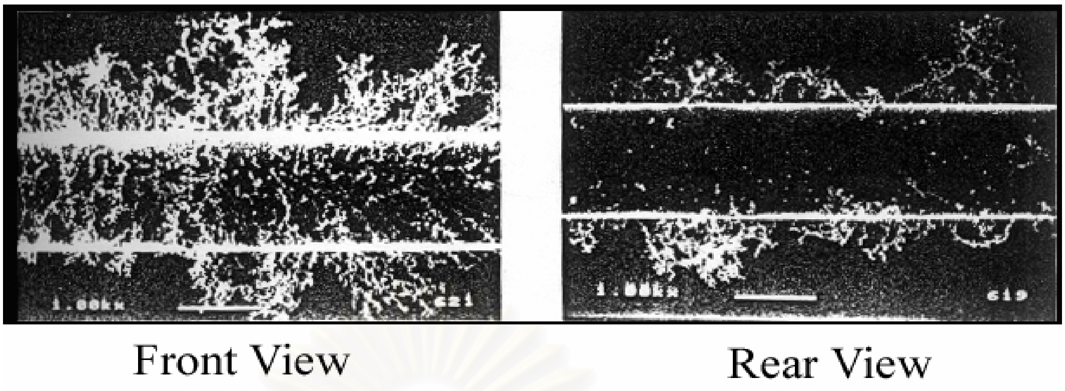
1.00kx
621
1.00kx
619
Front View
Rear View

**Figure 6.13** Experimental results of dendrite morphology on an electret fiber with high dust load for uncharged particles at conditions: $d_f$ =30 μm, $d_p$= 0.039 μm, $R_i$ = 0.013, u=15 cm/s, $\rho_p$=2.33 g/cm$^3$, $K_{In}$=0.004, Pe= 50000 and Stk = 0.015

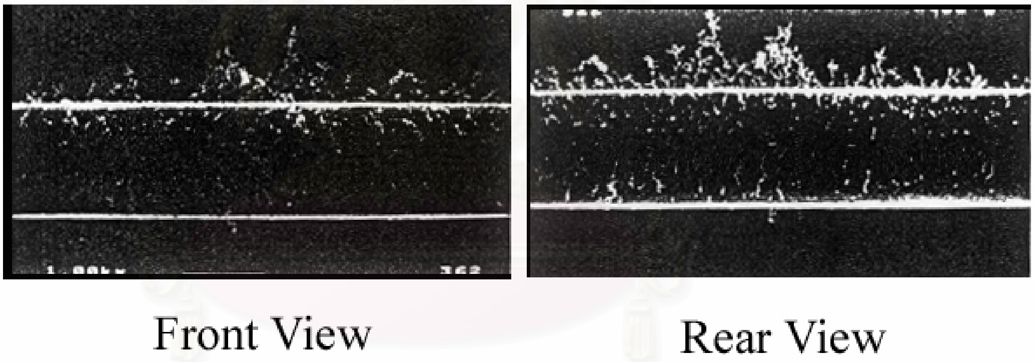
1.00kx
Front View
Rear View

**Figure 6.14** Experimental results of dendrite morphology on an electret fiber with low dust load for charged particles at conditions : $d_f$ =30 μm, $d_p$= 0.039 μm, Ri = 0.013, u=15 cm/s, $\rho_p$=2.33 g/cm$^3$, $K_C$=0.016, Pe= 50000 and Stk = 0.015

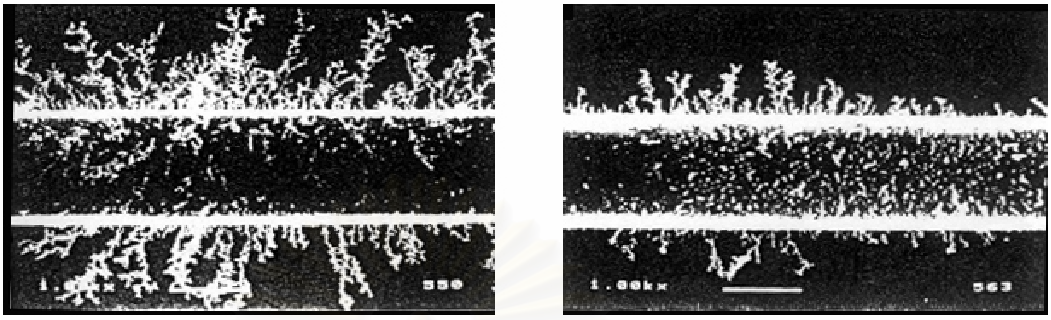

Front View Rear View

**Figure 6.15** Experimental results of dendrite morphology on an electret fiber with high dust load for charged particles at conditions: $d_f$ =30 μm, $d_p$= 0.039 μm, Ri = 0.013, u=15 cm/s, $\rho_p$=2.33 g/cm$^3$, $K_C$=0.016, Pe= 50000 and Stk = 0.015

### 6.2.2 Effect of electrical degradation factor

The concept of electrical degradation factor (ϕ) is introduced via equations (6.1) and (6.2). Here, the electrical degradation factor is assumed to be 0.005, 0.01 and 0.03, respectively. **Figure 6.16** shows the normalized collection efficiency for various electrical degradation factors. It can be seen that for the case of a high electrical degradation factor, the normalized collection efficiency decreases more rapidly and the minimum point is lower and occurs earlier than that of a low electrical degradation factor. In the present study, the appropriate electrical degradation factor is considered to be 0.01 for all simulation conditions.

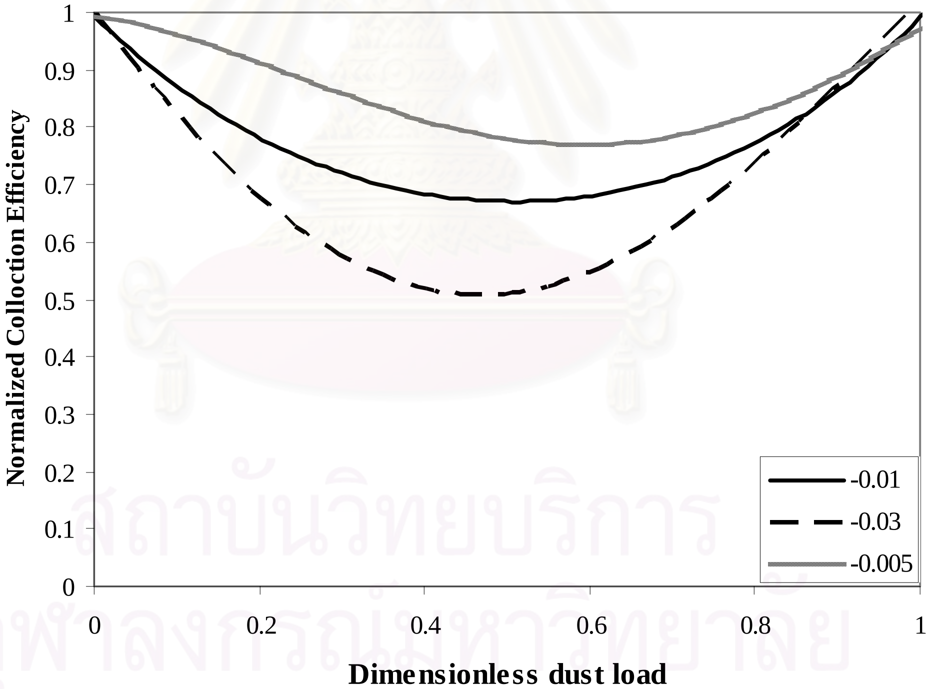

**Figure 6.16** Normalized collection efficiency for the case of $K_C = 0.2$ , $Ri = 0.0515$, $Pe = 75372$ and $\phi = 0.005, 0.01$ or0.03

### 6.2.3 Effect of interception parameter

Ri (Interception parameter) is an important parameter which has considerable effect on the agglomerative deposition phenomena of aerosol particles on an electret fiber. The concept of interception was explained in **section 3.2.2**. **Table 6.3** shows the interception parameter corresponding to various particle sizes. **Figure 6.17** compares the typical configuration of dendrites obtained in the present simulation for the case of $K_c = 0.20$, Ri= 0.0515 or Ri = 0.063, respectively. For both charged and uncharged particles, when $R_i$ is low, captured particles are more densely packed. But when $R_i$ increases, the dendrite morphology reveals more vacant area and looks more porous.

**Table 6.3** Interception parameter as a function of particle size (fiber diameter 20 μm)

| Dp ( micrometer) | Ri |
|---|---|
| 0.46 | 0.023 |
| 0.61 | 0.0305 |
| 1.03 | 0.0515 |
| 1.26 | 0.063 |

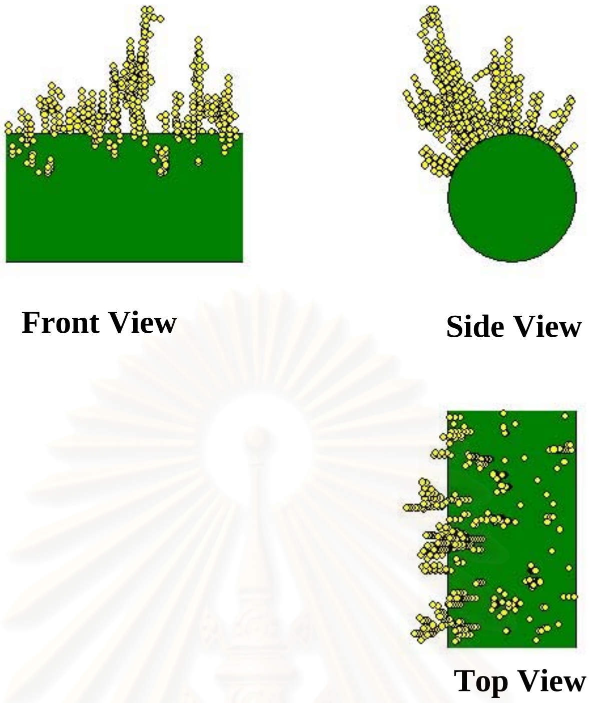
Front View
Side View
Top View

a) $K_c = 0.20$, Ri = 0.0515

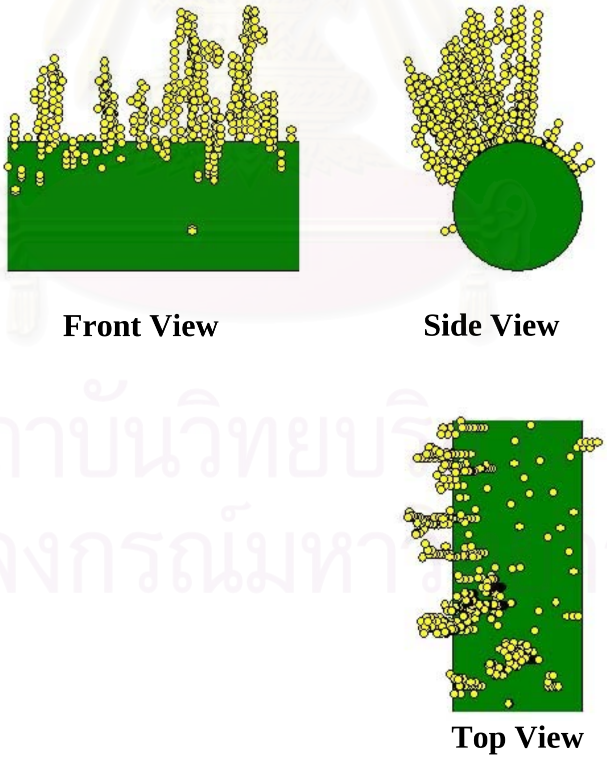
Front View
Side View
Top View

b) $K_c = 0.20$, Ri = 0.063

**Figure 6.17** Typical configuration of dendrites with $K_c = 0.20$, $\phi = 0.01$ a) Ri = 0.0515 ; b) Ri = 0.063

### 6.2.4 Effect of coulombic force parameter

Only $K_C$ (coulombic force parameter) is considered for the case of charged particles captured on an electret fiber. The concept of $K_C$ was explained in **section 3.2.6**. The accompanying degradation factor (ϕ) is assumed to be 0.01. **Figure 6.18** shows a typical example of dendrite morphology for the case of $K_C$ = 0.1, $R_i$ = 0.0515. **Figure 6.19** shows a typical configuration for the case of $K_C$ = 0.05 , $R_i$ = 0.0515. **Figure 6.17(a)** shows a typical configuration of for the case of $K_C$ = 0.2, $R_i$ = 0.0515. The effect of a high $K_C$ on the morphology makes the dendrites taller, straighter and more slender than those of a low $K_{C.}$ It can be seen that there are more scattered dendrites on the fiber surface for the case of a low $K_C$.

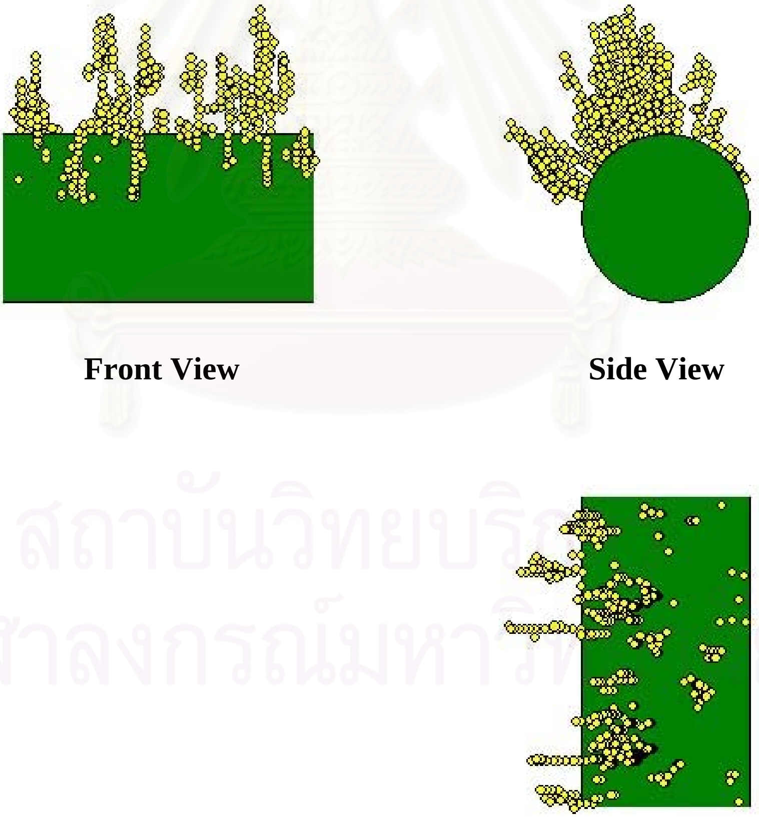

**Front View** **Side View**

**Top View**

**Figure 6.18** Typical configuration of dendrites for the case of $K_c$ = 0.10, Ri = 0.0515, Pe = 75372.

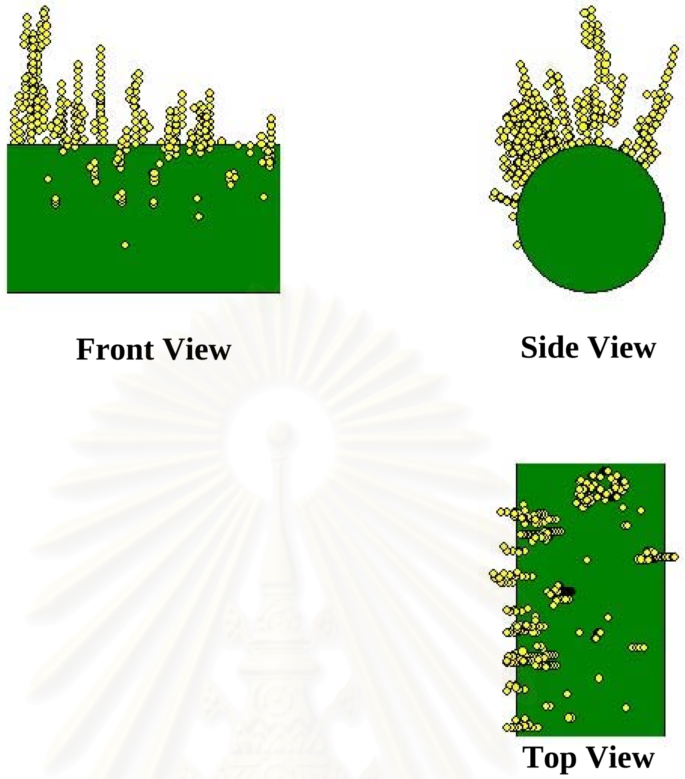
Front View
Side View
Top View

**Figure 6.19** Typical configuration of dendrites for the case of $K_c = 0.05$, Ri = 0.0515 Pe = 75372.

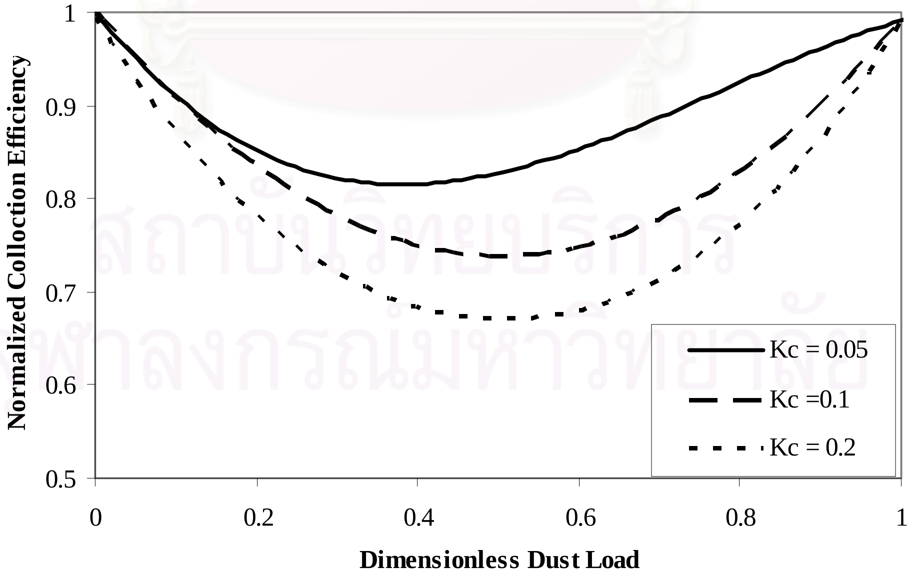

**Figure 6.20** The normalized collection efficiency for the cases of $K_C = 0.05$, 0.1 and 0.2 , respectively ( Ri = 0.0515, Pe =75732,$\phi$ = 0.01)

As mentioned above, the normalized collection efficiency is the ratio of the dust-loaded collection efficiency,$\eta$, to that of the clean fiber, $\eta_0$. **Figure 6.20** shows the normalized collection efficiency for the case of $K_C$ = 0.2, 0.1 and 0.05, respectively, with Pe = 75,372 and Ri = 0.0515. The dimensionless dust load is calculated as the ratio of the actual dust loading under filtration to the non-zero dust load at which $\eta/\eta_0 = 1$. It can be seen that normalized collection efficiency for the case $K_C$ = 0.05 remains the highest follow by the case of $K_C$ = 0.1 and $K_C$ = 0.2 ,respectively. For the case of high columbic force (high $K_C$), the initial collection efficiency of the clean fiber ($\eta_0$) is also very high; therefore the normalized collection efficiency for the case of highest $K_C$ can be reduced to the lowest value.

### 6.2.5 Effect of induce force parameter

**Figures 6.21, 6.22 and 6.23** show the typical configuration of dendrites for the case of $K_{In}$ = 0.20, 0.10 and 0.05, respectively. When the induced forces prevails, uncharged particles are collected all around the entire fiber surface and form chainlike agglomerates, which subsequently become irregular and complicated. Furthermore, these agglomerates grow almost perpendicular to the surface up to a certain height. For a low $K_{In}$, the shapes of dendrites are fatter and shorter than those of a high $K_{In}$ . In contrast, for the high $K_{In}$, the dendrites become taller and more slender and look somewhat straighter.

There are remarkable differences in the spatial distributions of charged and uncharged particles captured around an electret fiber. For uncharged particles, the dendrites are distributed more randomly and somewhat more uniformly on the whole fiber surface, growing almost perpendicular to the fiber surface. In contrast, for charged particles, the dendrites also form pearl chain structure along the electric force lines but are scattered mostly in the region with opposite charge to the particles' polarity. When particles are collected high above the effective reach of the electrostatic effect, they start to form random structured deposits (Kanaoka et al., 2001).

**Figure 6.24** shows the normalized collection efficiency for the case of $K_{In}$ = 0.2, 0.1 and 0.05 with Ri = 0.0515, $\phi$ = 0.01. As in the case of $K_C$, it can be seen that the minimum point of the normalized collection efficiency becomes lower and occurs earlier when $K_{In}$ is higher. In **Figure 6.24**, the normalized collection efficiency for the case $K_{In}$ = 0.05 is highest and the case of $K_{In}$ = 0.2 is lowest because the initial collection efficiency of clean fiber ($\eta_0$) for the case of the strongest induced force is highest.

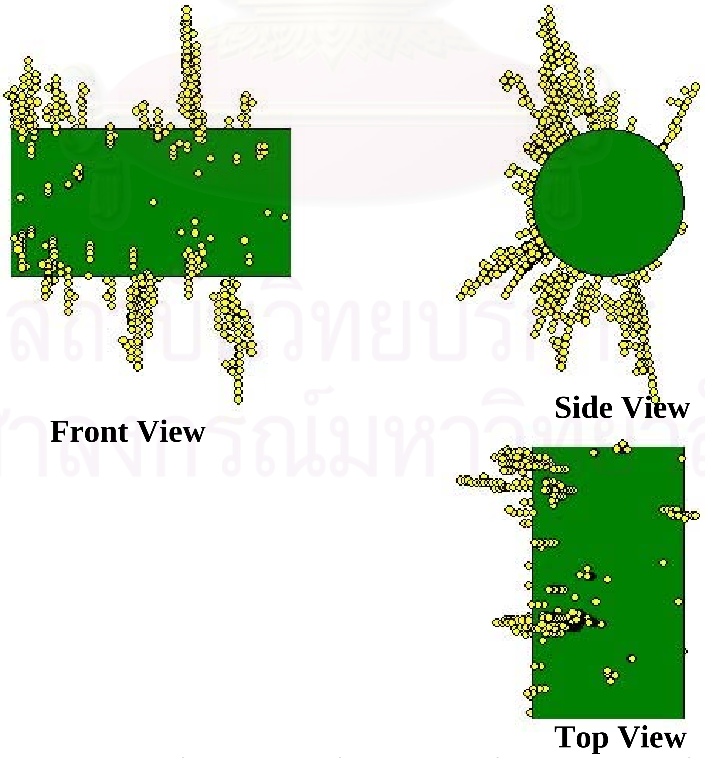

**Figure 6.21** Typical configuration of dendrites for the case of $K_{In}$ = 0.20, Ri = 0.0515, Pe = 75372, $\phi$ = 0.01

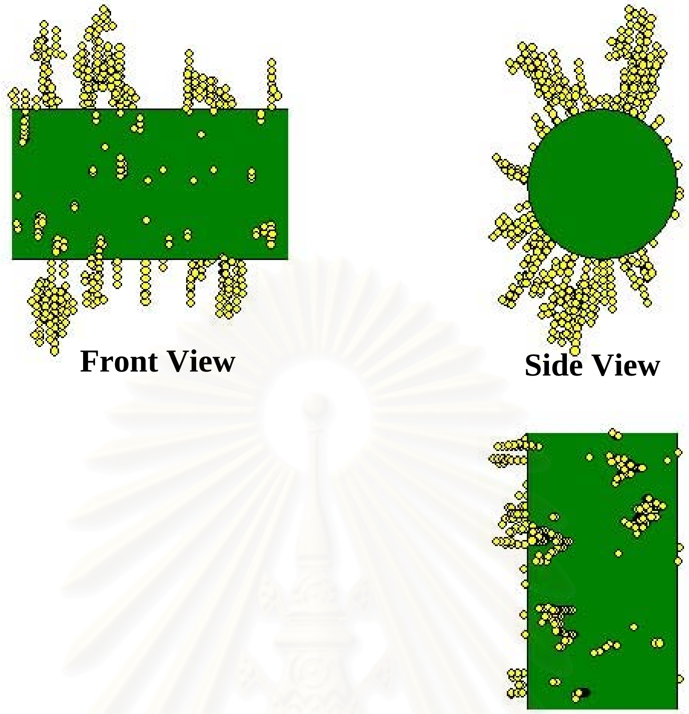
Front View
Side View
Top View

**Figure 6.22** Typical configuration of dendrites for the case of $K_{In}$ = 0.10, Ri = 0.0515, Pe = 75372, $\phi$ =0.01

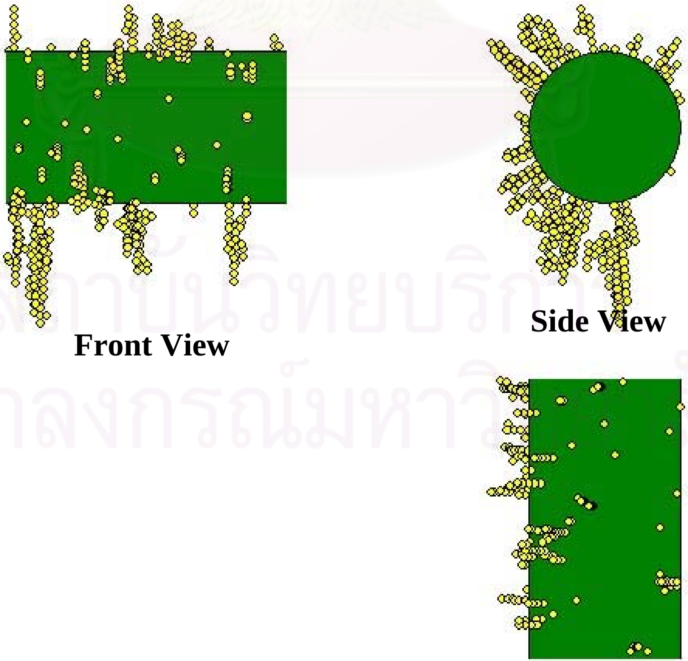
Front View
Side View
Top View

**Figure 6.23** Typical configuration of dendrites for the case of $K_{In}$ = 0.05, Ri = 0.0515, Pe = 75372, $\phi$ = 0.01

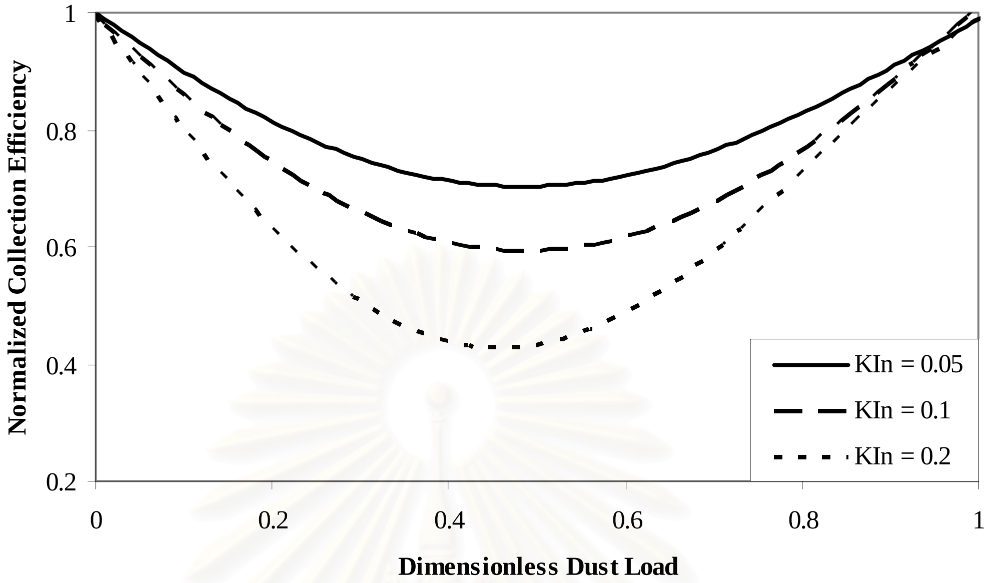

**Figure 6.24** Normalized collection efficiency for the cases of $K_{In}$ = 0.05, 0.1 and 0.2, respectively ( Ri = 0.0515, Pe = 75372,$\phi$ = 0.01)

### 6.2.6 Effect of Peclet number

When a particle is very fine, in the submicrometer order, the main deposition mechanism is Brownian diffusion. The meaning of Peclet number was explained in section 3.2.3. **Figures 6.25** , **6.26** and **6.27** show the typical configurations of dendrites for charged and uncharged particles at Pe = 1000, 5000 and 50000, respectively. At a low Pe, the shapes of the dendrite look comparatively tall, slim and straight for both charged and uncharged particles. It can be seen that the electret fiber can capture more particles especially the rear side of the surface when Pe is small. At a high Pe, the dendrites look shorter and fatter than the case of a low Pe.

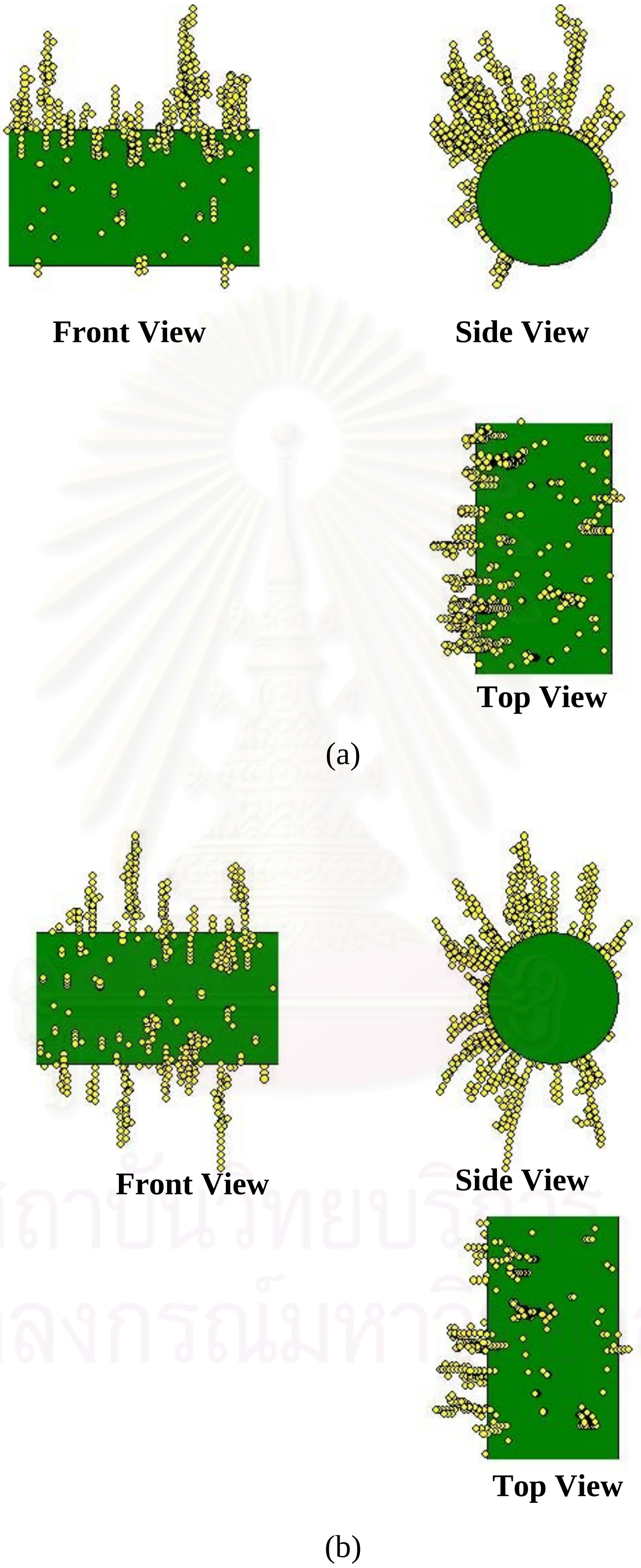
Front View
Side View
Top View
(a)
Front View
Side View
Top View
(b)

**Figure 6.25** Typical configurations of dendrites a) $K_c = 0.20$; b) $K_{In} = 0.20$ with $R_i = 0.0515$, $Pe = 1000$, $\phi = 0.01$

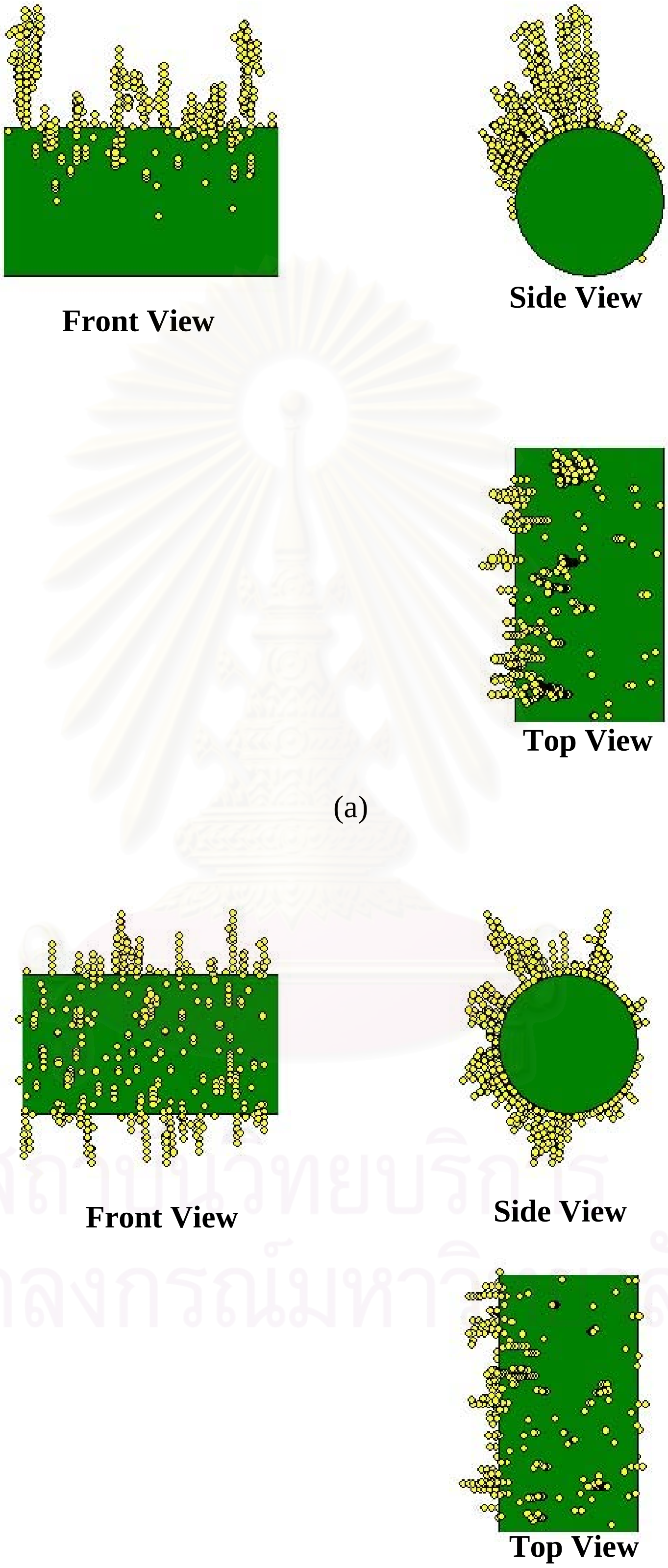
Front View
Side View
Top View
(a)
Front View
Side View
Top View

**Figure 6.26** Typical configuration of dendrites a) $K_c = 0.20$; b) $K_{In} = 0.20$ with $R_i = 0.0515$, $Pe = 5000$, $\phi = 0.01$

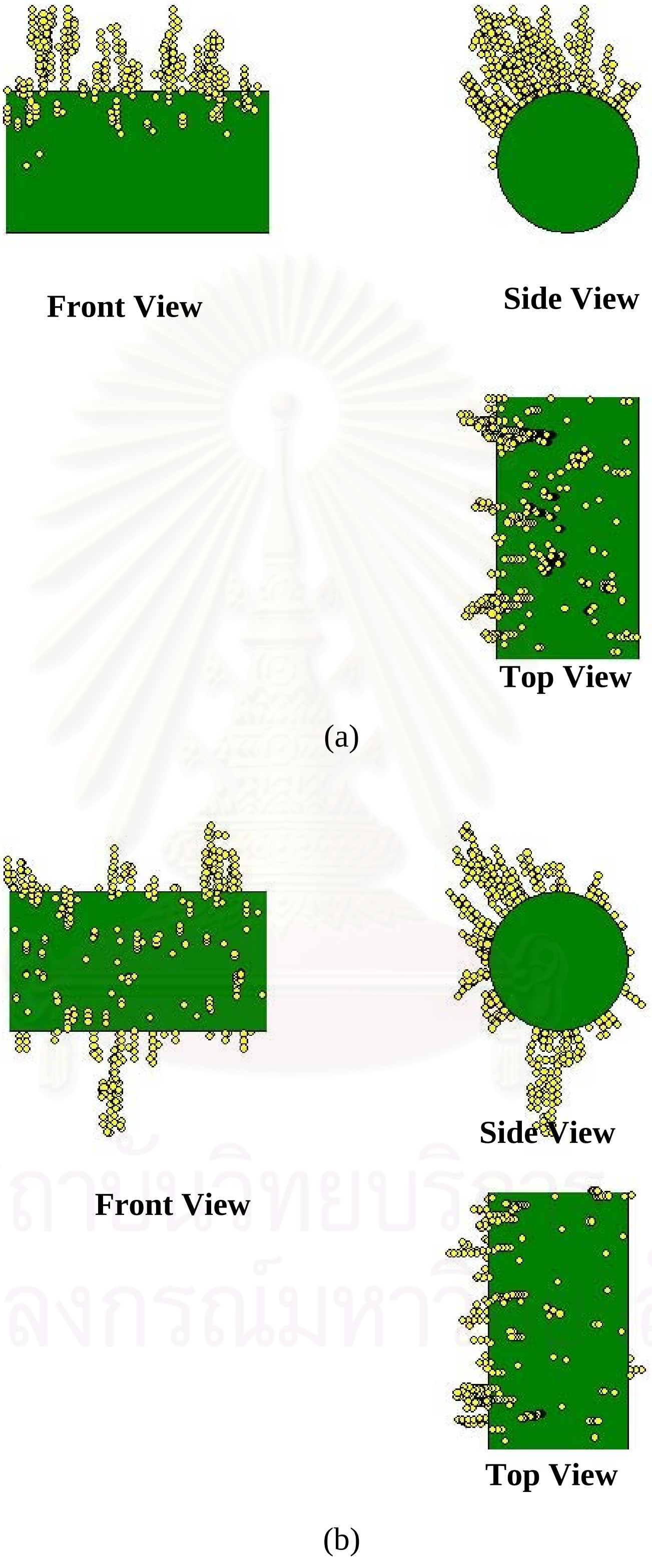
Front View
Side View
Top View
(a)
Front View
Side View
Top View
(b)

**Figure 6.27** Typical configurations of dendrites a) $K_c = 0.20$; b) $K_{In} = 0.20$ with $R_i = 0.0515$, $Pe = 50000$, $\phi = 0.01$

### 6.2.7 Correlation for the simulated collection efficiency enhancement factor

**Figure 6.28** shows the simulated single-fiber collection efficiency of charged particles over a size range 0.46 – 1.26 μm for $K_C = 0.2$ and $\phi = 0.01$. The initial single-fiber collection efficiency with respect to charged aerosol particles begins from a high initial value because the filter is initially clean and the electrostatic effect is still strong. The collection efficiency initially decreases with the dust load because of the gradual degradation of the electrostatic effect. As expected, the initial single-fiber collection efficiency ($\eta_0$) of small particles is lower than that of large particles, which agrees well with the experimental results. In addition, the minimum point of the single-fiber collection efficiency for small particles is lower and occurs earlier than that for large particles.

In the present study, the normalized collection efficiency against dimensionless dust load will be discussed under various conditions. The electrical degradation factor ($\phi$) is assumed to be 0.01 for all simulation conditions. **Figures 6.29 – 6.32** show the normalized collection efficiency with respect to charged particles. The normalized efficiency results obtained via the Monte-Carlo technique show good qualitative agreement but some quantitative differences from the correlated single-fiber experimental results (**Figure 6.3**). The discrepancy may be ascribed to 3 reasons:

1. The present simulations consider the agglomerative deposition of aerosol particles on a single fiber. The fibers are assumed to be arranged in parallel at equal spacing but the real filter mat are composed of numerous layers of many fine fibers arranged in random orientations.

2. In the simulations the effect of deposited particles on the local flow stream is assumed to be negligible.
3. No inter-bridging or crosslinking of agglomerates between adjacent fibers is considered. Nor is possible interactions between adjacent fibers.

**Figures 6.33 – 6.36** show the normalized collection efficiency with respect to uncharged particles. The degradation electrical factor is again assumed to be 0.01. As in the case of charged particles, the minimum point of the efficiency for smaller particles is lower and occurs earlier than that for larger particles. Maneeintr (2000) suggested that in the case of dominant electrical forces, the normalized collection efficiency, $\eta/\eta_0$, can be represented by two correlations: the initial stage and the subsequent stage, respectively. The present simulation results agree with Maneeintr's suggestion. The single-fiber collection efficiency can be represented by $\eta = \eta_{0E}[1+\lambda_E m] + \eta_{0M}[1+\lambda_M m]$. The electrical enhancement factor ($\lambda_E$) is shown to be smaller than the mechanical enhancement factor ($\lambda_M$) for all simulation results. As mentioned before, the electrical degradation factor is taken to be 0.01 for all simulation conditions. It was found that the electrical enhancement factor itself should be a logarithmic function of the dust load.

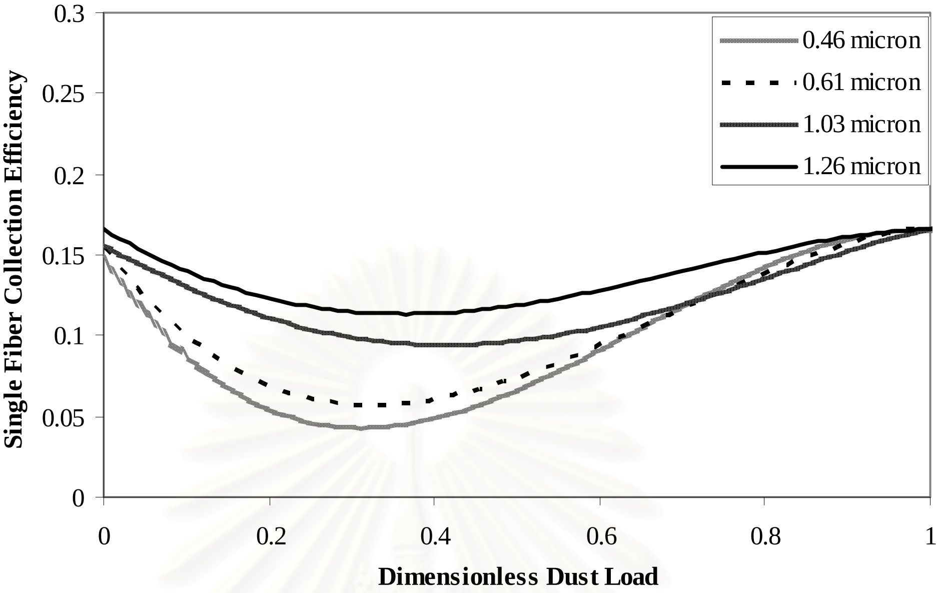

**Figure 6.28** Single fiber collection efficiency for the case of $K_C = 0.2$ and $\phi = 0.01$ for charged particles over a size range 0.46 – 1.26 micrometer.

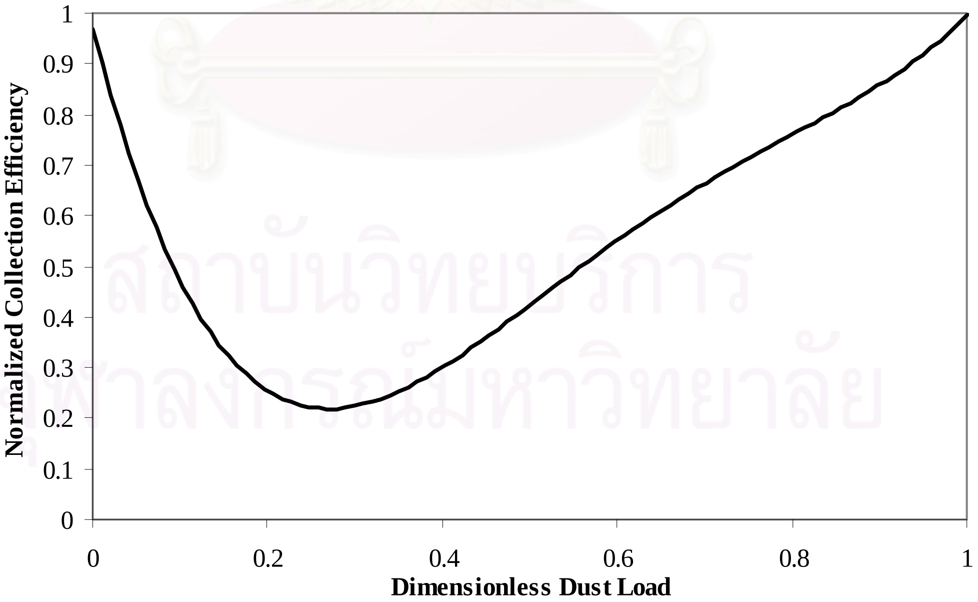

**Figure 6.29** Normalized collection efficiency for the case of $K_C = 0.2$ ,Ri = 0.023 and $\phi = 0.01$

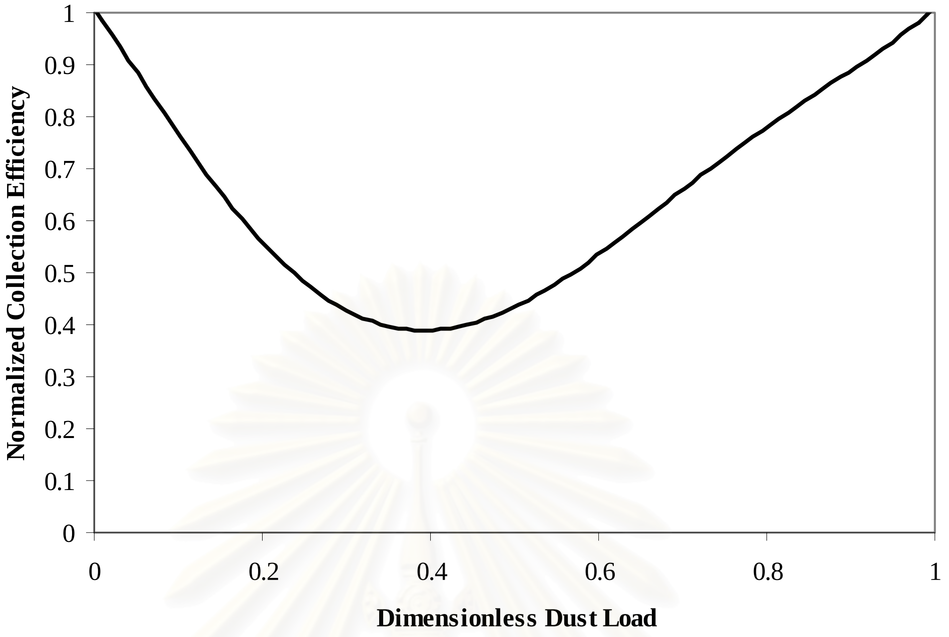

**Figure 6.30** Normalized collection efficiency for the case of $K_C = 0.2$ , $Ri = 0.0305$ and $\phi = 0.01$

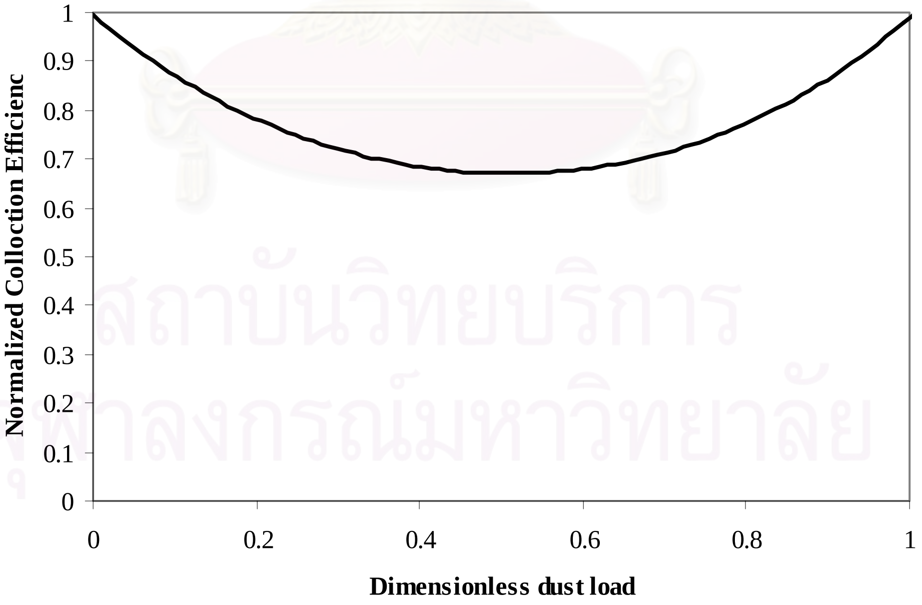

**Figure 6.31** Normalized collection efficiency for the case of $K_C = 0.2$ ,$Ri = 0.0515$ and $\phi= 0.01$

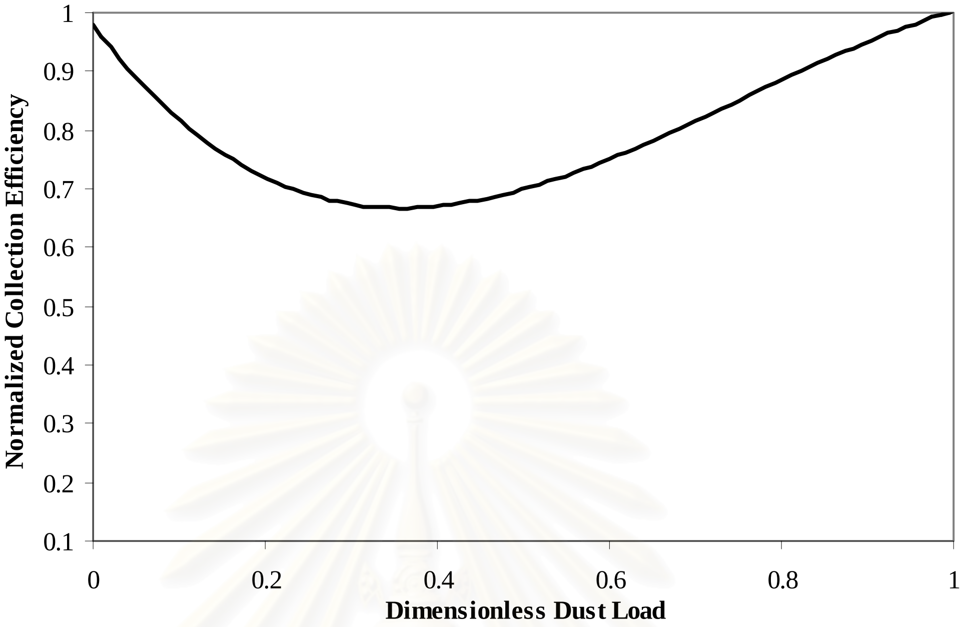

**Figure 6.32** Normalized collection efficiency for the case of $K_C = 0.2$ , $Ri = 0.063$ and $\phi = 0.01$

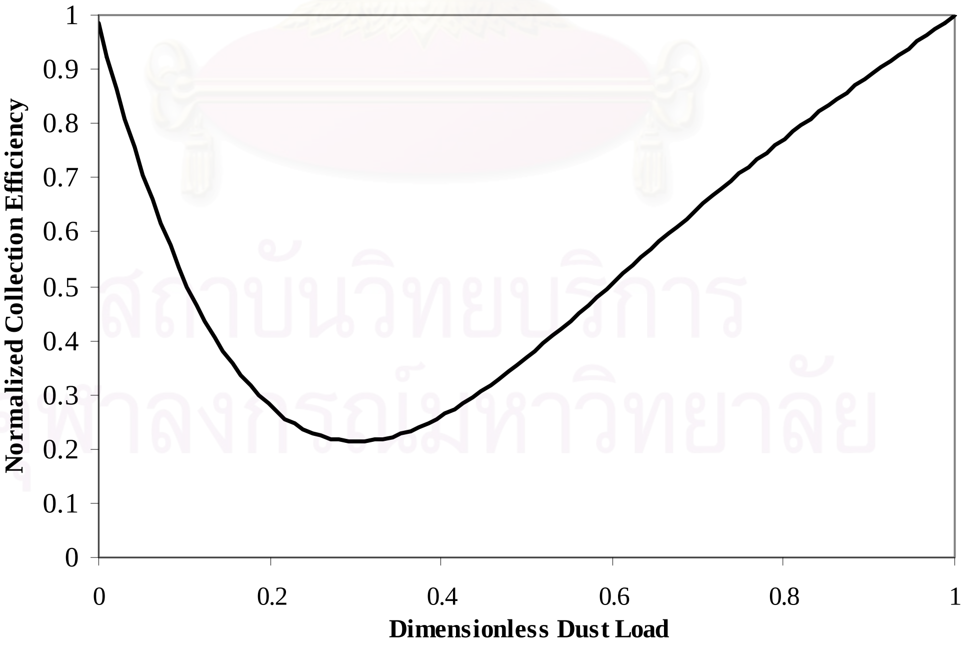

**Figure 6.33** Normalized collection efficiency for the case of $K_{In} = 0.2$ , $Ri = 0.023$ and $\phi = 0.01$

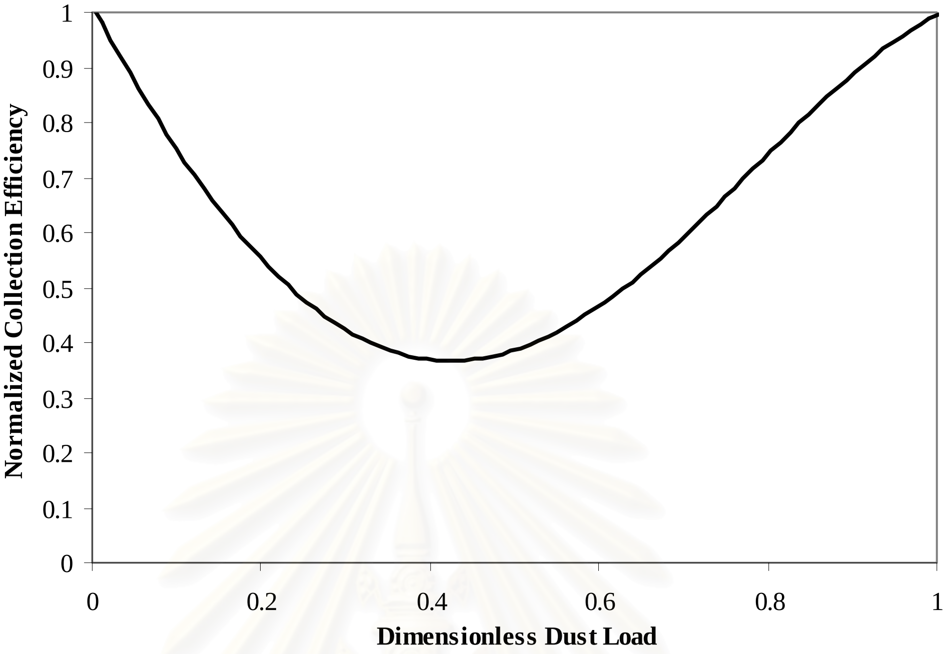

**Figure 6.34** Normalized collection efficiency for the case of $K_{In} = 0.2$ , Ri = 0.0305 and $\phi = 0.01$

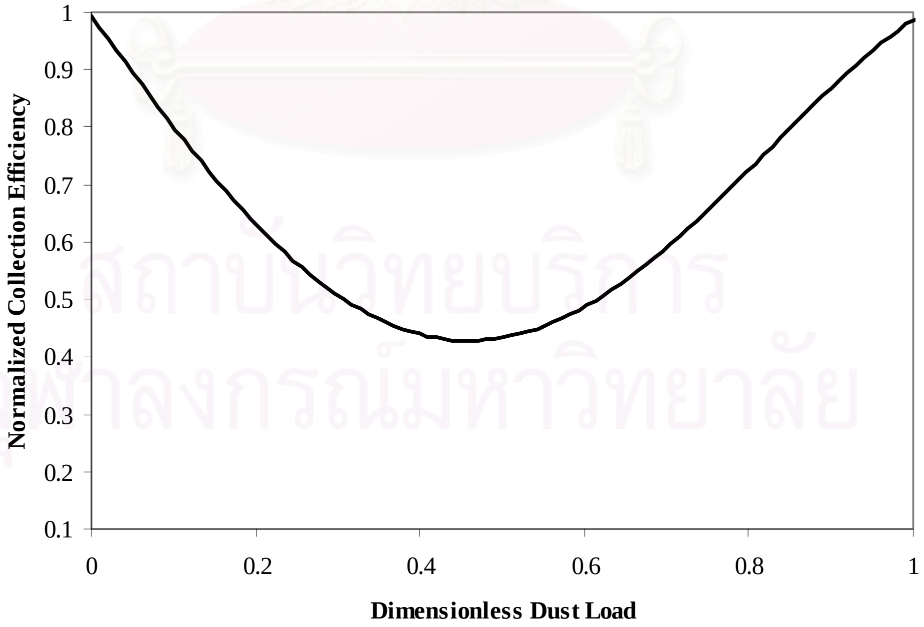

**Figure 6.35** Normalized collection efficiency for the case of $K_{In} = 0.2$ , Ri = 0.0515 and $\phi = 0.01$

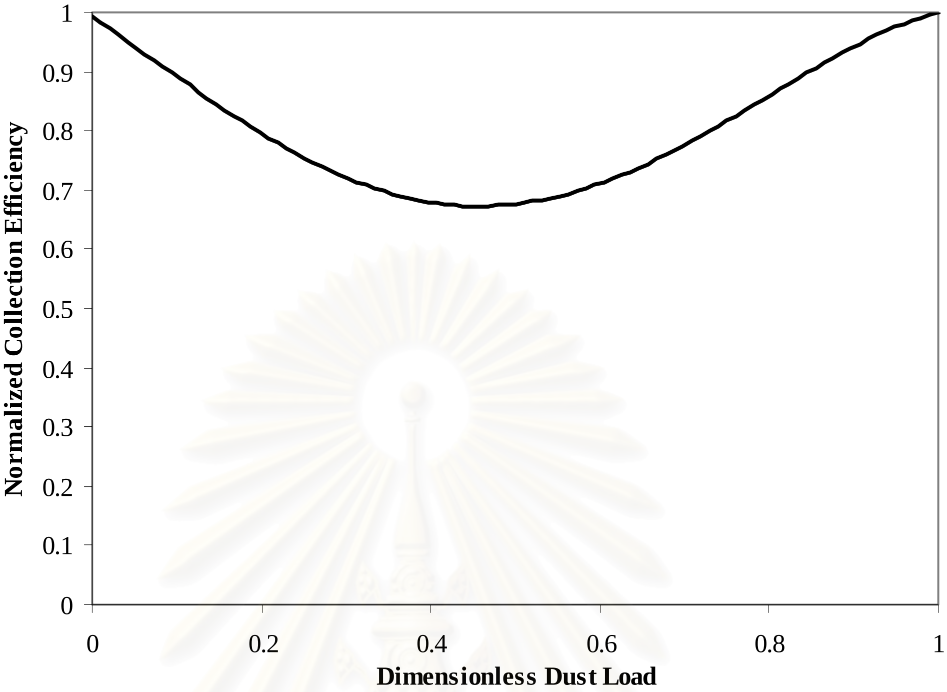

**Figure 6.36** Normalized collection efficiency for the case of $K_{In}$ = 0.2 ,Ri = 0.063 and $\phi$ = 0.01

## 6.3 Structural improvement to lengthen service life of the electret filter

The concept used to evaluate the filter service life was explained in **section 4.3**. We consider four different filters which have the same average packing density but different spatial distributions of packing density along the filter thickness. **Figure 6.37** compares the calculated penetration through the four different filters as a function of dust load. The penetrations through all four filters initially increase with dust load with filter A’s rising the most rapidly. After a period of time, the penetration through each filter reaches a maximum, starts to gradually decrease and becomes zero upon complete clogging. As expected, the values of maximum penetrations and clogging dust loads for the four filters are significantly different. Nevertheless, all filters have collection efficiencies higher than 99.99 % at all times. It should be noted that HEPA filters are required to have collection efficiencies higher than 99.97% with respect to 0.3 micrometer aerosol particles. In fact, the maximum penetrations of filters A, B, C and D are 0.004 %, 0.0045%, 0.006 % and 0.008 %, respectively. The maximum penetration of filter D is two times higher than filter A, but the dust load at clogging point of filter D, 12.8 kg/m$^3$, is about 3.5 times higher than that of filter A. Obviously, we can lengthen the filter service life up to 3.5 times by designing the filter structure as that of D, while maintaining aerosol collection efficiency above 99.99% at all times.

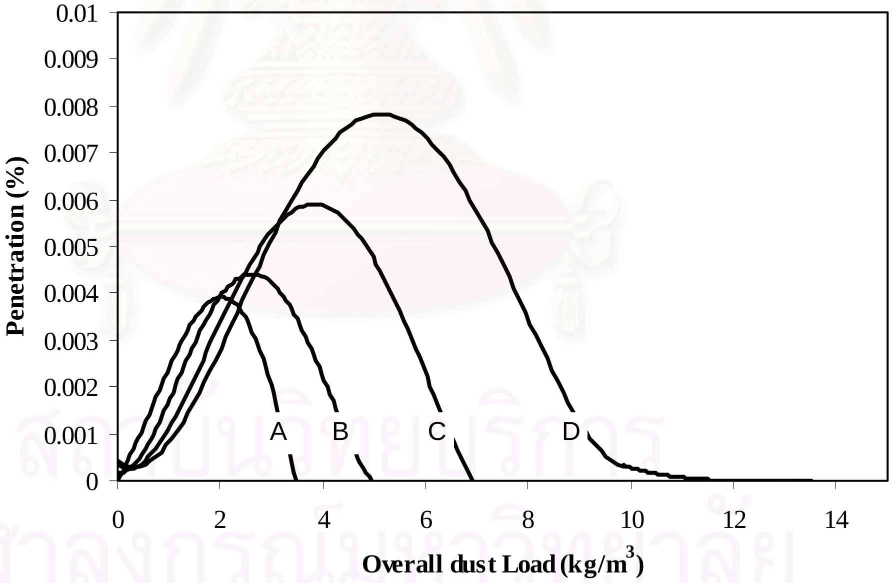

**Figure 6.37** Penetration through 4 different by packed electret filters under dust loading condition

Since the collection efficiency of all four filters are essentially 100%, a linear correlation between the dust load and filtration time is given as: dust load (kg/m$^3$) = 0.0011×time (hr). Therefore, the clogging times of filters A, B, C and D are around 3000 hrs, 4200 hrs, 6100 hrs and 13000 hrs, respectively.

The spatial distributions of dust load inside the 4 filters are shown in **Figure 6.38** as a function of dimensionless depth. From **Figure 6.38 (a)-(c)**, the maximum dust load of filters A- C always occurs at L = 0, the inlet side of the filter, and decreases steeply inside each filter. In **Figure 6.38(d)**, the maximum dust load initially appears at L = 0. After about 1200 hrs, the maximum dust load of filter D slightly shifts toward the outlet side. At 9002 hours, the maximum dust load appear at a dimensionless filter depth of 0.1 , and then the maximum dust load starts to shift to the inlet side of filter. At the clogging point, the maximum dust load appears at the front end of the filter after 13010 hours.

It should be pointed that normally air filters are not operated until they becomes completely clogged. As dust load increases, the accompanied pressure drop will increase, thereby reducing the actual air flow through the filter. Therefore, it is important to be able to predict the pressure drop of the filter as a function of dust load. The influence of dust load on the pressure drop of the electret filter has already been described in detail in **section 5.3**. In addition, the methodology available to predict the pressure drop for the case of non-electret filter has been given by Kanaoka (1998). It is reasonable to consider that the same approach is applicable to the electret filter. However, this is beyond the scope of the present study.

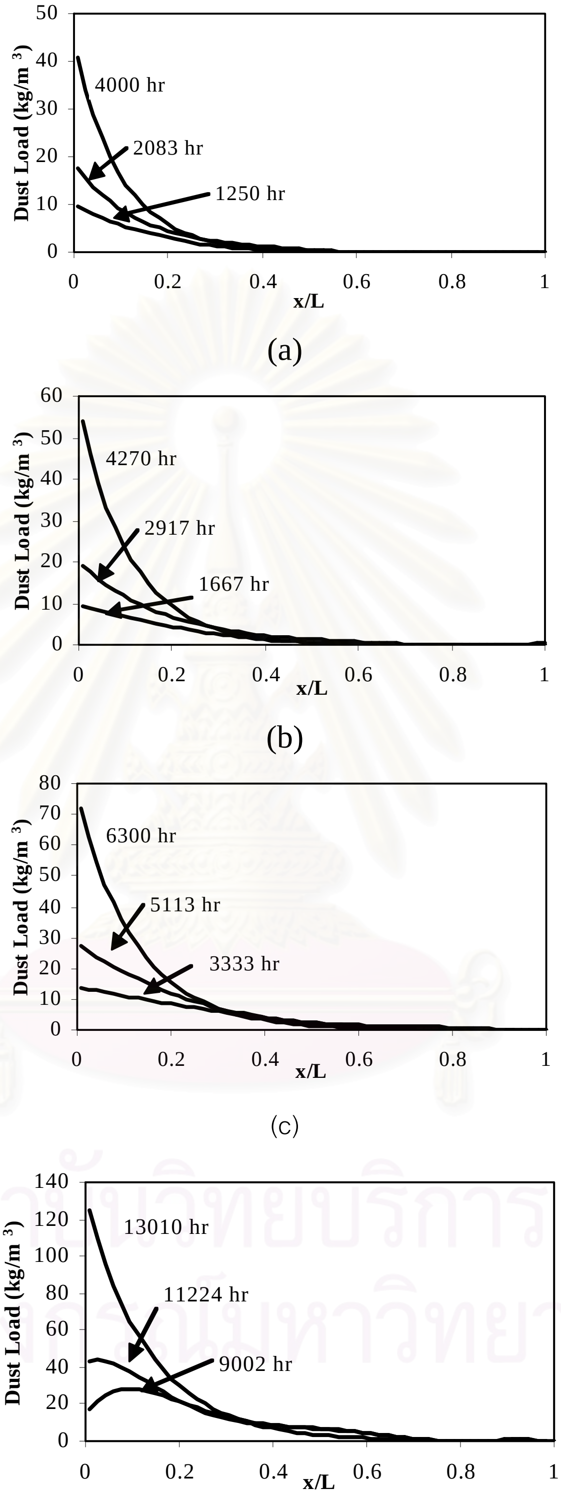

(a)

(b)

(c)

(d)

**Figure 6.38** Distribution of dust inside electret filters; (a) Filter A; (b) Filter B; (c) Filter C; (d) Filter D

# CHAPTER VII

# CONCLUSION AND RECOMMENDATION

In this study, correlation of the collection efficiency enhancement factor is estimated from reported experimental results (Walsh and Stenhouse, 1997). The three-dimensional stochastic model is utilized to simulate collection and agglomeration processes of particles on a cylindrical electret fiber. Conclusion and recommendation are summarized in this chapter.

## 7.1 Conclusion

Conclusion of this study are summarized as follows:

1. The collection efficiency of the electret fiber under dust loading can be approximated as the sum of the electrical and the mechanical collection efficiencies: $\eta = \eta_{0E}[1+(\beta \ln m+\gamma)m]+\eta_{0M}[1+\lambda m]$.

2. The electrical enhancement factor ($\lambda_E$) can be approximated as ($\beta$ ln m + $\gamma$).

3. The values of $\beta$ and $\gamma$ decrease as the size of aerosol particles increases. Charged particles have smaller $\beta$ and $\alpha$ values than uncharged particles. In addition, the differences of these two values for charged and uncharged particles increase as the particle size increases. The correlation yields

simulation results that agree well with the experimental results obtained by Walsh and Stenhouse (1997) for both charged and uncharged particles.

4. As shown the effect of interception**,** for both charged and uncharged particles, when Ri is low, captured particles are densely packed. But when Ri increases, morphology has more vacant area and looks more porous.

5. The effect of high $K_C$ on morphology makes the dendrite taller, straighter and more slender than that of low $K_{C.}$ There are more scattered dendrites on the fiber surface for the case of low $K_C$. The dendrites form pearl chain structure along the electric force lines but are scattered only in the region with opposite charge to the particles' polarity.

6. When induced force is prevailing, uncharged particles are collected all around the entire fiber surface and form chainlike agglomerates, which subsequently become irregular and complicated. For the low $K_{In}$, the shape of dendrite is fatter and shorter than that of high $K_{In}$ . In contrast, for high $K_{In}$, the dendrite becomes taller and more slender and looks straighter.

7. The initial single-fiber collection efficiency of charged aerosol particles begins from a high initial value because the filter is initially clean and the electrostatic effect is still strong. The collection efficiency initially decreases with the dust load because of the gradually degradation of the electrostatic effect. The initial single-fiber collection efficiency ($\eta_0$) of small particles is

lower than that of large particles which are shown agree well with the experimental results. In addition, the minimum point of the single-fiber collection efficiency of small particle is lower than that of large particles.

8. Simulation results show that it is possible to significantly lengthen the filter service life by packing the filter loosely on the front side and progressively more densely towards the back side, while maintaining aerosol collection efficiency above 99.99% at all times.

## 7.2 Recommendation

1. The three- dimensional stochastic simulation of the present study is simulated based on a single cylindrical fiber. In the real phenomena, the filter mats are composed of many fine fibers. The author recommends that future study should simulate by consider the effect of nearby fiber.

2. In the present study, only a single dominant electrical force – coulombic force for the case of charged and induced force for uncharged particles – is considered. In reality, however, both induced and coulombic forces are present simultaneously. If it is possible, the simulation process is should be combined effect of coulombic and induced forces.

# REFERENCES

Barot, D. T., Tien, C., and Wang, C. S. Accumulation of solid particles on single fibers fibers exposed to aerosol flows. AIChE Journal.26(1980):289-292.

Baumgartner, H., and Loffler, F. The collection performance of electret filters in the particle size range 10 nm-10μm. Journal of Aerosol Science.17 (1986a): 438-445.

Baumgartner, H., and Loffler, F. Experimental and theoretical investigation of the time-dependent collection performance of electret filters. 2nd Int.Aerosol Conf. (1986b):708-771.

Baumgartner, H., and Loeffler, F. Three-dimensional numerical simulation of the deposition of polydisperse aerosol particles on filter fibers-extend concept and preliminary results. Journal of Aerosol Science.18(1987):885-888.

Brown, R.C., Gray, W.R., Blackford, D.B., and Bostock, G.J. Effect of industrial aerosols on the performance of electrically charged filter material. Annals of Occupational Hygiene. 32(1988):271-294.

Brown, R.C. Air filtration. Oxford: Pergamon Press, 1993.

Davies, C.N. Air Filtration. Academic Press, 1973.

Emi, H., and Kanaoka, C. Most penetrating particle size in electret fiber filtration. Aerosols. (1984): 567-572.

Emi, H., Kanaoka ,C.,Otani, Y., and Ishiguro, T. Collection mechanisms of electret filter. Particulate Science and Technology. 5(1987):161-171.

Fuchs, N.A. Mechanics of Aerosols. Oxford:Pergamon Press,1964.

Ji, J.H. , Bae, G.N. , Kang, S.H. , and Hwang, J. Effect of particle loading on the collection performance of an electret cabin air filter for submicron aerosols. Journal of Aerosol Science. 34(2003):1493-1504.

Kanaoka, C., Emi, H., and Tanthapanichakoon, W. Conventive diffusional deposition and collection efficiency of aerosol on a dust-loaded fiber. American Institute of Chemical Engineers Journal. 29(1983): 895-902.

Kanaoka, C., Emi, H., and Ishiguro, T. Time dependency of collection performance of electret filters. 1st AAAR Conference. (1984):613-616

Kanaoka, C., Emi, H., Otani, Y., and Iiyama, T. Effect of charging state of particles on electret filtration. Aerosol Science and Technology. 7(1987):1-13.

Kanaoka,C., Performance of an air filter at dust-loaded condition. In Spurny,K.R.(Ed.), Advance in aerosol filtration. Schmallenberg,Germany: Lewis Publishers. (1998):323-334

Kanoka, C., Hiragi, S., and Tanthapanichakoon, W. Stochastic simulation of the agglomerative deposition process of aerosol particles on an electret fiber. Powder Technology.118(2001):97-106.

Kuwabara, S. The forces experienced by a lattice of elliptic cylinders in a uniform flow at small Reynolds numbers. Journal of Physical Society of Japan. 14(1959):522-527.

Lee, M., Otani, Y., Namiki, N., and Emi, H. Prediction of collection efficiency of high-performance electret filter. Journal of Chemical Engineering of Japan. 33(2002a): 57-62.

Myojo, T., Kanaoka, C. and Emi, H. Experimental observation of collection efficiency of a dust-loaded fibre. Journal of Aerosol Science.25 (1984):483-489.

Otani, Y., Emi, H., and Mori, J. Initial collection efficiency of electret filter and its durability for solid and liquid particles. Kona.11(1993):207-214.

Payatakes, A.C., and Tien, C. Particle deposition in fibrous media with dendritic-like pattern. Journal of Aerosol Science. 7(1976):85-100.

Payatakes, A.C., and Tien, C. Model of transient aerosol particle deposition in fibrous media with dendritic pattern. AIChE Journal. 23(1977):192-202

Payatakes, A.C., and Gradon, L. Dendritic deposition of aerosols by convective Brownian motion for small, intermediate and high Knudsen numbers. AIChE Journal. 26(1980):443-454

Pich, J.,Emi, H., and Kanaoka, C. Coulombic deposition mechanism in electret filters. Journal of Aerosol Science.18(1987):29-35.

Reist P. C. Aerosol Science and Technology. 2nd edition, McGraw-Hill, Inc.,(1993)

Romay, F. J., Liu, B.Y.H., and Chae, S.J. Experimental study of electrostatic capture mechanisms in commercial electret filters. Aerosol Science and Technology. 28(1998):224-234.

Stechkina, I.B., and Fuchs, N.A. Studies on fibrous air filter-I. Calculation of diffusional deposition in fibrous filters Annals of Occupational Hygiene. 9(1966):59-64.

Stechkina, I.B., Kirst, A.A., and Fuchs, N.A. Studies on fibrous aerosols filters-IV. Calculation of aerosol deposition in model filters in the region of maximum penetration. Annals of Occupational Hygiene.12(1969):1-8.

Tanthapanichakoon, W., Maneeintr, K., Charinpanitkul, W., and Kanaoka, C. Estimation of collection efficiency enhancement factor for an electret fiber with dust load. Journal of Aerosol Science. 34(2003):1505-1522.

Tien, C., Wang, C.S., and Barot, D.T. Chainlike formation of particle deposits in fluid-particle separation. Science,196(1977):983-985.

Wongsri, M., Tanthapanichakoon, W., Kanaoka, C.,and Emi, H., Convective diffusional collection efficiency of polydisperse aerosol on a dust-loaded fiber. Advanced Powder Technology. 2(1991):1-23.

Walsh, D.C. The behaviour of electrically active and prefilter fibrous filters under solid aerosol load. Ph.D Thesis. Loughborough University of Technology, 1995.

Walsh,D.C., and Stenhouse, J.I.T. The effect of particle size, charge and composition on the loading characteristics of an electrically active fibrous filter material. Journal of Aerosol Science.28(1997):307-321.

Wang C. S., Beizaie M., and Tien C. Deposition of solid particles on a collector;formulation of a new theory. AIChE Journal. 23(1977):879-889.

William, C. H. Aerosol Technology. New York: John Wiley & Sons, Inc,1998.

Yoshioka, N., Emi, H.,and Sone, H. Filtration of aerosols through fibrous packed bed with dust loading . Kagaku Kogaku (Chem. Eng. Japan). 33(1969):1013-1018.

# APPENDICES

# APPENDIX A

## Derivation of collection efficiency of electret filer under dust loading

The objective of this appendix is to present a derivation of collection efficiency equation of filter under dust loading. These equations are developed and shown in Kanaoka (1998)

$$\frac{\partial C}{\partial x} = -\frac{4}{\pi} \cdot \frac{\alpha}{1-\alpha} \frac{\eta_{\alpha m}}{d_f} C \tag{A.1}$$

$$\frac{\partial C}{\partial x} = -\frac{1}{v} \cdot \frac{\partial m}{\partial t} \tag{A.2}$$

$$\frac{\eta_{\alpha m}}{\eta_{\alpha 0}} = 1 + \lambda m$$

Collection efficiency

$$Em = 1 - \frac{C_0}{C_i} = 1 - \frac{\exp(-\lambda B C_i vt)}{\exp(-\lambda B C_i vt) + \exp(BL) - 1} \tag{A.3}$$

Dust load

$$m = -\frac{1}{\lambda} \cdot \frac{\exp(-\lambda B C_i vt) - 1}{\exp(-\lambda B C_i vt) + \exp(Bx) - 1} \tag{A.4}$$

where $B = \frac{4}{\pi} \cdot \frac{\alpha}{1-\alpha} \frac{\eta_{\alpha 0}}{d_f}$

Solution

From eq (A.1)

$$\frac{\partial C}{\partial x} = -\frac{4}{\pi} \cdot \frac{\alpha}{1-\alpha} \frac{\eta_{\alpha 0}(1+\lambda m)}{d_f} C \qquad (A.5)$$

if $B = \frac{4}{\pi} \cdot \frac{\alpha}{1-\alpha} \frac{\eta_{\alpha 0}}{d_f}$ therefore eq(A.5) becomes

$$\frac{\partial C}{\partial x} = -B(1+\lambda m)C \qquad (A.6)$$

if $f = C$
$g = 1+ \lambda m$

so, eq(A.6) becomes

$$\frac{\partial f}{\partial x} = -Bgf \qquad (A.7)$$

from $g = 1+ \lambda m$

$$m = \frac{(g-1)}{\lambda}$$

$$\frac{\partial m}{\partial t} = \frac{\partial}{\partial t}\left[\frac{g}{\lambda} - \frac{1}{\lambda}\right]$$

$$\frac{\partial m}{\partial t} = \frac{\partial}{\partial t}\left[\frac{g}{\lambda}\right] \qquad (A.8)$$

Substituting eq(8) into eq(2)

$$\frac{\partial f}{\partial x} = -\frac{1}{\lambda v} \cdot \frac{\partial g}{\partial t} \qquad (A.9)$$

eq(A.9) = eq(A.7)

$$\therefore \frac{\partial g}{\partial t} = Bgf\lambda v \qquad (A.10)$$

from eq(A.7)

$$\frac{\partial f}{\partial x} = -Bgf \qquad (A.7)$$

$$\frac{1}{f}\partial f = -Bg\partial x$$

$$\ln f = -Bg\partial x$$

$$g = \frac{-\ln f}{B} \cdot \frac{1}{\partial x} \qquad \text{(A.11)}$$

Substititing eq(A.11) into eq(A.10)

$$\frac{\partial}{\partial t}\left[\frac{-\ln f}{B\partial x}\right] = Bgf\lambda v$$

$$\frac{\partial \ln f}{\partial t \partial x} = -B^2 gf\lambda v \qquad \text{(A.12)}$$

from eq(A.10)

$$\frac{\partial g}{g} = Bf\lambda v\partial t$$

$$\ln g = Bf\lambda v\partial t$$

$$f = \frac{\ln g}{B\lambda v} \times \frac{1}{\partial t} \qquad \text{(A.13)}$$

Substituting eq(A.13) into eq(A.7)

$$\frac{\partial}{\partial x}\left[\frac{\ln g}{B\lambda v} \times \frac{1}{\partial t}\right] = -Bgf$$

$$\frac{\partial \ln g}{\partial x \partial t} = -B^2 gf\lambda v \qquad \text{(A.14)}$$

(A.12) – (A.14)

$$\frac{\partial \ln f}{\partial t \partial x} - \frac{\partial \ln g}{\partial t \partial x} = 0$$

$$\frac{\partial \ln(f/g)}{\partial t \partial x} = 0 \qquad \text{(A.15)}$$

$$\frac{f}{g} = \gamma e^{\alpha x + \beta t} \qquad \text{(A.16)}$$

$$f = g\gamma e^{\alpha x + \beta t}$$

$$\frac{\partial f}{\partial x} = g\gamma\alpha e^{\alpha x + \beta t} \qquad \text{(A.17)}$$

(A.17) = (A.7)

$$g\gamma\alpha e^{\alpha x+\beta t} = -Bgf$$

$$-\frac{1}{f} = \frac{B}{\gamma\alpha}e^{-\alpha x-\beta t} + K_1 \qquad (A.18)$$

from eq(A.16)

$$\frac{f}{g} = \gamma e^{\alpha x+\beta t} \qquad (A.16)$$

$$g = \frac{f}{\gamma e^{\alpha x+\beta t}}$$

$$\frac{\partial g}{\partial t} = -\beta\frac{f}{\gamma}e^{-(\alpha x+\beta t)} \qquad (A.19)$$

eq(A.17) = eq(A.10)

$$-\beta\frac{f}{\gamma}e^{-(\alpha x+\beta t)} = Bgf\lambda v$$

$$-\frac{1}{g} = \frac{B\lambda v\gamma}{\beta}e^{\alpha x+\beta t} + K_2 \qquad (A.20)$$

I.C. $t = 0$ , $m = 0$ , $g = 1$ ($g = 1+\lambda m$)
$X=0$ , $C = C_i$ , $f = C_i$

from eq(A.18) ; $f = Ci$ , $x = 0$

$$-\frac{1}{C_i} = \frac{B}{\gamma\alpha}e^{-\beta t} + K_1$$

$$K_1 = -\frac{1}{C_i} - \frac{B}{\gamma\alpha}e^{-\beta t} \qquad (A.21)$$

from eq(A.20) ; $g = 1$ , $t = 0$

$$-1 = \frac{B\lambda v\gamma}{\beta}e^{\alpha x} + K_2$$

$$K_2 = -1 - \frac{B\lambda v\gamma}{\beta} e^{\alpha x} \qquad \text{(A.22)}$$

so,

eq(A.18), (A.20) becomes

$$-\frac{1}{f} = \frac{B}{\gamma\alpha} e^{-\alpha x - \beta t} - \frac{1}{C_i} - \frac{B}{\gamma\alpha} e^{-\beta t} \qquad \text{(A.23)}$$

$$-\frac{1}{g} = \frac{B\lambda v\gamma}{\beta} e^{\alpha x + \beta t} - 1 - \frac{B\lambda v\gamma}{\beta} e^{\alpha x} \qquad \text{(A.24)}$$

eq(A.24) / eq(A.23)

$$\frac{f}{g} = \frac{\frac{B\lambda v}{\beta} - \frac{1}{\gamma e^{\alpha x + \beta t}} - \frac{B\lambda v x}{\beta} e^{-\beta t}}{\frac{-B}{\gamma\alpha} e^{-\alpha x - \beta t} - \frac{1}{C_i} - \frac{B}{\gamma\alpha} e^{-\beta t}} = \gamma e^{\alpha x + \beta t}$$

$\alpha$ = -B

$\beta$ = $-B\lambda C_i v$

$\gamma$ = Ci

$$-\frac{1}{f} = \frac{B}{-BC_i} e^{Bx + B\lambda C_i vt} - \frac{1}{C_i} - \frac{B}{-BC_i} e^{-B\lambda C_i vt} = -\frac{1}{C_0}$$

$$\frac{C_0}{C_i} = \frac{\exp(-\lambda BC_i vt)}{\exp(-\lambda BC_i vt) + \exp(Bx) - 1}$$

$$g = 1 + \lambda m = \frac{\exp(Bx)}{\exp(Bx) + \exp(-\lambda BC_i vt) - 1}$$

$$m = -\frac{1}{\lambda} \frac{\exp(-\lambda BC_i vt) - 1}{\exp(-\lambda BC_i vt) + \exp(Bx) - 1}$$

Collection efficiency

$$\mathrm{Em} = 1 - \frac{C_0}{C_i} = 1 - \frac{\exp(-\lambda B C_i v t)}{\exp(-\lambda B C_i v t) + \exp(BL) - 1} \qquad \text{(A.3)}$$

Dust load

$$m = -\frac{1}{\lambda} \cdot \frac{\exp(-\lambda B C_i v t) - 1}{\exp(-\lambda B C_i v t) + \exp(Bx) - 1} \qquad \text{(A.4)}$$

where $$B = \frac{4}{\pi} \cdot \frac{\alpha}{1-\alpha} \frac{\eta_{\alpha 0}}{d_f}$$

# APPENDIX B

## Publications resulting from this research work

### International research papers

1. W. Sae-lim, W. Tanthapanichakoon, and C. Kanaoka, “Correlation for the efficiency enhancement factor of a single electret fiber”, *Journal of Aerosol Science (In press)***.**
2. W. Sae-lim, W. Tanthapanichakoon, and C. Kanaoka, “Structural improvement to quadruple service life of a high-efficiency electret filter”, *Science and Technology of Advanced Materials (In press).*

### International proceedings

1. W. Sae-lim, W. Tanthapanichakoon, and C. Kanaoka, “Collection efficiency enhancement factor of an electret fiber under dust load”, *Proceeding of Regional Symposium on Chemical Engineering (RSCE 2004),* December 1-3, 2004, Bangkok, Thailand.
2. W. Sae-lim, W. Tanthapanichakoon, and C. Kanaoka, “Structural improvement to quadruple service life of a high-efficiency electret filter”, *International symposium on nanotechnology in environmental protection and pollution (ISNEPP 2005),* Jan 12-14,2005, Bangkok, Thailand

# VITA

Miss Weeraya Sae-lim, first daughter of Mr.Wichan and Mrs. Soelai Sae-lim, was born on July 30, 1980 in Songkhla, Thailand. She attended Hatyaiwittayalai School in Songkhla and graduated in 1997. In April 2001, she received her Bachelor Degree of Engineering in Chemical Engineering with 1st class honor from Faculty of Engineering, Prince of Songkhla University, Songkhla, Thailand. She enrolled her Doctoral Degree Program at Chulalongkorn University in 2001 under the Royal Golden Jubilee Ph.D. program. During April 2003 to April 2004, she lived in Japan to carry out a part of her dissertation. She was awarded a Ph.D. degree in Chemical Engineering in September, 2005.